



***Inter-comparison of Large  
Scale Optical Sensors Workshop***

***ESA/ESTEC 12-14 October 2004  
Noordwijk, The Netherlands***

# Workshop on Inter-Comparison of Large Scale Optical and Infrared Sensors

## Tuesday, 12 October

- |             |   |
|-------------|---|
| 09.00-09.30 | Opening and Introduction (Rast M.)  |
| 09.30-10.00 | MERIS radiometric and spectral calibration (Delwart S.)   |
| 10.00-10.30 | MODIS In-flight Calibration Methodologies (Xiong J.)  |
| 10.30-11.00 | Coffee Break  |
| 11.00-11.30 | Operational vicarious calibration of solar channels of the European meteorological geostationary satellites (Govaerts Y.) |
| 11.30-12.00 | Eight years MOS-IRS - Summary of calibration activities (Schwarzer H.)  |
| 12.00-12.30 | Revised Landsat-5 TM Radiometric Calibration Procedures and Postcalibration Dynamic Ranges (Chander G.)                   |
| 12.30-13.00 | In flight calibration of the CHRIS instrument onboard PROBA (Lobb D.)   |
| 13.00-14.00 | Lunch Break   |
| 14.00-14.30 | The calibration of the short-wavelength channels of the ATSR series of Instruments (Smith D.)                             |
| 14.30-15.00 | Advanced Calibration Concept of APEX (Nieke J.)   |
| 15.00-15.30 | Calibration and Validation with the EO-1 Observing Suite (Ungar S.)   |
| 15.30-16.00 | Coffee Break  |
| 16.00-16.30 | Calibration and Validation of Satellite Sensors at NOAA/NESDIS/ORA (Yoe J.)   |
| 16.30-17.00 | MISR Radiometric Validation Studies (Bruegge C.)  |

- 17.00-  
17.30 In-flight calibration issues of SCIAMACHY (Wuttke M.)
- 17.30-  
18.00 SCIAMACHY detectors calibration on-ground and in-flight (Lichtenberg G.)
- 18.00 Ice Breaker

### **Wednesday, 13 October**

- 09.00-  
09.30 Diffuser trade-off study vs spectral features: measurements and analysis (Bazalgette Courreges-Lacoste G.)
- 09.30-  
10.00 Validated data and removal of bias through Traceability to SI units (Fox N.)
- 10.00-  
10.30 The Establishment and Verification of Traceability for Remote Sensing Radiometry (Johnson C.)
- 10.30-  
11.00 Coffee Break
- 11.00-  
11.30 Multi-sensor database over desert sites for calibration purpose (Briottet X.)
- 11.30-  
12.00 Inter-comparison of Terra and Aqua MODIS (Xiong J.)
- 12.00-  
12.30 Cross-Calibration of the Landsat 7 ETM+ and EO-1 ALI Sensor (Chander G.)
- 12.30-  
13.00 Intercomparison of Surface Albedo Products from Various Spaceborne Sensors (Pinty B.)
- 13.00-  
14.00 Lunch Break
- 14.00-  
14.30 Intercomparison of terrestrial surface remote sensing products from various optical sensors (Gobron N.)
- 14.30-  
15.00 Comparison of the Earth's shortwave radiation measured by CERES and GERB instruments (Szewczyk P.)
- 15.00-  
15.30 A high-quality dataset of land-surface and atmospheric measurements for the comparison/cross-calibration of data. The Valencia Anchor Station (Lopez-Baeza E.)
- 15.30-  
16.00 Coffee Break

- 16.00-16.30 Vicarious calibration of ADEOS-2 GLI and Terra/Aqua MODIS using global data set for multi-sensor ocean-color applications (Murakami H.)
- 16.30-17.00 Intercomparison of atmospheric data using the Basic ENVISAT Atmospheric Toolbox (Niemeijer S.)
- 17.00-17.30 Using MERIS and MODIS for Land Cover Mapping in the Netherlands (Zurita Milla R.)
- 17.30-18.00 Drink

**Thursday, 14 October**

- 09.00-09.30 MERIS data access over diagnostic sites for calibration and validation purposes (Goryl P.)
- 09.30-10.00 Railroad Valley Playa for use in vicarious calibration of large footprint sensors (Thome K.)
- 10.00-10.30 A satellite cross-calibration experiment (Nieke J.)
- 10.30-11.00 Coffee Break
- 11.00-11.30 Inter-comparison of water leaving radiance data from operational ocean color sensors through in situ measurements (Zibordi G.)
- 11.30-12.00 Generating Comprehensive Earth Observation (EO) database for assessing the Canadian landmass response to climate change (Latifovic R.)
- 12.00-12.30 Spectral band difference effects for cross-calibration in the solar-reflective spectral domain (Thome K.)
- 12.30-13.00 Discussion
- 13.00-14.00 Lunch Break
- 14.00-15.30 Round Table
- 15.30-16.00 Coffee Break

## Diffusers trade-off study vs spectral features: measurements and analysis.

Grégory Bazalgette Courrèges-Lacoste<sup>1</sup>, Hedser van Brug, Jos Groote Schaarsberg  
TNO TPD, Optical Instrumentation division, Stieltjesweg 1, 2600 AD Delft (NL).

### Introduction

For the accurate radiometric calibration of earth observation instruments, diffusers are used as “white-references”. In the framework of on-ground calibration campaigns of instruments such as SCIAMACHY, GOME2, OMI (all using on-board diffusers), which took place at TNO TPD, a modulation of the reflectance signal in the spectral domain was discovered. The position and amplitude of the modulation depend on various factors: the diffuser material, the illumination and detection angles, the detection bandwidth, the wavelength, the used area of the diffuser or the way the diffuser is implemented in the optical design of the instrument (e.g. mesh, moving diffuser, ...). This modulation has been called *spectral features*. An overview of the spectral features on SCIAMACHY is given in [1].

### Diffuser trade-off study

In order to improve the measurement accuracy of earth observation instruments, TNO TPD performs in 2004 a diffusers trade-off study for the European Space Agency (ESA ESTEC). The objective of the study is to establish appropriate diffuser technology for on-ground calibration/validation and for on-board calibration systems to be used in future earth observation missions.

*Spectral features* measurement and modelling for a set of 5 diffuser types (see Table 1 below) in the spectral range 250 nm – 1600 nm (extrapolated to 2400 nm thanks to the TNO TPD *spectral features* model), is one of the studied phenomena.

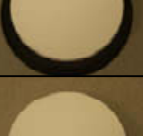
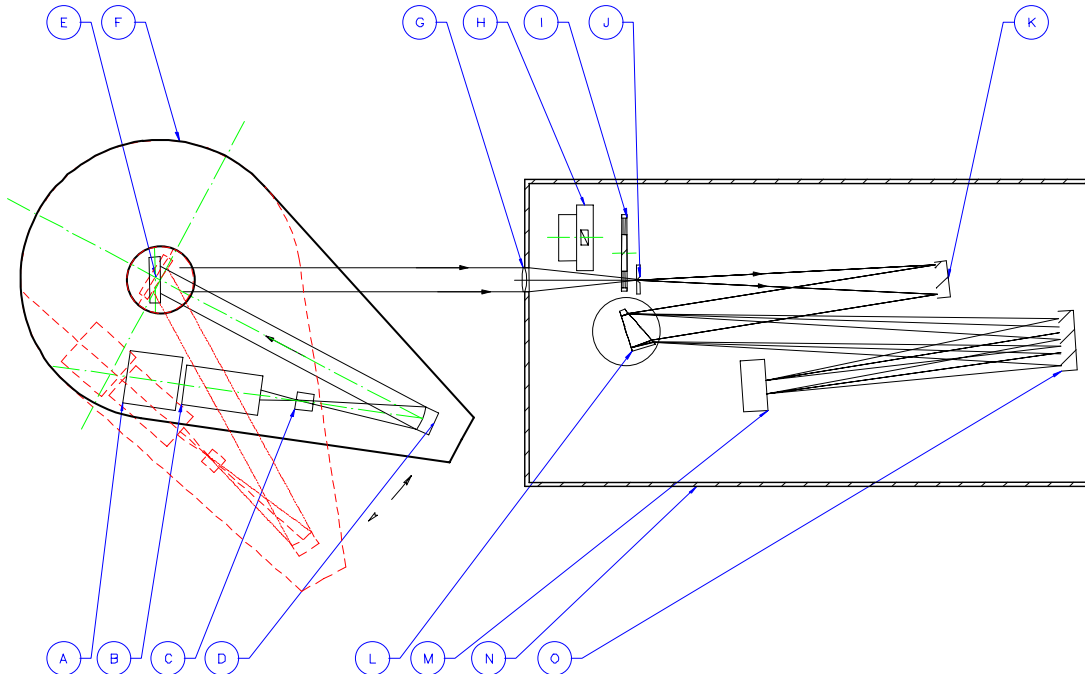
Diffuser type	Proprieties overview		Provider
Aluminium	Material = Aluminium Space qualified = Yes (SCIAMACHY, ...)		TNO TPD
QVD	Material = Quartz Space qualified = Yes (GOME2, OMI, ...)		TNO TPD
Spectralon™	Material = PTFE Space qualified = Yes (MERIS, MISR, ...)		Labsphere
Fluorion-99™	Material = PTFE Space qualified = No		Avian Technology
White tile	Material = depolished white ceramic Space qualified = No		NPL

Table 1 : diffusers of ESA diffuser trade-off study.

<sup>1</sup> G.B.C.L. (corresponding author). Tel. +31 15 269 28 17. Email: bazalgette@tpd.tno.nl.

### **Spectral features dedicated measurement set-up**

To achieve this goal a set-up specifically dedicated to *spectral features* measurements has been built and is used for the first time at TNO TPD. This set-up offers the possibility of measuring *spectral features* correlating their sensitive parameters to minimize their effect. An overview of the set-up is given in Figure 1 below.



**Figure 1 : Optical layout of the dedicated spectral features measurement setup.**

A	Light sources	I	Filter wheel
B	refocusing optics (aspheric mirrors)	J	entrance slit (variable)
C	variable pinhole (with additional polarization module)	K	Collimating mirror (sphere)
D	Collimating mirror	L	Prism and Grating turret
E	Rotational and movable diffuser/target	M	Detector array
F	Rotational illumination device	N	Black box
G	Spectrometer illumination entrance optics (lens/doublet)	O	Imaging mirror
H	Additional polarization device		

In this computer controlled set-up the diffuser and the light sources are placed on two co-axial rotation stages allowing variable illumination and detection angles. A selection of several light sources (e.g. Xenon, QTH, ...) is possible. The spectral range is 240 nm-1000 nm but can be extended to 1600 nm. Polarization measurements are also possible and will be implemented in the framework of the ESA study.

### **Origin of spectral features and spectral features model**

Diffusers are used in space applications to create an homogenous illumination of the entrance slit of the spectrometer. The spectrometer resolves the full white light spectrum into wavelength bands that are very small and hence are linked to large coherence lengths. In the image of the entrance slit, behind the dispersing element, speckle patterns for all the wavelengths can be observed.

*Spectral features* are resulting from the fact that not all speckle patterns are equally bright (the number of speckles in the entrance slit changes with wavelength), and that the observed speckle patterns depend strongly on illumination and observation angles of the diffuser, and on diffuser translations. The *spectral features* theoretical approach developed at TNO TPD is detailed in [2].

From our *spectral features* theory it follows that the amplitude of the *spectral features* increases with decreasing number of speckles per detector element (or entrance slit of the spectrometer). Since the size of the speckles increases linearly with the wavelength, with as a result an inversely proportional decrease in number of speckles, the effect of one speckle more or less will become larger with increasing wavelength. The amplitude of the spectral features is, according to our model, related to the relative change due to one speckle more or less in the entrance slit. Following this model the amplitude is expected to increase linearly with increasing wavelength.

Figure 2 below presents the result of *spectral features* modelling for a surface diffuser (Aluminium type). The *spectral features* can clearly be seen to grow with increasing wavelength. It can also be observed that the period of the structure scales with the wavelength. Preliminary measurements results of the diffuser trade-off study show strong comparison with modelling results.

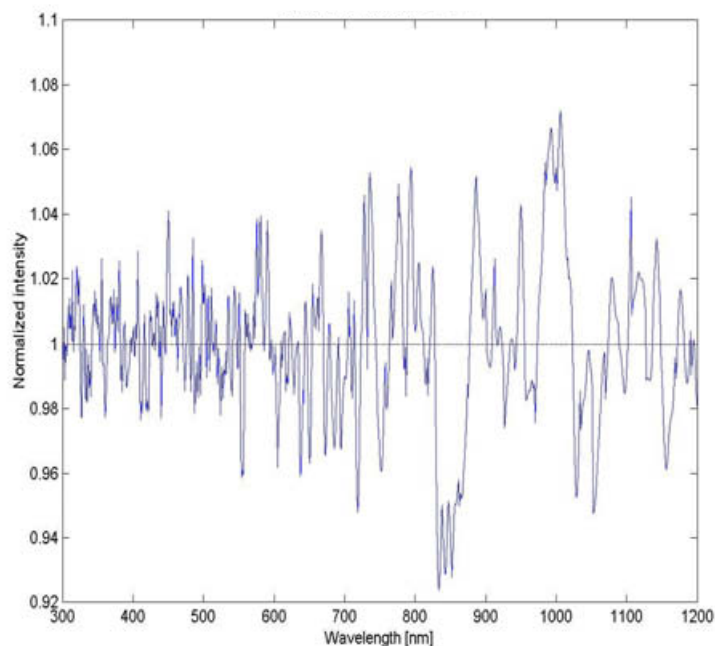


**Figure 2 : Ratio of two calculations performed for a surface diffuser and the optical layout of the TNO TPD spectral features dedicated set-up.**

### **Conclusion**

Internal TNO TPD knowledge reveals that the dependence of the *spectral features* on instrument properties, like focal lengths, spectral resolution, diffuser type, diffuser position, and diffuser angle-of-incidence, can be understood and predicted. Such known dependencies are very useful for the reduction of the *spectral features* in future instruments : if taken into account in the instrument design the *spectral features* can be reduced to acceptable levels (within the measurement noise).

### **References**

- [1] B. Ahlers et al., “*In-orbit detection of spectral features in SCIAMACHY*”, SPIE conference 5570. Maspalomas (2004).
- [2] H. van Brug et al., “*Speckles and their effects in spectrometers due to on-board diffusers*”, SPIE Conference 5542. Denver (2004).

## Abstract Sheet - Abstract number: 1

Author Name: Briottet, Xavier  
Organisation: ONERA  
Country: FRANCE  
Authors: Briottet, Xavier, ONERA, FRANCE (P)  
Briottet, Xavier, ONERA, FRANCE  
Henry, Patrice, CNES, FRANCE  
Miesch, Christophe, ONERA, FRANCE  
Topic: 1 Inter-comparison of satellite optical sensors da

### Multi-sensor database over desert sites for calibration purpose

This paper focuses on the vicarious calibration method based on desert sites. Such sites are now commonly used for multi-temporal and multi-angular calibrations, and for sensors inter-comparison.

To this end, ONERA and CNES had selected twenty desert sites located in the North of Africa and Arabia for their high temporal stability and high spatial uniformity. Since 1996, images of these sites are regularly acquired by a large amount of satellite image sensors like SPOT/high resolution, VGT1 and VGT2, ENVISAT/MERIS and AATSR, AVHRR/NOAA, ERS2/GOME and ATSR, TERRA/MODIS and MISR, ADEOS/POLDER1 and POLDER2. All these information are collected and stored in a database called SADE ("Structure d'Accueil de Données d'Etalonnage") which is presented here.

Today, this database is routinely used for the calibration monitoring of CNES sensors and for the inter-calibration of many international sensors taking into account their geometrical and spectral characteristics. Examples on multi temporal calibration and inter-comparison are given to illustrate the high potential of this database.

To improve the accuracy of the vicarious method over desert sites, the knowledge of the optical properties of the desert sites have to be improved. To this end, an original assimilation method is used to derive the visible/near-infrared spectral reflectance. In a first step, an appropriate ground spectral reflectance model with a small number of parameters is defined. Then an adjustment method using a heterogeneous set of satellite data extracted from the SADE database is used to recover the ground spectral model parameters. The validation stage is conducted by transferring this spectral ground model to the trop of atmosphere and comparing it with one available GOME spectral measurement. The comparison shows a good agreement on the spectral shape and the total bias of less than 3%.

Keywords: Desert Site, Vicarious Calibration, Data base, spectral reflectance

# Calibration refinements in support of MISR

Carol J. Bruegge, David J. Diner

*Jet Propulsion Laboratory, California Institute of Technology, Pasadena, California*

**ABSTRACT:** The Multi-angle Imaging SpectroRadiometer (MISR) is one of five instruments on-board the EOS/ Terra spacecraft, and has collected science data since March 2000. A multi-angle capability is provided by nine cameras, which view up to 70° forward and aft of the spacecraft track and enable unique geophysical retrievals. Throughout its mission, a calibration team has made periodic refinements to the process used to calibrate MISR. These have resulted in improved absolute, and band and camera-relative calibrations, as well as in derived geophysical data products. Data reprocessing is on-going, such that these refinements also improve previous data acquisitions. The calibration process is believed to be mature at this time, with no other changes anticipated. Bi-monthly deployments of the on-board-calibrator continue to monitor instrument response degradations, and provide correction coefficients needed to maintain the accuracy of the radiance products.

## I. OVERVIEW

The Multi-angle Imaging SpectroRadiometer (MISR) (Diner et al., 1998) is one of five instruments on-board NASA's Earth Observing System (EOS). With a 340 km swath width, MISR produces global data sets at nine day intervals or less, depending on latitude. The effective center wavelengths are 447, 558, 672, and 867 nm, as computed using a moments (centroid) analysis within the region delimited by the 1% response points (Bruegge et al., 2002). Each of the nine cameras has a unique name, and is associated with a specific view angle. The cameras view a target consecutively in the order Df (70.5° fore), Cf (60.0°), Bf (45.6°), Af (26.1°), An (nadir), Aa (26.1° aft), Ba (45.6°), Ca (60.0°), and Da (70.5°), with 7 minutes from first to last acquisition of a target. MISR has 14-bit quantization, and therefore has roughly 16,384 gray levels. The finite video offset and square-root encoding reduces this by about 300 counts.

In addition to the nine science cameras, MISR makes use of an on-board-calibrator (OBC). The OBC consists of two Spectralon diffuse panels, and six sets of photodiode detectors. The latter measure solar-reflected light from the panels, and provide a measure of the camera-incident radiance. These are regressed against the camera output, in order to provide the radiometric response for each of the 1504 CCD detector elements per line array, nine cameras, and four spectral bands per camera. One such photodiode set is on a goniometric arm, and allows panel bi-directional reflectance factor (BRF) degradation to be monitored. The OBC has been stable with time. This is attributed to the Spectralon handling and preparations procedures established preflight (Bruegge et al. 1993, Stiegman et al. 1993). A key step was the panel vacuum baking following BRF testing, thus removing volatile contaminants. Additionally, test panels were replaced with flight panels following spacecraft-level testing. These steps proved to be effective, in that Spectralon panels have degraded, on-orbit by only 0.5% (Chrien et al. 2002).

## II. PROCESS UPDATES

MISR requirements for bright targets include 3% absolute, and 1% band- and camera-relative calibrations. MISR radiometric accuracy has previously been documented (Bruegge et al., 2002) for homogeneous desert targets. Here vicarious calibration (VC) experiments, in conjunction with sensor cross-comparison studies and on-board-calibrator (OBC) error assessments, have demonstrated MISR radiometric accuracy for targets which fall mid-range in the sensor's dynamic range - 0.3 to 0.4 in top-of-atmosphere (TOA) reflectance. Vicarious calibration experiments are intensive field campaigns, located at uniform desert sites such as Railroad Valley, Nevada. These are conducted annually for MISR, by the Jet Propulsion Laboratory (JPL) staff (Abdou et al. 2002). Unique tools for this JPL operation include AirMISR (Diner et al. 1998), an ER-2 based aircraft prototype for MISR, as well as the PARABOLA instrument (Bruegge et al. 2000, Abdou et al. 2000), a surface based radiometer which measures upwelling and downwelling radiance in 5° samplings. For these desert VC experiments the surface reflectance term dominates the TOA radiance. Under clear sky and low aerosol conditions, typical for southwestern sites, radiances are measured within an uncertainty of 3%. Vicarious calibrations are used to validate the radiometric scale of some sensors. In the case of MISR, the June 2000 vicarious campaign was used to calibrate the on-board-calibrator, which in turn produces radiometric gain coefficients for the cameras on a bi-monthly basis.

The utilization of the 2000 VC campaign to set the absolute scale for MISR was the first of five process improvements, summarized in Table 1. In 2001 the team began to conduct vicarious calibration experiments both at swath center and swath edge. The results indicated an agreement was within the VC precision for the swath center results, but a few percent higher at the edges. A review of the calibration processing code disclosed an indexing error and resulting inversion of the BRF database used to correct for differences between the photodiode and camera view angles of the panel. This was quickly corrected.

Table 1. MISR calibration process updates. The date the algorithm was first implemented is given in Column 4, and the Level 1B radiance product version which captures this change given in Column 5.

<b>Correction name</b>	<b>Description</b>	<b>Analysis technique</b>	<b>Implementation date</b>	<b>subsequent L1B2 version</b>
VC adjust	On-board calibrator tuned to ground truth	Vicarious Calibration, Lunar Lake 2000	2/24/2001	7
Linear offaxis	Coding error: Indices reversed in Spectralon BRF database	Vicarious Calibration at swath edge	10/24/2001	10
PSF correction	Edge enhancement	Preflight measurements, on-orbit edge analysis	11/12/2002	16
Band adjust	3% decrease in the Red, 1.5% in the NIR.	Vicarious Calibration, 2000-2004 campaigns	12/5/2003	22
Camera adjust	Channel adjustments	Symmetry and lunar studies	11/30/2004	23

In 2002 a correction for instrument point-spread function effects was implemented (Bruegge et al., 2004). Preflight testing had indicated that a point source of light would be smeared across the line array. Cross-pixel attenuation was less than 0.1 for adjacent pixels, decreasing sharply to  $10^{-5}$  within 25 pixels distance. This small light smearing is not sufficient to cause radiometric errors except under extreme conditions (such as over dark ocean targets in the vicinity of bright cloud or ice targets). The implementation of a PSF correction scheme thus improves radiometry for contrast target cases.

A band-relative adjustment has been made to MISR data beginning December 2003. The need for this change was again revealed through vicarious calibration experiments. An analysis of three years of data has shown the radiances from the Red Band to be consistently high. Subsequent to this study the radiances for this band were reduced by 1.5% (Bruegge et al., 2004).

The final response adjustment has come about from a symmetry study where the response of the fore- vs. aft-pointing cameras was compared (Diner et al., 2004). This, and supporting evidence from lunar observations, resulted in camera-to-camera response changes that were typically less than 1%, but as large as 2.5% for one camera. The nadir calibration response has not changed as a result of this study.

These process changes have been validated by cross-comparison studies using MERIS, and MODIS, and by dark water vicarious calibration studies. These studies are made using the MISR nadir camera, in that only AirMISR is capable of viewing at the extreme down-track view angles observed by MISR. These studies have shown MISR radiances to be about 3% higher than MODIS radiance products, due to a difference in the radiometric standard used to calibrate the instrument. MODIS makes use of their on-board calibrator to establish the scale, including knowledge of the diffuse panel reflectance, determined via a solar ratioing radiometer; as stated earlier, MISR relies upon vicarious calibration as its radiometric standard. Agreement among MISR and MERIS radiances are within 2%. Dark water VC studies have confirmed MISR's radiometric response over dark targets (Kahn et al, 2005). The final validation of MISR calibration has come from the science community. Sensitivity studies have shown that a few percent correction in band or camera relative calibration can change the reported aerosol optical depth by 0.02. With the current system it is believed

that MISR aerosol products are typically accurate to  $\pm 0.03$  (Diner et al., 2004). These accuracies rival those obtained from surface sun photometers, such as those used within the AERosol RObotic NETwork (AERONET).

### III. ACKNOWLEDGMENTS

The work described in this paper is being carried out at the Jet Propulsion Laboratory, California Institute of Technology, under contract with the National Aeronautics and Space Administration. MISR data products are processed and made available by the The Atmospheric Sciences Data Center, Langley Research Center.

A number of support individuals have assisted in the acquisition and analysis of MISR calibration data, including Wedad Abdou, Nadine Chrien, Barbara Gaitley, Mark Helmlinger, Ralph Kahn, Mike Smyth, David Nelson, Kyle Miller, Tom Thaller, and Tom Nolan.

### IV. REFERENCES

- Abdou, W., C. Bruegge, M. Helmlinger, J. Conel, S. Pilorz, & B. Gaitley 2002. *Vicarious calibration experiment in support of the Multi-angle Imaging SpectroRadiometer (MISR)*, IEEE Trans. Geosci. Remote Sens., 40(7):1500-1511.
- Abdou, Wedad A., Mark C. Helmlinger, James E. Conel, Stu Pilorz, Carol J. Bruegge, Barbara J. Gaitley, and John V. Martonchik, 2000. *Ground measurements of surface bidirectional reflectance factor (BRF) and hemispherical directional reflectance factor (HDRF) using the portable Apparatus for Rapid Acquisition of Bidirectional observation of the land and atmosphere (PARABOLA III)*, J. Geophys. Res., 106:11,967 - 11,976.
- Bruegge, Carol J., Wedad A. Abdou, David J. Diner, Barbara J. Gaitley, Mark C. Helmlinger, Ralph A. Kahn, and John V. Martonchik (2004). Validating the MISR radiometric scale for the ocean aerosol science communities. Proceedings of the The International Workshop on Radiometric and Geometric Calibration, December 2-5, 2003, Gulfport, Mississippi. A.A. Balkema Publishers, Rotterdam, Netherlands.
- Bruegge, Carol J., Nadine L. Chrien, Robert R. Ando, David J. Diner, Wedad A. Abdou, Mark C. Helmlinger, Stuart H. Pilorz, & Kurtis J. Thome 2002. *Early Validation of the Multi-angle Imaging SpectroRadiometer (MISR) Radiometric Scale*, IEEE Trans. Geosci. Remote Sens., 40(7):1477-1492.
- Bruegge, Carol J., Mark C. Helmlinger, James E. Conel, Barbara J. Gaitley, Wedad A. Abdou, 2000. *PARABOLA III: a sphere-scanning radiometer for field determination of surface anisotropic reflectance functions*, Remote Sensing Reviews, 19:75-94.
- Bruegge, C., A. Stiegman, R. Rainen, A. Springsteen, 1993. *Use of Spectralon as a diffuse reflectance standard for in-flight calibration of earth-orbiting sensors*, Opt. Eng., 32(4):805-814.
- Chrien, N., C. Bruegge, & R. Ando, 2002. *Multi-angle Imaging SpectroRadiometer (MISR) on-board calibrator (OBC) in-flight performance studies*, IEEE Trans. Geosci. Remote Sens., 40(7): 1493-1499.
- Diner D.J., Barge, L.M., Bruegge, C.J., Chrien, T.G., Conel, J.E., Eastwood, M.L.Garcia, J.D., Hernandez, M.A., Kurzweil, C.G., Ledebor, W.C., Pignatano, N.D., Sarture, C.M., Smith, B.G. (1998). The Airborne Multi-angle Imaging SpectroRadiometer (AirMISR): instrument description and first results. IEEE Trans. Geoscience and Remote Sens., 36 (4), 1339 - 1349. Kahn, R., W-H. Li, J. Martonchik, C. Bruegge, D. Diner, B. Gaitley, W. Abdou, O. Dubovik, B. Holben, S. Smirnov, Z. Jin, and D. Clark, 2005. MISR low-light-level calibration, and implications for aerosol retrieval over dark water, J. Atmos. Sci., in press.
- Diner, D., J. Beckert, T. Reilly, C. Bruegge, J. Conel, R. Kahn, J. Martonchik, T. Ackerman, R. Davies, S. Gerstl, H. Gordon, J-P. Muller, R. Myneni, R. Sellers, B. Pinty, & M. Verstraete 1998. *Multi-angle Imaging SpectroRadiometer (MISR) description and experiment overview*, IEEE Trans. Geosci. Rem. Sens., 36:1072-1087.
- Diner, David J., Ralph A. Kahn, Carol J. Bruegge, John V. Martonchik, Wedad A. Abdou, Barbara J. Gaitley, Mark C. Helmlinger, Olga V. Kalashnikova, and Wen-Hao Li, 2004. Refinements to MISR's radiometric calibration and implications for establishing a climate-quality aerosol observing system. SPIE 5652, Passive Optical Remote Sensing of the Atmosphere and Clouds IV, Honolulu, Hawaii, 2004.
- Kahn, R., W-H. Li, J. Martonchik, C. Bruegge, D. Diner, B. Gaitley, W. Abdou, O. Dubovik, B. Holben, S. Smirnov, Z. Jin, and D. Clark, 2005. MISR low-light-level calibration, and implications for aerosol retrieval over dark water, J. Atmos. Sci., in press.
- Stiegman, A.E., C.J. Bruegge, A.W. Springsteen, 1993. *Ultraviolet stability and contamination analysis of Spectralon diffuse reflectance material*, Opt. Eng. 32(4):799-804.

## **Abstract Sheet - Abstract number: 23**

Author Name: Chander, Gyanesh  
Organisation: SAIC/EDC/USGS  
Country: UNITED STATES  
Authors: Chander, Gyanesh, SAIC/EDC/USGS, UNITED STATES (P)  
Markham, Brian, LPSO/GSFC/NASA, UNITED STATES

### **Revised Landsat-5 TM Radiometric Calibration Procedures and Postcalibration Dynamic Ranges**

The Landsat 5 (L5) Thematic Mapper (TM) sensor provides the longest-running continuous data set of moderate spatial-resolution remote sensing imagery, dating back to its launch in March 1984. Effective May 5, 2003, L5 TM data processed and distributed by the U.S. Geological Survey (USGS) Earth Resources observation System (EROS) Data Center (EDC) will be radiometrically calibrated using a new procedure and revised calibration parameters. This change will improve absolute calibration accuracy, consistency over time, and consistency with Landsat-7 (L7) Enhanced Thematic Mapper Plus (ETM+) data. Users will need to use new parameters to convert the calibrated data products to radiance. The new procedure for the reflective bands (1–5,7) is based on a lifetime radiometric calibration curve for the instrument derived from the instrument's internal calibrator, cross-calibration with the ETM+, and vicarious measurements. The thermal band will continue to be calibrated using the internal calibrator.

## **Abstract Sheet - Abstract number: 24**

Author Name: Chander, Gyanesh  
Organisation: SAIC/EDC/USGS  
Country: UNITED STATES  
Authors: Chander, Gyanesh, SAIC/EDC/USGS, UNITED STATES (P)  
Meyer, David, SAIC/EDC/USGS, UNITED STATES  
Helder, Dennis, SDSU, UNITED STATES

### **Cross-Calibration of the Landsat 7 ETM+ and EO-1 ALI Sensor**

As part of the Earth Observer 1 (EO-1) Mission, the Advanced Land Imager (ALI) demonstrates a potential technological direction for Landsat Data Continuity Missions (LDCM). To evaluate the ALI's capabilities in this role, a cross-calibration methodology has been developed using image pairs from the Landsat 7 (L7) Enhanced Thematic Mapper Plus (ETM+) and EO-1 (ALI) to verify the radiometric calibration of the ALI with respect to the well-calibrated L7 ETM+ sensor. Results have been obtained using two different approaches. The first approach involves calibration of near-simultaneous surface observations based on image statistics from areas observed simultaneously by the two sensors. The second approach uses vicarious calibration techniques to compare the predicted Top-of-Atmosphere (TOA) radiance derived from ground reference data collected during the overpass to the measured radiance obtained from the sensor. The results indicate that the relative Sensor Chip Assemblies (SCA) gains agree with the ETM+ Visible and Near Infrared (VNIR) bands to within two percent and the Short Wave Infrared (SWIR) bands to within four percent.

# VALIDATED DATA AND REMOVAL OF BIAS THROUGH TRACEABILITY TO SI UNITS.

N. P. Fox

*National Physical Laboratory, Hampton Rd, Teddington, Middx, TW11 0LW, UK.*

## 1. Introduction

In recent years there has been an increasing demand for improved accuracy and reliability of Earth Observation (EO) data. Stimulated not only by our desire to understand better the workings of our planet and the cause and impact of climate change, but also because improvements in models allow us to discriminate better between data. A further driver is the increasing reliance on the combination of data from different sensors and sources (satellites, aircraft and in-situ) to establish more sophisticated data products. These will be important for “operational services” of the future, as envisaged in initiatives such as GMES (Global Monitoring of Environment and Security) of the EU and ESA. This combination of data from different sources can only be carried out if each data set has a clear, reliable statement of uncertainty.

When only relative spatial maps are required, it is only radiometric resolution (Signal to Noise) and uniformity of response of the sensor that are critical. In these applications absolute accuracy is of lower importance. However, as soon as temporal information is required, combination of data from more than one source (satellite or ground) or where the data may form a baseline for a future long-term study (as in most climate change research), accuracy and a clear knowledge of its associated uncertainty, is essential. This in turn requires “traceability” of measurement to an internationally agreed system of units (SI). The term traceability in this context has a clear definition<sup>1</sup>, requiring a full analysis and description of uncertainties and an unbroken chain of calibrations back to an internationally recognised primary standard, usually maintained by a national metrology institute (NMI) such as NPL or NIST. This requirement has been formally recognised by CEOS with the adoption at its 14<sup>th</sup> plenary in November 2000 ([www.ceos.org](http://www.ceos.org)) of the following resolutions:

*1/ All EO measurement systems should be verified traceable to SI units for all appropriate measurands.*

*2/ Pre-launch calibration should be performed using equipment and techniques that can be demonstrably traceable to and consistent with the SI system of units, and traceability should be maintained throughout the lifetime of the mission.*

## 2. Radiometric traceability for EO data products

Although the above resolutions are an important step, “traceability” will only become a reality when the EO community have a clear understanding of the benefit i.e. “*to improve the likelihood of data products derived from a remote sensing instrument being a quantitative description of the bio/geo-physical parameter that it is seeking to measure and that such measurements are invariant with time and are robust enough for regulatory, policy or commercial decisions*”.

There are a variety of methods used in the pre-flight calibration of EO sensors but the most common for optical imagers usually involves the filling of the entrance aperture of the instrument with a source of known radiance. The traceability of this radiance source should in principle be linked back to an NMI such as NPL or NIST. Figure 1 (Left hand panel) illustrates the traceability chain for establishing the primary scales of NPL. A similar schematic exists for most of the worlds NMIs. The primary standard is an absolute detector called a cryogenic radiometer which compares the heating effect of optical radiation with that of electrical power. The operation at cryogenic temperatures improves the accuracy and sensitivity<sup>2</sup>. A more detailed description of the techniques and procedures (of relevance to the EO community) can be found elsewhere<sup>3</sup> and references therein.

It should of course be noted from fig 1 (right hand panel) that the most critical issue facing the EO community is most probably not the pre-flight calibration, but that of establishing and maintaining traceability “in-orbit”. This is particularly so for satellite sensors operating in the visible and near-infrared where there are many examples of pre-launch calibration coefficients needing revision due to changes in the sensor following storage and the launch into orbit. Frequently

revisions need to be made through the life of the mission due to degradation of the instrument in the hostile space environment.

Figure 2 (taken from Los<sup>4</sup>) shows measurements of NDVI (Normalised Difference Vegetation Index) of a nominally stable desert site (results should be linear with time as there is little by the NOAA AVHRR series of instruments). It demonstrates the difficulty in ensuring both long-term stability in-flight and consistency between instruments, even when they are of the same design. In this example, when there is no on-board calibration systems, the results can only be used through the use of a vicarious ground calibration to apply correction factors to normalise results to a common baseline.

How such calibration updates should best be determined is a fairly hot debate between the advocates of on-board calibrators and those of vicarious techniques. Within each category there are a further range of options, e.g. an “on-board” calibration system, can itself be a ground calibrated reference such as a black body for thermal infrared, or a hybrid system where for example the reflectance of a diffuser is determined on the ground and an a-priori measurement of a reference source is used to provide the link to radiance e.g. exo-atmospheric solar irradiance.

In competition, or perhaps more appropriately, complementarily, are vicarious techniques, such as views of the Moon or Earth deserts. Whilst these in principle offer the opportunity to fully fill the aperture of the satellite sensor with spatially uniform spectral radiance and, in the case of Earth deserts, can be directly measured, they still require a knowledge of atmospheric conditions and their absolute uncertainty to SI, is no better than that claimed for the on-board techniques.

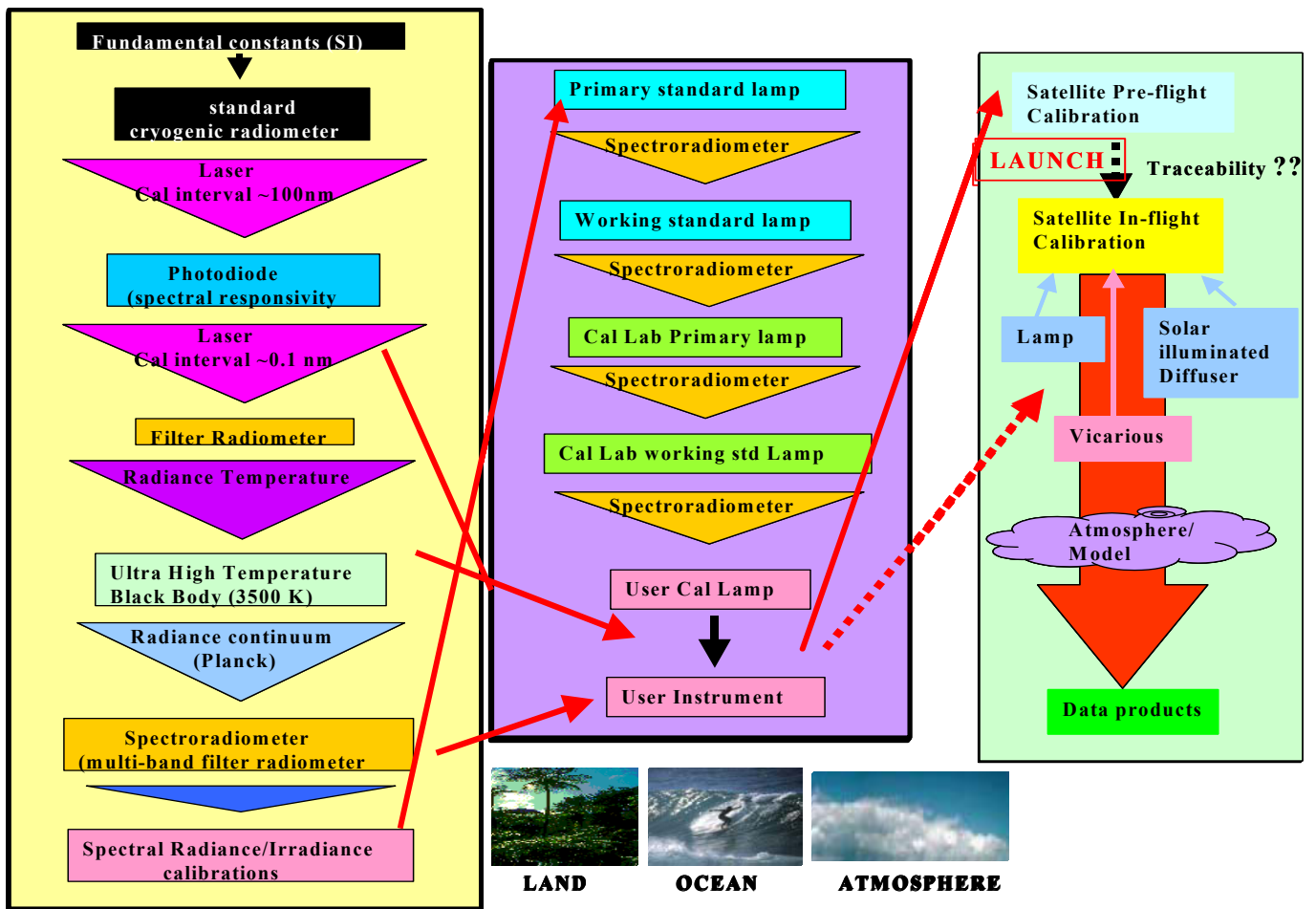


Figure 1. Schematic representation of the route of traceability for the EO community. The left and middle panels describe the typical procedure from the primary standard to the user. The right hand panel illustrates the difficulty in obtaining traceability for a satellite instrument post-launch. The solid red lines show good traceability routes, the dashed a best efforts.

In most cases there is little to choose between the techniques on offer, all are pretty good at monitoring change, but when determining radiometric accuracy in terms of SI units, all are relatively poor, with accuracies ranging from 3 to 10 %. If such uncertainties are to be improved, then the following issues need to be addressed.

- What is the attainable accuracy of radiation measurements in the visible and near infrared with on board calibrators?
- What is attainable through vicarious techniques?
- Are the results from on-board and vicarious techniques in agreement?
- What is the accuracy for the end user?

### 3. Options for the future

One option for the future to significantly improve accuracy and traceability of EO data, would be the implementation of a dedicated calibration mission such as proposed in TRUTHS (Traceable Radiometry Underpinning Terrestrial- and Helio- Studies)<sup>5,6</sup>. This proposal is for a mission to establish a set of calibration reference targets, Earth deserts, Sun and Moon to transfer calibrations of radiance or irradiance to other in-flight sensors. This is broadly similar to current best practice for vicarious calibrations. However, in TRUTHS, the calibration coefficients of these targets would be regularly updated through observation and calibration by instruments onboard a small satellite. TRUTHS instruments would be calibrated using a novel on-board procedure which mimics that performed on the ground by NMIs when establishing primary scales, see figure 1, left hand panel. This procedure includes the flight of a primary standard and so traceability to SI can be fully and regularly established in-flight, with very high radiometric accuracy (<0.5% for spectral radiance) avoiding any problems due to drift either pre- or post- launch. A more detailed description can be found in Fox et al<sup>5,6</sup>.

Whilst TRUTHS offers the complete solution, the principles and techniques it proposes can be used independently. For example, the in-flight calibration system can be incorporated onto any earth viewing imager, to improve its in-flight

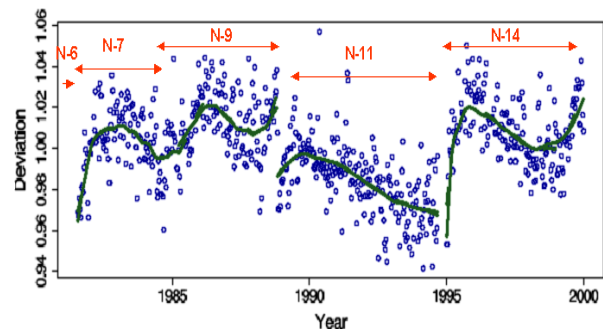


Figure 2. Plot showing change in NDVI of a nominally stable desert site as measured by AVHRR on the NOAA series of satellites (N6, N7, N9, N11 and N14).

calibration. Of course the establishment and regular recalibration of reference targets will only occupy a small amount of the observing capacity of any mission and thus the bulk of this can be used for direct scientific activities.

Similarly, it is perhaps timely to consider the establishment of a global network of a small number of calibration test sites to acquire benchmark data sets for example GIANTS (Global Instrumented And Networked Test Sites) as proposed by Teillet et al<sup>7</sup>. The use of “standard” ground reference calibration test sites as a means of cross-calibration and validation of satellite sensors is well established. In many cases, dedicated campaigns have been organized using teams supported by the respective instrument. In some cases, particularly atmospheric chemistry applications, use has been made of existing ground networks of validation equipment, much of which is automated. In the case of land imagers, some test sites have become recognized “standards”, e.g., White Sands alkali flats and Railroad Valley Playa in the Central USA, La Crau in Southern France and of course the SADE data base of CNES. These and other sites have been well characterized and shown to be relatively homogeneous spatially and temporally stable (at least in the short-term). However, significant differences have been observed by different sensor teams when using the same target area for vicarious calibration activities. This is caused by biases originating from subtle differences in the methodologies used, instrumentation and calibration traceability. Such biases can also occur for networked sites, although these can be reduced by the use of common instrumentation and standard methodologies. Each site requires a common set of automated instrumentation, including Sun photometers; standard meteorological parameters; video images of the site in real time; down-welling solar irradiance; and surface spectral reflectance/radiance. All instruments should be automated and transmit data

independently. Continuous year round availability of a single calibration site is difficult to achieve and highly susceptible to local weather conditions, for an extreme example, snow. However, having a global network of essentially interoperable test sites overcomes this limitation.

In the context of the TRUTHS mission, data from the ground will correlate with absolute information from TRUTHS satellite such that other satellite sensors need only be stable in the short term. This is easier to achieve than absolute calibration. However, in the near term in the absence of such a satellite, calibration updates would need to be carried out by ground support teams or aircraft overpass.

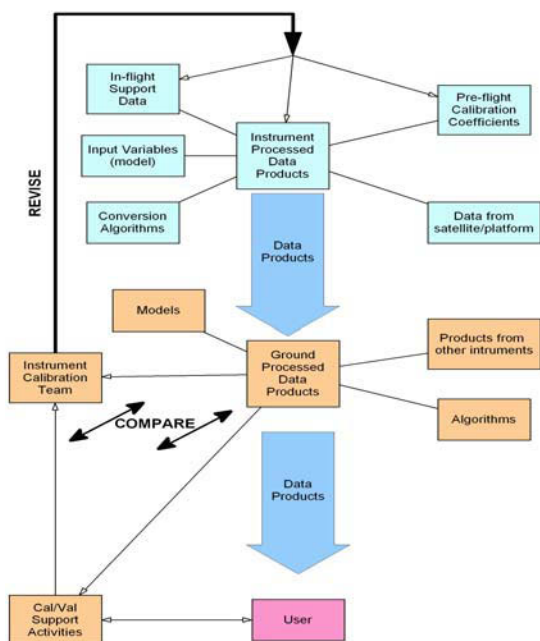


Figure 3. Schematic representation of the production process for a data product from a typical satellite sensor.

#### 4. Summary

This short paper has highlighted some of the issues and potential solutions to improve the traceability and accuracy of the satellite sensor radiometric characteristics. However, it should be noted that to ensure that the final EO data product is of adequate quality to meet the needs of the user community requires all aspects of the data production process to be reliable and “quality assured”. Figure 3 illustrates the complexity together with the critical interactions and processes that must also be fully traceable with clear statements of uncertainty in order to fully meet the needs of the users and to ensure that the “operational services” envisaged by GMES are reliable, efficient and economically self-sustaining into the future.

This goal requires the establishment of an infrastructure that encourages calibration, intercomparisons, and above all the

publication of clear, fully documented routes of traceability. These routes must contain statements and breakdown of uncertainties for all steps in the derivation of an EO data product, pre-flight, post-launch, and all algorithms and models used.

#### 5. References

1. ISO International vocabulary of basic and general terms in metrology (1993)
2. Fox N.P. Radiometry with cryogenic radiometers and semiconductor photodiodes, *Metrologia* 32: 535-534 (1996)
3. Fox N.P. Validated Data and Removal of Bias through Traceability to SI Units” ISPRS book series **vol 2** Post-Launch Calibration of Satellite Sensors p31-42 (2004)
4. Los, S.O., Estimation of the ratio of sensor degradation between NOAA-AVHRR channels 1 and 2 from monthly NDVI composites. *IEEE Transactions on Geoscience and Remote Sensing*, 36: 206-213 (1998).
5. Fox, N.P, Aiken, J, Barnett, J.J., Briottet, X., Carvell R., Frohlich C., Groom. S. B., Hagolle, O., Haigh J. D, Kieffer, H. H., Lean, J., Pollock, D. B., Quinn T., Sandford M.C.W., Schaepman M., Shine K. P., Schmutz W. K. Teillet P. M., Thome K. J., Verstraete M. M., Zalewski E., Traceable Radiometry Underpinning Terrestrial- and Helio- Studies (TRUTHS), *Proc. SPIE* 4881: 395-406, (2003)
6. Fox, N.P, Aiken, J, Barnett, J.J., Briottet, X., Carvell R., Frohlich C., Groom. S. B., Hagolle, O., Haigh J. D, Kieffer, H. H., Lean, J., Pollock, D. B., Quinn T., Sandford M.C.W., Schaepman M., Shine K. P., Schmutz W. K. Teillet P. M., Thome K. J., Verstraete M. M., Zalewski E., Traceable Radiometry Underpinning Terrestrial- and Helio- Studies (TRUTHS), *Adv. Space Res*, 32: 2253-2261. (2003)
7. Teillet, P.M., K.J. Thome, N. Fox and J.T. Morisette, Earth observation sensor calibration using a global instrumented and automated network of test sites (GIANTS), *Proceedings of SPIE*, 4550: 246-254 (2001).

## **Abstract Sheet - Abstract number: 21**

Author Name: Gobron, Nadine  
Organisation: EC-JRC  
Country: ITALY  
Authors: Gobron, Nadine, EC-JRC, ITALY (P)  
Pinty, Bernard, EC-JRC, ITALY  
Aussdat, Ophlie, EC-JRC, ITALY  
Taberner, Malcolm, EC-JRC, ITALY  
Mlin, Frederic, EC-JRC, ITALY  
Verstraete, Michel, EC-JRC, ITALY  
Topic: 1 Inter-comparison of satellite optical sensors da

### **Intercomparison of Terrestrial Surface Remote Sensing Products from Various Optical Sensors**

The biophysical activities on land surfaces are documented from spectral measurements made in space. Advances in the understanding of radiation transfer and availability of higher performance instruments have led to the development of a new generation of geophysical products able to provide reliable, accurate information on the state and evolution of terrestrial environments. Specifically, a series of optimized algorithms have been developed to estimate the Fraction of Absorbed Photosynthetically Active Radiation (FAPAR) for various instruments. Such an approach allows the synergistic use of FAPAR products derived from different sensors and the construction of global FAPAR time series independent from the life time of these specific sensors. An inter-comparison procedure will be presented and results from the exercise conducted with SeaWiFS, MERIS (ENVISAT), and MODIS (Terra) products will be shown.

# OPERATION VICARIOUS CALIBRATION OF SOLAR CHANNELS OF THE EUROPEAN METEOROLOGICAL GEOSTATIONARY SATELLITES AND ITS IMPACT ON GEOPHYSICAL PRODUCT EXTRACTION

Y.M. Govaerts\*

(<sup>1</sup>) EUMETSAT, Postfach 10 05 55, D-64295 Darmstadt, Germany Fax: +49 (0)6151 807-838

## Abstract

This paper presents the solar channel calibration of the Meteosat first and second generations and its impact on the derivation of geophysical products.

## 1 Introduction

EUMETSAT is currently operating simultaneously three Meteosat First Generation (MFG) spacecrafts and Meteosat Second Generation (MSG). SEVIRI, the main radiometer on-board MSG, measures the reflected solar radiation within three spectral bands centered at 0.6, 0.8 and 1.6  $\mu\text{m}$ , and within a broad band similar to the VIS channel of MVIRI, the radiometer on-board the MFG satellites. As no in-flight calibration device is available for the solar channels of all these instruments, an operational vicarious method, based on simulated radiances over bright desert targets, has been developed at EUMETSAT. This method should ensure the calibration during the entire duration of the MSG mission, i.e., more than 12 years as well as of the entire archived MFG data back to 1981. The duration of each Meteosat spacecrafts is given in Section (2).

The present study fulfils two objectives. First, the uncertainties associated with the characterisation of the “calibration reference”, i.e., the modelled radiances, are evaluated. The proposed method relies on the comparison between simulations and calibrated observations acquired by spaceborne instruments. To this end, Envisat/MERIS, Envisat/AATSR, ERS2/ATSR-2, SeaStar/SeaWiFS and VEGETATION data have been collected over the calibration targets. These data have next been simulated accounting for the actual observation conditions of each instrument (see Section 3). The vicarious calibration method derives an absolute calibration coefficient for each processed channel and monitors the degradation of the sensor. Results are presented in Section (4). The impact of this calibration on the derivation of geophysical parameters is evaluated next on surface albedo has been derived from Meteosat-7, -5 and GMS-5 spacecrafts (Section 5).

\*paper presented at the CEOS-IVOS Workshop on the Intercomparison of Large Scale Optical Sensors at ESTEC from the 12th to the 14th of October

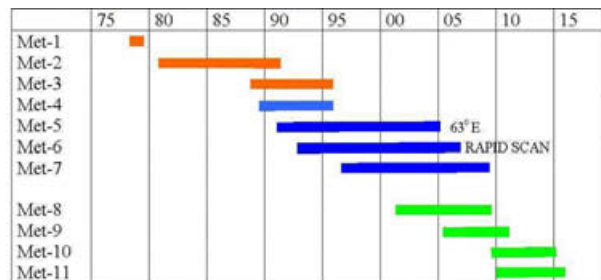


Figure 1: Past, current and future Meteosat spacecrafts in-flight duration.

## 2 The Meteosat solar channel data

The Meteosat archive is essentially composed of image data acquired in three bands: visible (VIS) 0.4–1.1  $\mu\text{m}$ , water vapour (WV) 5.7–7.1  $\mu\text{m}$  and infrared (IR) 10.5–12.5  $\mu\text{m}$ . This data set originates from seven different spacecrafts as can be seen in Figure (1), divided into three different periods: pre-operational (Meteosat-1 to -3), operational (Meteosat-4 to -6) and a transition phase to MSG (Meteosat-7). The MFG data run from 1981 and are expected to end in 2005 for the 0° mission. This mission is currently being replaced by the MSG mission which operational phase started in early 2004 with Meteosat-8 and will last at least until 2012. SEVIRI is the main radiometer on-board the MSG spacecraft. It scans the Earth disc every 15 minutes within 11 spectral channels located between 0.6  $\mu\text{m}$  and 14  $\mu\text{m}$  and a high resolution broadband visible channel (HRV) (Schmetz et al. 2002).

## 3 Meteosat calibration reference

Stable desert targets (Cosnefroy et al. 1996) have been selected in order to secure a consistent calibration reference during the entire duration of the MFG and MSG missions. The accuracy and precision of the simulations over these targets have been evaluated comparing simulations with calibrated observations acquired by spaceborne instruments (Govaerts and Clerici 2004). To this end, ERS2/ATSR-2, SeaStar/SeaWiFS, VEGETATION and Envisat/MERIS and AATSR data have been collected over the desert targets sim-

BAND		MERIS	ATSR-2 AATSR	SeaWiFS	VGT
BLUE	0.4	442	–	443	B0
GREEN	0.5	560	550	555	–
RED	0.6	665	660	670	B2
NIR	0.8	865	870	865	B3
SWIR	1.6	–	–	–	MIR

Table 1: Selected spectral bands for each instrument.

ulated accounting for the actual observation conditions and spectral response of each instrument (Table 1). This analysis reveals (not show here) that the monthly mean relative bias between observations and simulations averaged over all targets remains low, but exhibits a small seasonal trend. These results indicates that the reference can be used for the calibration of the MVIRI and SEVIRI solar channels with an expected accuracy of  $\pm 5\%$  (Table 2).

	MERIS	ATSR2	SeaWiFS	VGT
Blue	+5.2%	–	-0.6%	+2.3%
Green	+3.7%	+0.2%	-0.7%	–
Red	+4.4%	+3.3%	-1.1%	+5.2%
NIR	+5.5%	+3.0%	-1.8%	+3.6%
SWIR				

Table 2: Average bias in percent with respect to the Meteosat calibration reference. Positive values indicate greater observation values with respect to simulation.

## 4 Operational calibration method

The estimation of the calibration coefficients is affected by calibration reference uncertainties and the instrument characteristic errors. It is therefore necessary to estimate the corresponding impact on the calibration coefficient accuracy and, if possible, to minimize this error. The proposed calibration algorithm is thus designed to minimize the error propagation while deriving a calibration coefficient and to verify the consistency of this estimation. A complete description of the method can be found in Govaerts et al. (2004).

MET-8/SEVIRI solar channels have been regularly calibrated since February 2003. These calibration hasn't revealed sensor drift larger than 1% per year. The value of these coefficients can be found in the SEVIRI image file header. Estimated calibration error is within 5% for each solar channels. Results for the calibrations of MFG are available summarized on Table (4).

## 5 Impact on geophysical product extraction

Since July 1998, EUMETSAT is operating simultaneously two geostationary Meteosat spacecrafts, located respec-

M	L. date	$C_f(t_0)$	$\delta C_f(t_0)$	$D_f(t)$	$\delta D_f(t)$	$\widetilde{E}_0$
4	03/06/89	0.733	0.0299	5.2389	2.8305	599.5
5	03/02/91	0.818	0.0733	2.8221	2.3042	690.6
6		N/A	N/A	N/A	N/A	N/A
7	09/02/97	0.915	0.0223	5.7453	1.7249	690.8

Table 3: Calibration results for the VIS band onboard MFG spacecrafts. **Launch date** is the derived calibration coefficient at launch time in  $\text{Wm}^{-2}\text{sr}^{-1}/\text{DC}$ ,  $\delta C_f(t_0)$  is the corresponding error in  $\text{Wm}^{-2}\text{sr}^{-1}/\text{DC}$ .  $D_f(t)$  is the daily degradation rate in  $\text{Wm}^{-2}\text{sr}^{-1}/\text{DC day}^{-1}10^{-5}$  and  $\delta D_f(t)$  is the corresponding error in the same unit.  $\widetilde{E}_0$  is the exo-atmospheric solar irradiance the VIS band in  $\text{Wm}^{-2}$ .

tively at  $0^\circ$  longitude (Meteosat-7) and  $63^\circ$  East (Meteosat-5). The two spacecrafts observed a large common area over which any geophysical products derived from both spacecrafts should be similar if there respective calibration is consistent and the retrieval algorithms correct.

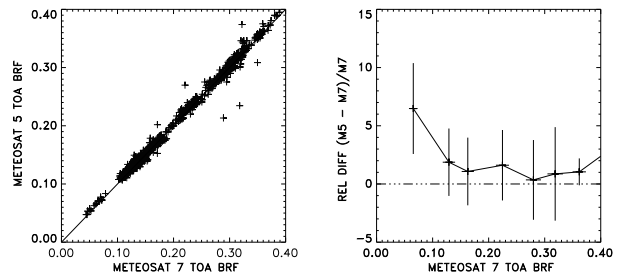


Figure 2: **LEFT:** Scatter plot of cloud free TOA BRFs observed by Meteosat -7 and -5 along the  $31.5^\circ\text{E}$  latitudinal transect, *i.e.*, with identical viewing zenith angles and differences in sun zenith angles not exceeding  $\pm 2^\circ$ . **RIGHT:** Relative difference in percent between the Meteosat-5 and -7 TOA BRF as a function of the Meteosat-7 TOA BRF.

Let us first address the issue of TOA BRF comparison. The characteristics of the Meteosat-5 and -7 radiometer VIS band should be, in principle, similar, as their radiometers have been produced in the same batch and according to identical specifications. Both instruments are routinely calibrated with the same vicarious method that relies on simulated radiance over bright desert targets (Govaerts et al. 2004). The inter-calibration consistency between the two instruments needs also to be addressed as uncertainties in the characterization of the VIS band have already been reported (Govaerts 1999). To this end, Top-of-Atmosphere (TOA) BRFs derived for both instruments have been collected under identical viewing zenith angles for differences in sun zenith angles not exceeding  $\pm 2^\circ$ . There is a good agreement between both instruments as can be seen in Fig. (2), except over dark sea surface. Over terrestrial surfaces, observations are consistent, Meteosat-5 reflectances overestimating only by about 1–2% those observed by Meteosat-7.

Surface albedo is derived from both spacecrafts with the algorithm proposed by Pinty et al. (2000a). This product

is generated at the Meteosat full spatial resolution which corresponds to a North-South and East-West sampling distance of about 2.5 km at the sub-satellite point (Pinty et al. 2000b). On the average, surface albedo values retrieved from Meteosat-7 observations exceed by about 0.015, or 6% in terms of relative difference, those retrieved from Meteosat-5 (Govaerts et al. 2004) (Fig. 3). Problems related to the accuracy of the instrument characterization are not excluded at this stage to explain the mean difference (Govaerts 1999), which is within the calibration error reported in Govaerts et al. (2004). Nonetheless, observed albedo differences remain small and below typical accuracy required by climate studies. The surface albedo algorithm has also been applied to the Japanese geostationary satellite GMS-5 for the same period. In this case the density plot between Meteosat-5 and GMS-5 shows an important bias between both data set as a result of a poor calibration of this latter instrument (Fig. 4).

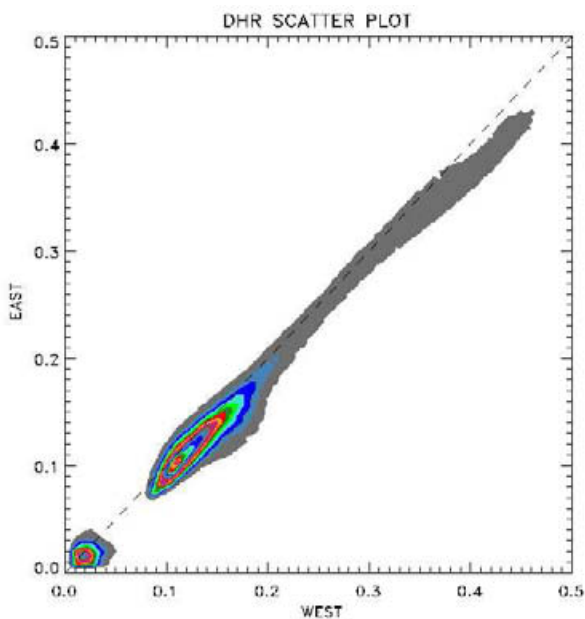


Figure 3: Density plot between the surface albedo retrieved from Meteosat-7 (WEST) and Meteosat-5 (EAST) in May 2001.

## 6 Conclusions and recommendations

This paper describes the calibration reference that is used for the operational vicarious calibration of the MVIRI and SEVIRI solar channels. This reference consists of simulated TOA radiances, using a data set of surface and atmospheric properties. A comparison between calibrated spaceborne data and simulations reveals that the relative bias between simulations and calibrated observations do not exceed 6% when a large number of observations are averaged over all targets. The systematic calibration of the Meteosat solar channels permits the derivation of consistent geophysical variables. In particular, the calibration of Meteosat-5 and -7 allows the retrieval of a consistent surface albedo.

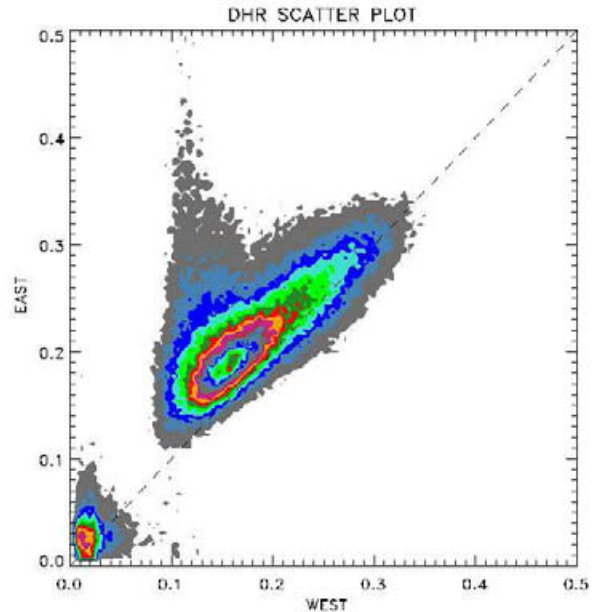


Figure 4: Density plot between the surface retrieved from Meteosat-5 (WEST) and GMS-5 (EAST) in May 2001.

## REFERENCES

- Cosnefroy, H., M. Leroy, and X. Briottet (1996). Selection and characterization of Saharan and Arabian desert sites for the calibration of optical satellite sensors. *Remote Sens. Environ.* 58, 101–114.
- Govaerts, Y., A. Lattanzio, B. Pinty, and J. Schmetz (2004). Consistent surface albedo retrieval from two adjacent geostationary satellites. *Geo. Res. Letters* 31, doi:10.1029/2004GL020418.
- Govaerts, Y. M. (1999). Correction of the Meteosat-5 and -6 VIS band relative spectral response with Meteosat-7 characteristics. *Int. J. Remote Sens.* 20, 3677–3682.
- Govaerts, Y. M. and M. Clerici (2004). Evaluation of radiative transfer simulations over bright desert calibration sites. *IEEE Trans. Geosci. Remote Sens.* 42, 176–187.
- Govaerts, Y. M., M. Clerici, and N. Clerbaux (2004). Operational Calibration of the Meteosat Radiometer VIS Band. *IEEE Trans. Geosci. Remote Sens.* 42, 1900–1914.
- Pinty, B., F. Roveda, M. M. Verstraete, N. Gobron, Y. Govaerts, J. V. Martonchik, D. J. Diner, and R. A. Kahn (2000a). Surface albedo retrieval from Meteosat: Part 1: Theory. *J. Geophys. Res.* 105, 18099–18112.
- Pinty, B., F. Roveda, M. M. Verstraete, N. Gobron, Y. Govaerts, J. V. Martonchik, D. J. Diner, and R. A. Kahn (2000b). Surface albedo retrieval from Meteosat: Part 2: Applications. *J. Geophys. Res.* 105, 18113–18134.
- Schmetz, J., P. Pili, S. Tjemkes, D. Just, J. Kerkmann, S. Rota, and A. Ratier (2002). An introduction to Meteosat Second Generation. *BAMS* 83, 977–992.

# THE ESTABLISHMENT AND VERIFICATION OF TRACEABILITY FOR REMOTE SENSING RADIOMETRY, WITH AN EYE TOWARDS INTERCOMPARISON OF RESULTS

**B. Carol Johnson,<sup>1</sup> Joseph P. Rice, and Steven W. Brown**

*Optical Technology Division  
National Institute of Standards and Technology  
Gaithersburg, MD 20899 USA*

## Traceability and the Measurement Problem

The study of global climate change is a critical, long-term application of remote-sensing radiometry. Values for physical quantities are derived from radiometric observations, typically using models and ancillary data. One consequence of these complicated relationships is that values for radiometric uncertainties are often not stated, even though the results depend on the accuracy of the radiometric measurements. Recent workshops attempt to reconcile this issue [1, 2]. The conclusion is that in many cases the current observing systems do not meet the accuracy and stability requirements necessary for climate-change research [1].

One necessary condition to solve this problem is to require that the results of the measurements from orbit be traceable<sup>2</sup> to stated references, usually national or international standards. Noteworthy advantages of maintaining traceability include a common reference base and quantitative measures of assessing the agreement of results for different sensors or measurements at different times. Evaluation and documentation of uncertainty in the results is an integral part of establishing traceability. The determination of exo-atmospheric total solar irradiance is one example of the significance of rigorous adherence to establishing traceability. Continuous measurements from space, with the derived irradiance values traceable to reference standards, began in 1978. The results from different missions disagree by amounts greater than the observed instrument precision, see Ref. [4]. It is difficult to interpret these results because, in the typical presentation of the various results, the results are presented without uncertainties. Without stated uncertainties, it is impossible to assess the level of agreement.

The National Institute of Standards and Technology (NIST) and other national metrology laboratories and standards organizations have established policies and documentation for terms such as “NIST traceable” [5]. These considerations are worth reviewing in light of radiometric measurements from space and in relationship to efforts between the Optical Technology Division (OTD) and other U.S. agencies. For example, there is nothing in the definition of traceability regarding temporal overlap or interval length for the

---

<sup>1</sup> Contact information: NIST, MS 8441, Gaithersburg, MD 20899-8441, +1 301 975-2322 (tel), +1 301 869-5700 (fax), [cjohnson@nist.gov](mailto:cjohnson@nist.gov).

<sup>2</sup> Traceability – property of the result of a measurement or the value of a standard whereby it can be related to stated references, usually national or international standards, through an unbroken chain of comparisons all having stated uncertainties [3].

measurements in the unbroken chain of comparisons. Pre-flight measurements by the sensor of an external laboratory standard source and an internal “on-board” source, followed by post-launch, on-orbit measurements of the internal source and an Earth target, give results that are traceable to the radiometric values of the initial laboratory standard source. Of course, the uncertainties in each step, which may include effects that are difficult to quantify (e.g., the stability of the on-board source or the effects of storage, shipment, and launch) must be described in complete detail. A second point is that the measurements in the chain of comparisons are not always of the same quantity, thus requiring quantifiable physical models. Examples include: 1) blackbody standards whose radiometric properties are traceable to contact measurements of the cavity temperature; and 2) detector standards based on cavity absorbers, which compare the optical power absorbed to the electrical power required to achieve the same heating. Clearly, knowledge of factors such as aperture area, diffraction effects, and cavity emittance (source standards) or cavity non-equivalence (detector standards) is required for describing these traceability chains. A third point is that the results of measurements or values of standards do not have to represent quantities that are part of the International System of Units (SI) to be “NIST traceable.” In the assignment of values of transmittance, reflectance, or absorptance to filters, windows, mirrors, or other optical components, the underlying measurements of radiance flux can be absolute or relative, since ratios determine the final values. In these situations, artifacts are critical and comparisons are more difficult to design and implement.

#### Assessment of Claims of Traceability

In remote sensing radiometry, reference standards (detectors, sources, reflectance targets, and temperature sensors) are used by the responsible institution to assign pre-flight calibration coefficients to the satellite sensors. NIST policy on traceability states that it is the responsibility of the instrument vendor to support their claim of traceability,<sup>3</sup> and it is the responsibility of the end user to assess the validity of this claim. The end users, e.g. programs at the National Aeronautics and Space Administration (NASA), the National Oceanic and Atmospheric Administration (NOAA), the Department of Defense (DOD), or other U.S. agencies have collaborated with the NIST OTD in the assessment step; as a result we have developed and deployed portable, calibrated radiometers and sources and organized comparisons of artifacts. The chain of comparisons for establishing traceability for these NIST instruments or artifacts is as short as possible, the characterization is extensive, and there are elements of redundancy. As a result, the uncertainties are adequate to assess and validate the uncertainties of the vendor’s assignments of radiometric quantities to the ground support equipment used to calibrate the satellite sensors.

In the reflected solar region (~250 nm to ~2.5  $\mu\text{m}$ ), the vendor typically establishes traceability using lamp standards of spectral irradiance that are combined with standards of spectral reflectance for realizing spectral radiance values. NIST-developed filter radiometers, spectroradiometers, and integrating sphere sources have been used numerous times, primarily in support of NASA’s Earth Observing System (EOS)

---

<sup>3</sup> See Ref. [5] for description of the elements required to support claims of traceability.

Program. In some cases, these efforts resolved outstanding discrepancies [6]. In the emitted thermal spectral region ( $\sim > 2.5 \mu\text{m}$ ), the vendor typically establishes traceability using calibrated temperature sensors in custom blackbody sources. A two-channel filter radiometer that operates in a vacuum chamber or ambient conditions has successfully validated a number of vendor blackbodies, including ones used for sea-surface temperature [7]. Values of bi-directional reflectance distribution function (BRDF) for reflectance standards have been validated by round-robin comparisons [8], and a comparison of aperture-area determinations relevant for total solar irradiance studies is underway [9]. Spectral transmittance values were determined for witness filters in the High Resolution Infrared Radiation Sounder (HIRS) NOAA program by NIST over a range of filter temperatures and compared to the vendor results; in some cases there were significant discrepancies [10]. For more information on other examples of assessing claims of traceability, see Ref. [2], pages 7 to 16, and the review article [11].

### Instrument Characterization

An objective of this October 2004 Infrared and Visible Optical Sensors Subgroup workshop on calibration was to discuss the protocols for comparisons of Level 2 and 3 products<sup>4</sup> for different sensors. The significance of sensor characterization for deriving accurate products is often not recognized. Thorough characterization is as important as establishing traceability, because measurements from orbit of Earth scenes are not well represented by the pre-flight reference source standards—differences exist in terms of spectral shape, polarization, magnitude, spatial and angular content, and temporal scales. A part of the NIST OTD efforts focus on instrument characterization and development of correction procedures.

This point is illustrated with examples of the determination of a sensor's spectral response functions. Differences in the relative spectral shape of ocean scenes and reference sources with incandescent lamps result in large errors in ocean-color products (e.g. chlorophyll *a*) unless the sensor has an ideal spectral response—finite at one wavelength and zero everywhere else—or a correction algorithm is applied [12]. This algorithm, developed for an array spectrograph, uses system-level characterization measurements that were implemented with laser-generated, tunable flux which filled the sensor's entrance pupil. The telescopes used to develop the U.S. Geological Survey (USGS) Lunar Irradiance Model, which is the basis of on-orbit inter-satellite lunar comparisons, use filters for spectral selection. The system-level spectral responses were modeled using filter transmittance results with collimated flux. In 2003, USGS, NASA, and NIST made system-level measurements for several of the channels using a portable, tunable laser system. Shifts of the center wavelength of up to 2.5 nm were observed; most likely, the differences exist because the filter is not illuminated by collimated light when mounted in the telescope. In atmospheric sounding, measurements at infrared wavelengths are used to retrieve surface temperature, atmospheric temperature profiles, and other physical quantities. Small errors in the spectral response functions can cause large errors in the retrieved brightness temperatures. It is difficult to verify the vendor's

---

<sup>4</sup> Refers to derived geophysical variables; Level 2 products are in terms of the original spatial resolution and location, Level 3 products are in terms of uniform space-time coordinates.

assessment of these functions because they are specific to each sensor. Additional research, such as comparison of system-level measurements to combined component-level measurements or development of new methods to assess the accuracy of infrared spectral response characterization results, should be pursued.

## Summary

Establishment of traceability is necessary for placing results and estimates of their uncertainty on an absolute scale. There are a number of factors that must be considered when comparing independent measurements. Sensor characterization is important for effective removal of systematic effects. These effects can easily lead to results that are in error by more than the stated uncertainty.

## References

- [1] Satellite Instrument Calibration for Measuring Global Climate Change, *NISTIR 7047*, Washington DC: U.S. Government Printing Office, (2004).
- [2] Post-Launch Calibration of Satellite Sensors, *ISPRS Book Series Volume 2*, S. A. Morain and A. M. Budge, Eds., New York: A. A. Balkema, (2004).
- [3] International Vocabulary of Basic and General Terms in Metrology, *VIM 2nd ed.*, Geneva: International Organization for Standardization, Sec. 6.10 (1993).
- [4] T. J. Quinn and C. Frohlich, *Nature*, **401**, 841-841, (1999); and <http://spot.colorado.edu/~koppig/TSI>
- [5] <http://ts.nist.gov/traceability>
- [6] S. W. Brown, B. C. Johnson, S. F. Biggar, E. F. Zalewski, J. Cooper, P. Hajek, E. Hildum, P. Grant, R. A. Barnes, and J. J. Butler, *Appl. Optics*, submitted (2005).
- [7] J. P. Rice, J. J. Butler, B. C. Johnson, P. J. Minnett, K. A. Maillet, T. J. Nightingale, S. J. Hook, A. Abtahi, C. J. Donlon, and I. J. Barton, *J. Atmos. & Oceanic Tech.*, **21**, 258-276 (2004).
- [8] E. A. Early, P. Y. Barnes, B. C. Johnson, J. J. Butler, C. J. Bruegge, S. F. Biggar, P. R. Spyak, M. M. Pavlov, *J. Atmos. & Oceanic Tech.*, **17**, 1077-1091 (2000).
- [9] B. C. Johnson, M. Litorja, and J. J. Butler, *Proc. SPIE*, **5151**, 454-462 (2003).
- [10] C. Cao, M. Weinreb, and S. Kaplan, Satellite Calibration Conference (CalCon), Logan, Utah (2004).
- [11] J. P. Rice and B. C. Johnson, *Proc. SPIE*, **4450**, 108-126 (2001).
- [12] S. W. Brown and B. C. Johnson, *Metrologia*, **40**, S81-S83 (2003).

# GENERATING COMPREHENSIVE AND CONSISTENT SATELLITE CLIMATE DATA RECORDS OVER THE CANADIAN LANDMASS

Rasim Latifovic, Alexander Trishchenko, Ji Chen, Bill Park

## 1. Introduction

Generating accurate and comprehensive spatial data from satellite observations of Canada on national scale is one of the major goals of the project “Earth Science on National Action on Climate Change”. This project is part of the Program “Reducing Canada’s Vulnerability to Climate Change” conducted by the Earth Sciences Sector of the Department of Natural Resources Canada. The satellite data records represent important component of climate data records which are critical for studying vulnerability of natural and managed systems to climate change. Long-term observations sustained over decades are a prerequisite for providing climate data needed by scientists, decision makers and stakeholders to make adaptive choices to improve resilience to climate change and vulnerability. These data are also of great importance for maintaining economic vitality and sustainable development. Satellite data contain valuable measurements of the Earth’s atmosphere and surface properties. Starting in early 80’s satellite observations span now over two and half decades and constitute valuable source of information about various geophysical parameters, such as cloud fraction, albedo, leaf area index, land cover, and land and water temperatures.

This paper and accompanying presentations describe advanced system developed at the Canada Centre for Remote Sensing (CCRS) for automatic processing of Level 1B coarse resolution satellite data into higher-level products required for climate research and applications. Primary objective of this work is to produce consistent and comprehensive satellite climate data records CDRs over Canada from observations collected by the NOAA-6 to NOAA-17 (1980-2004) and SPOT/VGT 1&2 (1998-2004) satellites. We are also working on expanding our database to include data acquired by present and future sensors such as MODIS/Terra and Aqua, NPOESS/VIIRS, and ENVISAT/MERIS.

In order to facilitate accomplishment of the first objective a new processing system, called Earth Observation Data Manager (EODM), was designed based on the best knowledge and experience gained at Canada Center for Remote Sensing (CCRS) over the last decade. The, GEOcoding and COMpositing New version, (GeoCompN) ([Adair et al., 2002](#), [Cihlar et al., 2002](#)) is the previous system for processing data collected by AVHRR sensors onboard NOAA-11 and -14. It was designed and implemented as a collaborative effort of PCI Geomatics of Richmond Hill, Ontario, Canada and CCRS. Although, designed for terrestrial monitoring the operational use of GeoCompN has reveal the following several important concerns unique to the processing of long-term satellite data:

- Long-term commitment to system improvement i.e. continual algorithm refinement, calibration, validation, data collection and analysis.
- The need to monitor the lifetime performance of multiple observing platforms simultaneously carrying on forward near-real time processing.
- Periodic reprocessing and reanalysis to improve quality of data products.
- Archiving and providing users with timely access to data and metadata.
- Processing and archiving extremely large volumes of data engage significant computational resources.

CDR's specific requirements cannot be fully satisfied by the existing processing system, designed for providing a daily single best observation over a given location. Such temporal resolution is not adequate for generating some of thematic satellite climate records as cloud coverage or diurnal surface temperature. Additional requirements unique to generating satellite CDRs that cannot be met with existing commercial systems are the need for constant software maintenance, algorithm refinement and implementation as new information and methods become available. Thus, software development and maintenance is an important component of the system and should be supported by the science teams responsible for generating the climate data record.

## 2. System overview

Earth Observation Data Manager (EODM) is the new system that processes coarse satellite resolution data into various geophysical data products. Presently, EODM provides end-to-end processing of AVHRR and post-seasonal correction of SPOT VGT S10 data. The NOAA-6 to NOAA-17 AVHRR data are supported by four primary functions: 1) data ingest and calibration, 2) geometric correction, 3) resampling and 4) composite product generation. These functions enable production of a basic product that includes TOA reflectance from bands 1 and 2, reflectance/radiance from band 3A/3B, brightness temperature from bands 4 and 5, and auxiliary data such as viewing geometry and relative composite date. EODM's design is tailored to the specific requirements for satellite data to be utilized for climate studies. The system has the following components and features:

- 1) Calibration module that performs radiance calibration, satellite-to-satellite spectral cross calibration and functions that support analysis and refinement of internal calibration data.
- 2) Geometric correction module based on a new approach developed and implemented to ensure high rate of successfully processed orbits. An important system characteristic needed for constant sampling within the diurnal, seasonal, and long-term inter-annual cycle.
- 3) The resampling designed to achieve high georeferencing accuracy at every pixel location required for performing long-term trend analysis. Quality control procedure reports an overall accuracy and flags areas in an orbit where desired accuracy is not achieved. New detailed database of ground control points that cover North America in uniform way was generated for automated ground control point matching used for removing unsystematic geometric errors.
- 4) Processing of orbits acquired during day and night over summer and winter season.
- 5) Product specific clear-sky compositing procedure based on flexible multi criteria approach. For example, the compositing criteria for producing composite products over water bodies are based on analysis of cloud mask and selecting minimal reflectance in the visible band, while compositing over land is based on a cloud mask and maximum NDVI criteria.

The AVHRR or SPOT/VGT S10 products derived by compositing processed level 1B data at the TOA level are further refined through the post-seasonal corrections to derived surface level products. This is achieved through the ABC3 methodology (Atmospheres, BRDF, Cloud Correction of Composite data) presented in [Cihlar \*et al.\*, \(2004\)](#). ABC3 performs atmospheric corrections of top of atmosphere (TOA) reflectance using semi-analytical algorithm with coefficients tuned to MODTRAN4 exact computations [Trishchenko, \(2002\)](#). The atmospheric correction algorithm incorporates also local topographic effects to account for inclined surface within pixel area

Trishchenko et al., (2000). Surface reflectance normalization to a common viewing geometry is implemented using a non-linear temporal angular BRDF model (NTAM) Latifovic et al., (2003), which corrects for the surface anisotropic effects present in composite data. Detecting and replacing contaminated observations is performed using the CECANT algorithm Cihlar et al., (1999). Systematically corrected surface level primary data products are used for generating higher-level thematic climate data record (i.e. geophysical variable such as snow and ice, cloud fraction, albedo, leaf area index, land cover, lake temperature etc).

## Conclusion

Long-term observations sustained over decades are a critical first-step in providing the data necessary for studying climate variability and change. Decision makers and stakeholders need synthesis products generated from such data to be able to make better decisions for improving resilience to the impacts resulting from climate change.

Generation of satellite based climate data record assume fulfillment of unique requirements, including periodical reprocessing, reanalysis and support with continuous research and development that involves a broad science community. EODMs system architecture is designed to facilitate the needs for constant improvements as the new methodologies become available, including assimilation of data from present and future satellite sensors, such as ENVISAT–MERIS, NPOESS –VIIRS.

Initial steps in generating thematic satellite based CDRs over Canada are achieved through design and implementation of in this article briefly described system. It will facilitate processing of satellite data but also research and development to create new TCDRs over 25 year long record.

## Reference:

Adair, M., Cihlar, J., Park, B., Fedosejevs, G., Erickson, A., Keeping, R., Stanley, D., & Hurlburt, P. (2002). GeoComp - n, an advanced system for generating products from coarse and medium resolution optical satellite data. Part 1: System characterization. *Canadian Journal of Remote Sensing*, 28:1-20

Cihlar, J., Chen, J. M., Li, Z., Latifovic, R., Fedosejevs, G., Adair, M., Park, W. M., Fraser, R., Trishchenko, A., Guindon, B., Stanley, D., Morse, D., (2002). GeoComp-n, an advanced system for the processing of coarse and medium resolution satellite data. Part 2: Biophysical products for northern ecosystems; *Canadian Journal of Remote Sensing*, Vol. 28, No. 1, pp. 21-44

Cihlar, J., R. Latifovic, J. M. Chen, A. Trishchenko, Y. Du, G. Fedosejevs, and B. Guindon, 2004. Systematic corrections of AVHRR image composites for temporal studies. *Remote Sensing of Environment*, 89, 217-233

Cihlar, J., Latifovic, R., Chen, J., and Li, Z. 1999. Near-real time detection of contaminated pixels in AVHRR composites. *Canadian Journal for Remote Sensing* 25: 160-170.

Latifovic, R., Cihlar, J., & Chen, J. M. (2003). A comparison of BRDF models for the normalisation of satellite optical data to a standard sun-target-sensor geometry. *IEEE Transactions on Geoscience and Remote Sensing*, 41, No.7

Trishchenko, A.P, Z. Li, W. Park, J. Cihlar 2000. Correction for the BRDF and Topographic Effects in Satellite Retrieval of Surface Spectral Reflectance in Solar Spectral Region. *IRS 2000 Current Problems in Atmospheric Radiation*, Proceedings of the Inter. Radiation Symposium St. Petersburg, Russia 24-29 July 2000 Smith and Timofeyev (Eds) ,

Trishchenko, A. P, B. Hwang, Z. Li, 2002, Atmospheric correction of satellite signal in solar domain: Impact of improved molecular spectroscopy. *Proc. 12<sup>th</sup> ARM Science Team Meeting*, 7pp. (available at [http://www.arm.gov/docs/documents/technical/conf\\_0204/trishchenko-ap.pdf](http://www.arm.gov/docs/documents/technical/conf_0204/trishchenko-ap.pdf))

# SCIAMACHY DETECTORS: CALIBRATION ON-GROUND AND IN-FLIGHT

G. LICHTENBERG

National Institute for Space Research Netherlands (SRON), Sorbonnelaan 2, NL-3584 CA Utrecht, lichten@sron.nl

## 1. INTRODUCTION

SCIAMACHY is a scanning nadir and limb spectrometer covering the wavelength range from 240 nm to 2390 nm in 8 channels. The instrument is polarisation sensitive and measures the Q fraction of the polarisation in 6 broadband sensors covering the wavelength range of the instrument. Additionally the U fraction of the polarisation is measured around 850 nm. SCIAMACHY was launched in February 2002 on the ENVISAT platform. During the on-ground calibration the polarisation sensitivity and the radiometric sensitivity was extensively measured for a range of scanning angles. This article describes the basic concepts of the SCIAMACHY calibration and discusses some aspects of the in-flight performance of the IR detectors. The presentation given at the workshop covers additional aspects of the calibration and also contains a number of lessons learned for future instruments which are not repeated here. More information can be obtained at the SCIAMACHY calibration webpage [http://www.sron.nl/~SCIA\\_CAL/](http://www.sron.nl/~SCIA_CAL/) (e.g. a daily updated transmission plots for the IR channels 7 and 8).

## 2. CALIBRATION CONCEPT

The experience of GOME where various air-vacuum effects led to calibration problems showed that spectrometers should be calibrated under thermal vacuum (T/V) conditions. In the case of SCIAMACHY a calibration done completely under T/V conditions was not possible, because several mirror incidence angles had to be covered and the vacuum tank was too small to allow the necessary rotation of the instrument. Therefore a combination of T/V and ambient measurements was used. The radiometric sensitivity and the polarisation sensitivity of the instrument were measured under T/V conditions for *one* reference angle and all necessary instrument modes (limb, nadir and irradiance). In order to be able to calibrate all incidence angles on the mirrors (or diffusers), component level measurements of all possible mirror combinations and mirror-diffuser combination were made under ambient conditions. The ambient measurements were done for a set of angles (including the reference angle measured under T/V conditions) and a set of wavelengths. The reference angle measurement is used to transfer the results from the ambient measurement to the T/V measurement. Measurements are done for unpolarised light, s- and p-polarised light and  $\pm 45$  polarised light. Additionally to the on-ground calibration, in-flight calibration measurements with internal light sources (WLS=White Light Source and SLS=Spectral Line Source) and solar measurements are used to track changes of the instrument. The combination of T/V measurements with the ambient measurements gives ideally the correct instrument response for all incidence angles at begin of life of the instrument. The degradation measured in-flight takes into account changes of the instrument over time (see figure 2.1).

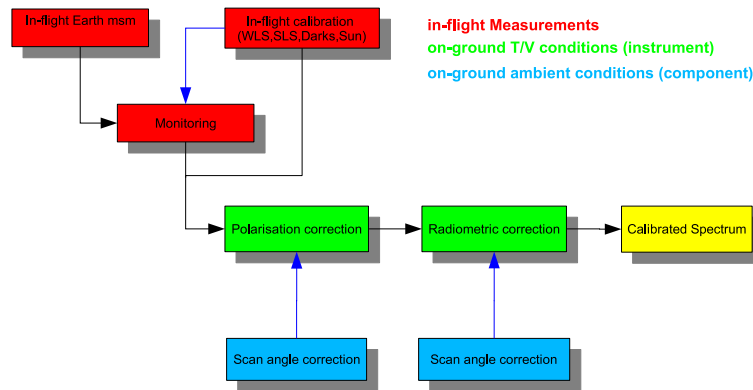


FIGURE 2.1. Calibration concept for SCIAMACHY. The different colours symbolise the different types of measurements used during the calibration.

### 3. IN-FLIGHT PERFORMANCE

Two types of detectors are employed in SCIAMACHY: For the UV/VIS spectral range standard Si Reticon detectors are used. For the IR wavelength range EPITAXX InGaAs detectors with custom designed optics and readout electronics are used. The in-flight performance of the UV/VIS detectors is as expected from on-ground measurements (or better). For the remainder of this article we will therefore concentrate on the IR detectors, i.e. channels 7&8. Both channels are cooled to around 145 K with a passive radiant cooler that looks into deep space. Soon after the cool down it was discovered that an ice layer was developing on both detectors (see figure 3.1). The ice layers is of macroscopic thickness, the maximum layer thicknesses observed are 230 and 600  $\mu\text{m}$  for channels 7 and 8 respectively, if one assumes pure water ice. Possible sources of water include the carbon fibre structure of ENVISAT and the MLI.

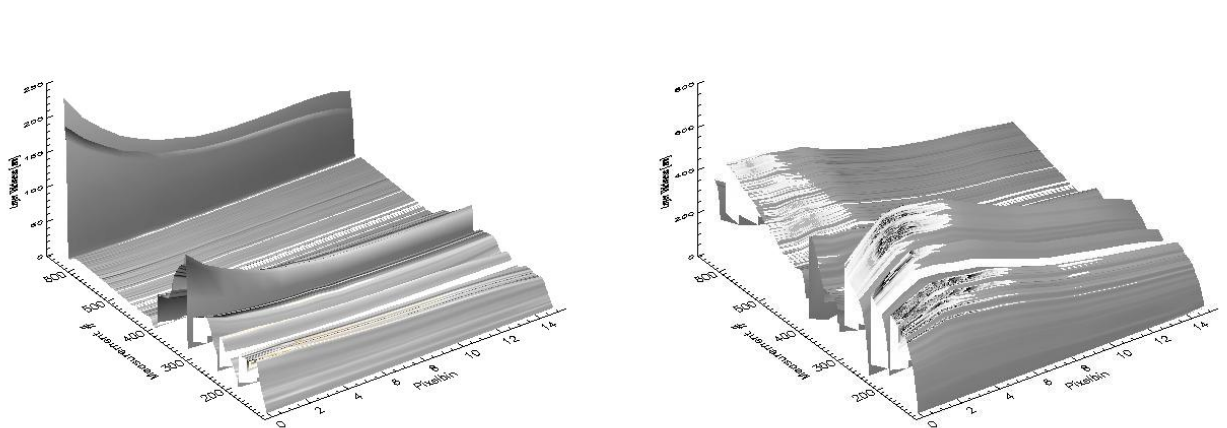


FIGURE 3.1. Ice layer thickness over time and averaged over 64 pixels. Left: Channel 7. Right: Channel 8. The height (z-axis) indicates the thickness of the ice layer in  $\mu\text{m}$ , along the x-axis (left to right) the pixel /wavelength band is shown. The y-axis shows the time (as measurement number). Data from January 2003 to July 2004 are plotted. During this time six decontaminations were performed.

The layer thickness varies over the channels as can be seen in figure 3.1. Lower pixel numbers (blue end of the channels) have more ice on them than higher pixel numbers. The reason for this behaviour is unknown (although one might expect differences in layer thickness). During nominal operations decontaminations

are performed in regular time intervals, i.e. the layers are removed regularly by heating the detectors. While channel 8 shows the expected exponential layer growth with time after each decontamination, channel 7 behaves more irregularly. After individual decontaminations, channel 7 showed 3 types of behaviour: (1) an expected exponential layer growth, (2) an accelerated growth causing a signal loss of up to 50% in 2 weeks with subsequent slow *decrease* of layer thickness afterwards and (3) a state in which the ice layer grows slowly for 3 weeks and then stays stable at a signal loss of around 10%. The reason for the different behaviour of channel 7 after the decontaminations and the difference in ice layer growth between channel 7 and 8 (which are of the same design) are not understood. One possibility is a second cold trap somewhere in the detector housing of channel 7 that is “triggered” only under some circumstances. The ice layers made some changes in the calibration and in the retrieval of trace gases necessary. Since a significant part the dark signal consists of thermal background which is attenuated by the ice layer just as the science signal, the dark measurement now has to be performed every orbit (instead of every 400 orbits). The slitfunction of the instrument is changed because the ice scatters the incoming light. The change is dependent on the structure of the ice and thus difficult to correct. An empirical correction based on known trace gas contents is currently under investigation. The transmission loss can be corrected because in-flight calibration measurements are possible with the sun and internal light sources.

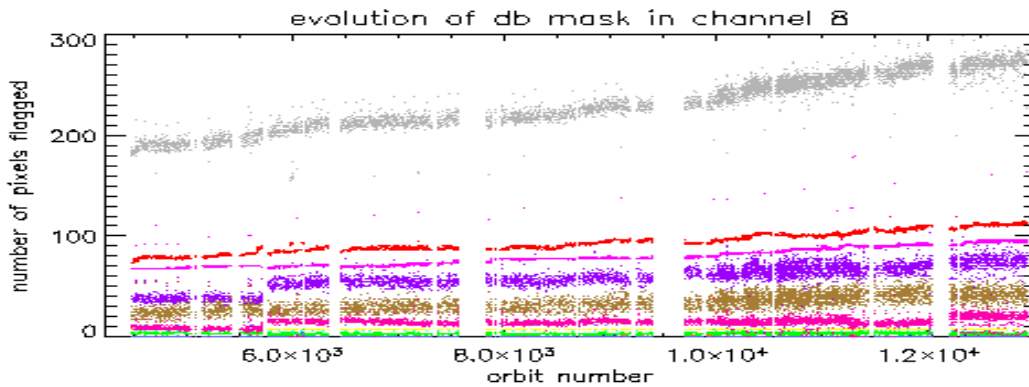


FIGURE 3.2. *Number of bad&dead Pixels in channel 8 as a function of orbit number. The colours symbolise the different types of bad pixels. The grey curve shows the total number of bad pixels.*

Another effect that was recently discovered is the increase of so called “bad pixels” in the IR channels. These pixels show random telegraph noise, excessive noise or are disconnected. The underlying reason for the bad pixels is a lattice mismatch between the InP substrate and the light detecting InGaAs layer. The increase of bad pixels is most likely caused by ion particle impact. It is not yet clear if the increase of bad pixels will stop in the future (possible if some pixels are more susceptible for radiation damage than others) or if it will continue to increase. SRON has set up a monitoring facility that produces a daily mask to filter out bad pixels for retrieval.

#### 4. CONCLUSIONS

The calibration of SCIA under thermal vacuum conditions avoided GOME type problems like air-vacuum effects that are introduced by the calibration. The use of uncoated mirrors in SCIAMACHY reduced the degradation in the UV significantly compared to GOME. The calibration under thermal vacuum conditions should become standard for all optical instruments that contain elements that are likely to change under long term vacuum conditions such as dichroics and coated mirrors or lenses. The development of the ice layers and the unexpected change of the number bad pixels show that it is of vital importance to have in-flight calibration capabilities. The ice layer on the detectors require adjustments in operations and data processing. After these are implemented SCIAMACHY will reach its full potential.

# IN-FLIGHT CALIBRATION OF THE CHRIS INSTRUMENT ON PROBA

**Mike Cutter and Dan Lobb**

*Sira Technology Ltd, South Hill, Chislehurst, Kent, BR7 5EH, England.*

*E-mail: Mike.Cutter@sira.co.uk Dan.Lobb@sira.co.uk*

## 1 CHRIS – platform and orbit

The CHRIS instrument (Compact High Resolution Imaging Spectrometer), developed by Sira Technology Ltd, is a hyperspectral radiometer, providing images of Earth in the visible and near-IR spectral region. It is the largest instrument payload on the ESA platform PROBA (Project for On-Board Autonomy), which was launched from the Indian PSLV on the 22<sup>nd</sup> October 2001. The platform is in a sun-synchronous polar orbit (10.30 am equator crossing) with an apogee of 673km and a perigee of 560km. PROBA is a highly manoeuvrable small satellite, capable of large, rapid rotations on pitch and roll axes, with fine control over pitch and roll rates.

## 2 CHRIS objectives

The CHRIS instrument is designed partly as a technology demonstrator: it has been developed at very low cost and is used to evaluate the performance of a compact spectrometer design form and to provide experience in operation of hyperspectral systems. However, the hyperspectral data produced by the instrument has been found valuable for a range of science applications, particularly in studies on land surfaces, but also in applications to coastal zones and aerosols. The instrument uses the agility of the PROBA platform to provide BRDF data – in general recording images of each designated target area at 5 different view direction in each target overpass, as indicated in Figure 1, as well as across-track pointing for target acquisition. The platform also provides slow pitch during imaging in order to increase the integration time of the instrument, by a “slow-down factor” of approximately 4.

## 3 CHRIS basic performance

Basic performance and design characteristics of CHRIS on PROBA are summarised in the table below. The design form is capable of extension into the short-wave IR (out to 2500nm). Currently, the platform data storage and telemetry system allows 1 complete image set to be transmitted to ground per day.

Parameter	Value
Image area at perigee	13 km square
Image set for BRDF	typically 5 images up to 3 sets per day
Spatial sample	17 m at perigee
Spectral range	415nm to 1050nm
Spectral resolution	1.25nm to 11nm

Parameter	Value
Digitisation	12 bits
Gain stages	4 levels (1, 2, 4, 8)
Signal-to-noise ratio	200 at 0.2 albedo
Mass	< 14 kg
Power imaging	8 W primary
Size	790 x 260 x 200 mm <sup>3</sup>

## 4 Main instrument design

The instrument is an imaging spectrometer of basically conventional form, with a telescope forming an image of Earth onto the entrance slit of a spectrometer, and an area-array detector at the spectrometer focal plane. The instrument operates in a push-broom mode during Earth imaging. The CHRIS optical design is shown in figure 1.

The telescope is an axially-symmetrical two-mirror catadioptric system, with a focal length of 746mm, a 2° swath width and a pupil diameter of 200mm. The spectrometer design is based on an Offner relay, using three mirrors - two concave and one convex – to provide unit magnification between the entrance slit and the detector focal plane. Curved prisms are introduced into the light path between the entrance slit and first mirror, and between the last mirror and detector, to introduce the required spectral spread. All curved components, are spherical and all refracting elements are made in fused quartz. Rectangular baffle plates are introduced to control stray light reaching the telescope focal plane without reflections at the mirrors.

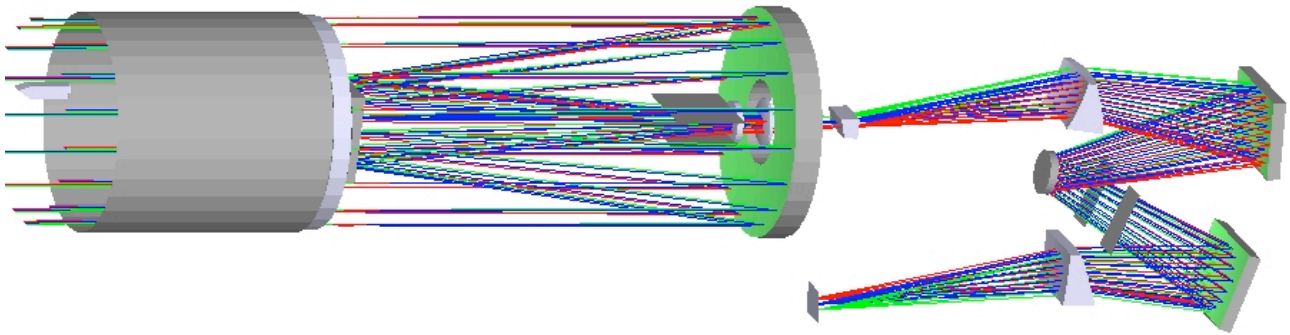


**Figure 1 CHRIS optics design, showing baffles and location of solar calibration device**

The detector is a frame-transfer CCD with 760 active columns providing spatial resolution, and 140 rows providing spectral resolution in the nominal image area. The analogue gain of the detector electronics can be switched between 4 levels; given digitisation to only 12 bits, this gain switching is desirable to increase dynamic range (particularly to deal with low detector response at extremes of the spectral range). The instrument is controlled via “configuration files” that are uploaded to the platform with image requests. The configuration files include the spectral bands to be read out and analogue gain settings. It is also possible to double the across-track sample distance by binning at the read-out port, and/or choose to read only half of the field width. When spatial coverage requirements are relaxed, it becomes possible to read out much larger numbers of resolved spectral bands.

The system does not include a shutter, so that the detector generates signal during the frame transfer period, introducing a “smear” error. One of the 19 output bands read out at maximum spatial resolution is always recorded from an area of the detector that nominally receives no light – this provides a signal proportional to the required smear correction for each detector column read, and also corrects for stray light.

## 5 Solar calibration device

The design of the solar calibration device is indicated in Figure 2. It is a reflecting prism integrated with one lens surface, providing a focal length of 25mm. The device is designed to receive direct sunlight on its external face, when the platform is over the Antarctic, on the dark side of the terminator, and the instrument is pointed towards nadir. The lens focuses an image of the sun in front of the telescope aperture, with an angular spread that effectively fills the instrument field. In operation of the solar calibration device, the platform attitude is controlled to point the instrument towards nadir over a dark area of Antarctic, and rotated in yaw so that sun-light is received on the device. Several readings are taken while the sun traverses the  $2^\circ \times 4^\circ$  field of the device, to check for effects of particulate contamination in the small area of pupil that is sampled.

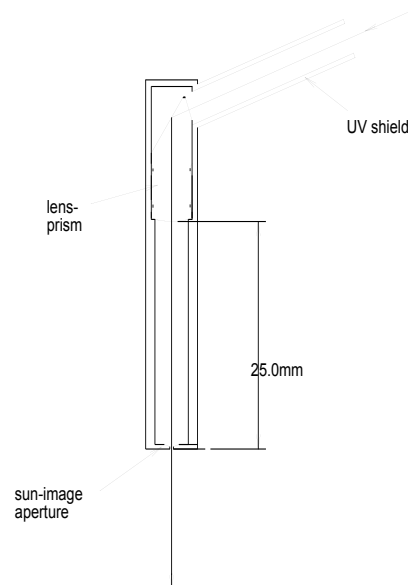


**Figure 2 Solar calibration device**

## 6 In-flight calibration methods, critical problems and assessments

In-flight calibration measurements can be considered under the headings: offsets, response and wavelengths. Offset corrections – including electronics offsets, dark signal and CCD smear – are made

using dummy reads, masked pixels and dedicated smear bands. These corrections are relatively straightforward, and they are believed to be satisfactory. Linearity measurements, using an internal LED, also give satisfactory results.

The main concerns are with response (gain) measurements, which generally present the most significant problems for calibration of imaging radiometers operating in the solar spectral region (including visible and near-IR for CHRIS). The “solar calibration device”, described above, is the CHRIS in-flight absolute calibrator. Vicarious calibration for response has also been undertaken by some investigators, and is likely to be used for the most confident absolute data calibration. Sira and investigators have used a variety of flat-fielding (or “de-stripping”) methods, correcting for small residual errors in response uniformity across the field.

### Wavelength shifts and slit-image shifts

Principle problems, for CHRIS calibration, include variation in the wavelengths defined by detector rows, due to launch shifts and changes of temperature which move the dispersed image with respect to the detector. The in-flight shifts are due mainly to predictable changes in refractive index of the dispersing prisms – changes of a few nanometres are produced with seasonal changes, at about 1nm per degree in the worst-affected part of the spectrum. Wavelength shifts are measured in flight, to about 1nm rms, using the atmospheric oxygen absorption band at 765nm. However, the wavelength shifts also affect radiometric calibration. The pre-flight absolute calibration data require careful interpretation, and corrections must be made in flight for the radiometric response correction coefficients. There is also a temperature effect on the location of slit images in the along-slit direction – this complicates the process of flat-fielding, since the response non-uniformity of the instrument is produced by a combination of non-uniform transmission along the slit, with detector pixel non-uniformity. The process must be updated with seasonal temperature changes.

### Solar calibration device – results and assessment

The solar calibration device has the essential advantage, for the low-cost CHRIS instrument, that it provides a reference radiance through a fixed (and dedicated) part of the aperture – thus requiring no mechanism.

The concomitant disadvantage is that it samples only a small part of the aperture. Although calibrated on ground, it cannot measure effects of changes in non-uniform contamination across the aperture. The device is therefore unlikely to be considered for a more demanding mission with a reasonable budget. In practice it has been found to give fairly good absolute calibration – this may be judged from comparison between pre-flight absolute spectral response measurement and in-flight measurements assuming ASTM data for solar irradiance, as shown in Figure 3.

The device was found to be ineffective in flat fielding, since it produces an irradiance distribution at the detector that is affected by very fine surface polish imperfections (called “orange peel”) on all optical surfaces. This effect is due to the very small size of the sun image illuminating the optics, which produces Schlieren effects. In a future rebuild of CHRIS, it is likely that the lens of the solar calibration device will be replaced by a small transmitting diffuser having high gain (although in this case speckle effects must be investigated).

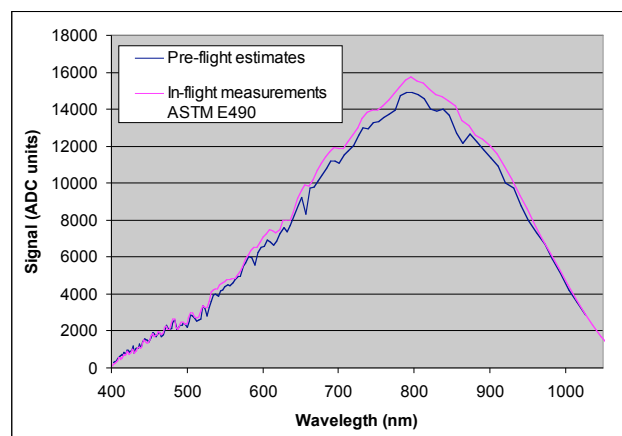


**Figure 3 Pre-flight/in-flight response comparison**

## **7 Conclusions**

The CHRIS instrument is providing useful data for a wide group of users, and is now in its third year of operation, following commissioning (although designed for only one year). Calibration of data has presented problems, but now appears likely to provide confidence at a few-% accuracy level, based mainly on vicarious results. Main lessons learned from CHRIS operation include the importance of spectrometer stability, including in-flight stability in wavelength calibration.

# A HIGH-QUALITY DATASET OF LAND-SURFACE AND ATMOSPHERIC MEASUREMENTS FOR THE COMPARISON/CROSS-CALIBRATION OF DATA FROM LARGE SCALE OPTICAL EARTH OBSERVATION SENSORS IN SPACE. THE VALENCIA *ANCHOR STATION*

E. Lopez-Baeza<sup>1</sup>, S. Alonso<sup>2</sup>, A. Comerón<sup>3</sup>, R. Diaz-Pabon<sup>2</sup>, C. Domenech<sup>1</sup>, J.F. Gimeno-Ferrer<sup>1</sup>, J. Jorge<sup>4</sup>, A. Labajo<sup>2</sup>, N. Pineda<sup>4</sup>, D. Pino<sup>5,\*</sup>, A. Rius<sup>5</sup>, F. Rocadenbosch<sup>3</sup>, K. Saleh<sup>1,#</sup>, M. Sicard<sup>3</sup>, R. Tarruella<sup>4</sup>, J. Torrobella<sup>5</sup>, and A. Velazquez<sup>1</sup>

1. *Climatology from Satellites Group, University of Valencia, Spain*

E. Lopez-Baeza, C. Domenech, J.F. Gimeno-Ferrer, K. Saleh<sup>#</sup>, A. Velazquez

#Also at: *INRA Bordeaux, France*

2. *Spanish Institute for Meteorology, Spain*

S. Alonso, R. Diaz-Pabon, A. Labajo

3. *Lidar Laboratory, Polytechnic University of Catalonia, Spain*

Comeron, F. Rocadenbosch, M. Sicard

4. *Polytechnic University of Manresa, Spain*

J. Jorge, N. Pineda, R. Tarruella

5. *Institute for Space Studies of Catalonia, CSIC, Spain*

D.Pino<sup>\*</sup>, A. Rius, J. Torrobella

<sup>\*</sup>Also at: *Polytechnic University of Catalonia, Barcelona, Spain*

## EXTENDED ABSTRACT

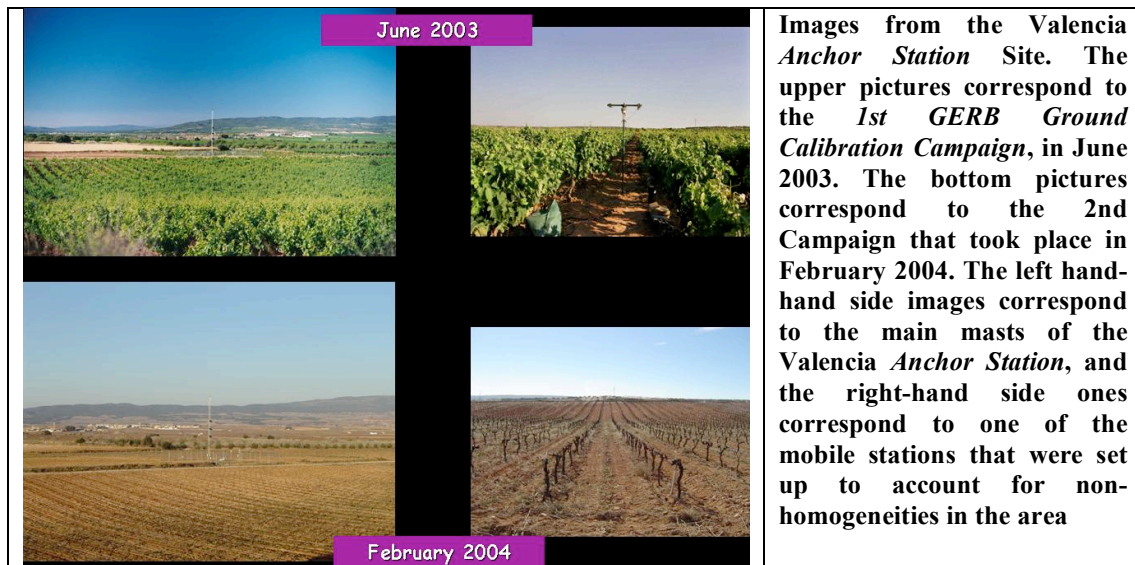
The Valencia *Anchor Station* is a reference meteorological station for validation of remote sensing data and products, specifically from low spatial resolution remote sensing instruments. It was set up by the University of Valencia (Spain) in December 2001 at the natural region of *Utiel-Requena Plateau*, a reasonable homogeneous area of about 50 x 50 km<sup>2</sup>. A number of intensive field campaigns have recently been developed at this site in connection with different Earth Observation missions, such as EuroSTARRS-2001 and SMOS-REFLEX 2003, both related to ESA SMOS (*Soil Moisture and Ocean Salinity*) Mission, and the two first *GERB Ground Validation Campaigns* that took place, respectively, in June 2003 and February 2004 during GERB's *Commissioning Period*. In these two latter campaigns, the CERES instruments onboard the Terra and Aqua NASA satellites played a crucial role in helping to defining and establishing a methodology for validation of very low spatial resolution satellite data and products. This is being accomplished thanks to the special and specific PAPS (*Programmable Azimuth Plane Scanning*) acquisitions that have been programmed over the Valencia *Anchor Station* Site for different observation conditions.

As an outcome from the two *GERB Ground Validation Campaigns*, a high-quality land-surface and atmospheric dataset is being built. This is composed of measurements of

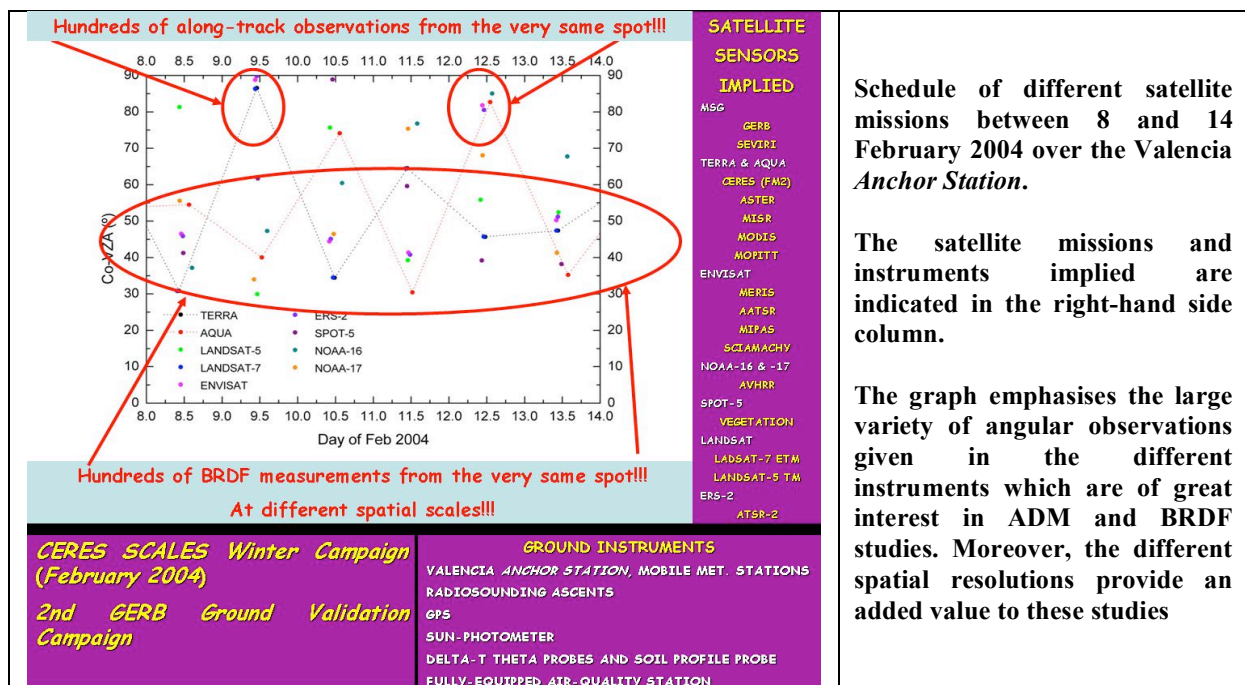
- radiosonde ascents exactly on spot and at the time of the corresponding satellite overpass (*Terra* or *Aqua*)
- GPS precipitable water content
- atmospheric transmissivity
- lidar scans

together with the operational meteorological observations at two different levels (2 m and 15 m) from the Valencia *Anchor Station* and from other mobile stations strategically placed at other land-surface conditions to account for the site main heterogeneities.

Details of the 1st *GERB Ground Validation Campaign* that took place at this site between 13 and 30 June 2003 may be found in Lopez-Baeza et al (2003).



The 2nd *GERB Ground Validation Campaign*, developed also at this site from 9 to 12 February 2004, was particularly defined and programmed taking into account a large number of satellite remote sensing instruments simultaneously coinciding their observations over the *Anchor Station* area under different conditions. Among these instruments, we may refer SEVIRI and GERB onboard MSG, the *Terra* and *Aqua* payloads, all the ENVISAT instruments, NOAA-AVHRR-16 and -17, LANDSAT-7 ETM and LANDSAT-5 TM, SPOT-VEGETATION and ERS2 (ATSR-2).



The purpose of this paper is to show the interest and quality of the ground dataset being gathered so far. To do that, we show the good agreement achieved between radiative transfer simulations obtained from STREAMER (Key and Schweiger, 1998) using these ground and

atmospheric measurements, and CERES top of the atmosphere radiances. Conditions for the radiative transfer simulations for the February 2004 campaign are given in the table below.

## **Radiative Transfer Simulations of the CERES TOA Radiances (Feb. 2004 Campaign)**

**CERES Geometrical Observation Conditions for the specific date and target (Valencia *Anchor Station*).**

**Atmospheric Profiles (Mid-latitude winter atmosphere)**

- **Water Vapour: Radiosounding ascents scaled to 94-95 STREAMER atmospheric levels constrained by the water vapour total-column GPS measurement**
- **Ozone: Profile scaled to TOMS measurements**
- **Aerosols: Rural aerosols (background tropospheric aerosols, 50 km visibility, background stratospheric aerosols)**

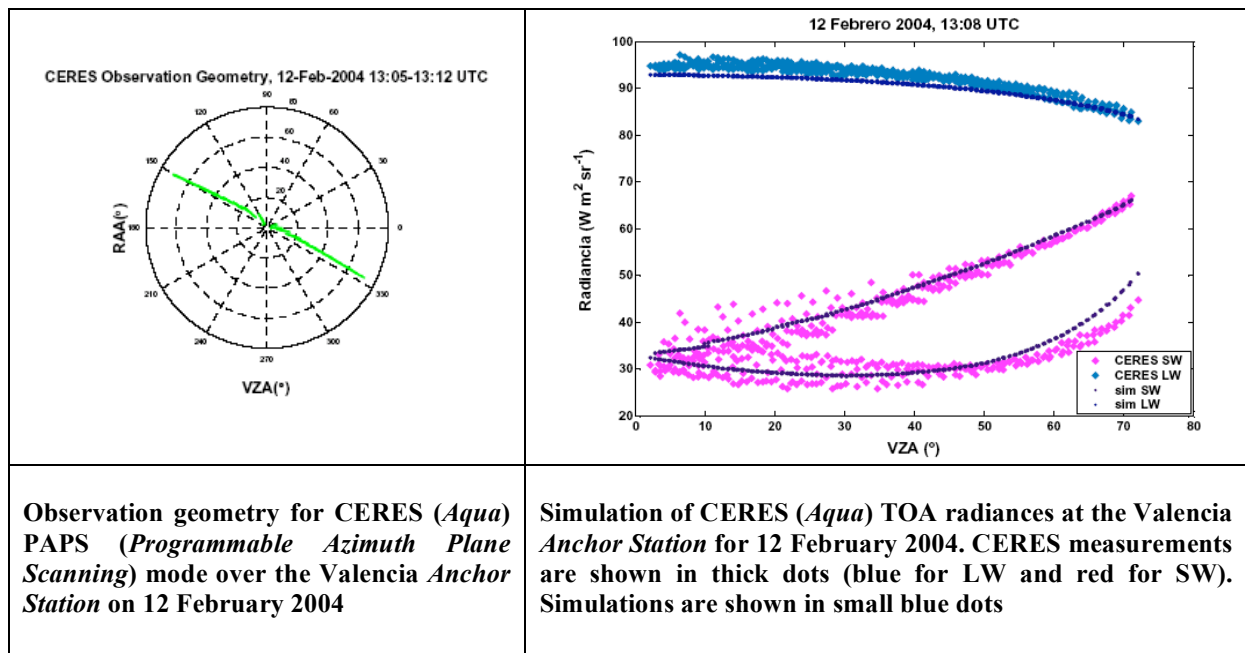
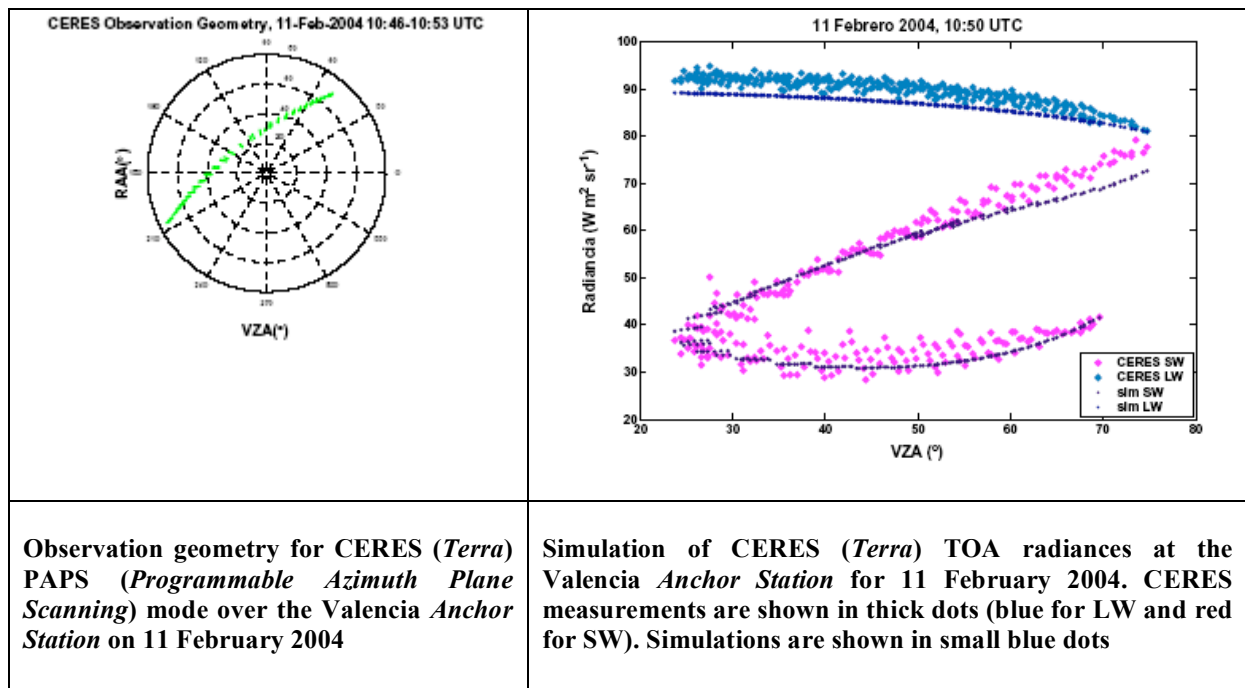
**Surface Parameters**

- **Spectral Albedo: from ASTER spectral library (*John Hopkins University*)**
- **BRDF: Model from Ahmad & Deering (1993) for 0.662 and 0.826  $\mu\text{m}$  applied to the study area by using broadband albedo measurements from the Valencia *Anchor Station* and mobile stations and spectral albedo above**
- **Surface Emissivity: from CERES/SARB database (See also Wilber et al., 1999)**
- **Surface Temperature, Albedo, etc.: from the Valencia *Anchor Station* and mobile stations used**
- **Land uses: 76.6% bare soil + 23.4% vegetation from LANDSAT-5 classification**

**Input parameters from the campaign dataset used in the radiative transfer simulations with STREAMER**

The following figures show two examples of the top of the atmosphere (TOA) radiance simulations obtained for that campaign, one for CERES onboard *Terra* and the other for CERES onboard *Aqua*.

--	--



This dataset is offered to define independent values of different geophysical parameters that may be used as reference for the comparison and cross-calibration of a large variety of remote sensing instruments of different spatial, spectral, radiometric, angular, revisiting time, etc., observation conditions. Besides, the possibility of defining and designing specific Cal/Val activities in the site is also envisaged.

## ACKNOWLEDGMENTS

This work has been carried out in the framework of the SCALES Project of the *Spanish Programme on Space Research (Ministry for Science and Education)*. One of us (A. Velazquez) holds a doctorate student grant in this framework.

We would like to thank the *Spanish Institute for Meteorology* for their contribution on the radiosonde ascents and the *Institute for Space Studies of Catalonia* for their contribution on the GPS measurements.

Most of the radiative transfer simulations and the interpretation work have been carried out during a visiting stay of one of us (A. Velazquez) at *NASA Langley Research Centre* (Hampton). We appreciate all the help and support received there, especially from G. Lou Smith, Z. Peter Szewczyk, Norman G. Loeb and Tom P. Charlock.

The bare soil spectral reflectance used in this work has been reproduced from the *ASTER Spectral Library* through the courtesy of the *Jet Propulsion Laboratory, California Institute of Technology*, Pasadena, California. Copyright © 1999, *California Institute of Technology*. ALL RIGHTS RESERVED.

## REFERENCES

Ahmad, S.P. and D. W. Deering (1992): A simple Analytical Function for Bidirectional Reflectance. *J. Geophys. Res.*, 97, D17, pages 18867-18886

Key, J. and A.J. Schweiger (1998): Tools for atmospheric radiative transfer: Streamer and FluxNet, *Computers & Geosciences*, 24(5), 443-451.

Lopez-Baeza, E., Belda, F., Bodas, A., Crommelynck, D., Dewitte, S., Domenech, C., Gimeno, J., Harries, J., Jorge, J., Pineda, N., Pino, D., Rius, A., Saleh, K., Tarruella, R., Velazquez, A. (2003): *SCALES: SEVIRI and GERB CAL/VAL area for large-scale field experiments*. International Symposium on Remote Sensing. Remote Sensing of Clouds and the Atmosphere VIII (Remote Sensing Europe 2003, SPIE). Barcelona, (Spain), 8-12 September 2003

Wilber, A.C., D.P. Kratz, and S.K. Gupta (1999): *Surface Emissivity Maps for Use in Satellite Retrievals of Longwave Radiation*. NASA/TP-1999-209362

Contact details (address, telephone, fax, e-mail address) of the corresponding author

Dr Ernesto Lopez-Baeza  
*Climatology from Satellites Group*, Remote Sensing Research Unit  
Department of Thermodynamics  
Faculty of Physics. University of Valencia  
Calle Dr Moliner, 50. Burjassot. 46100 Valencia (Spain)  
Tel.: +34.96.3543118 / 3544350    Mobile: +34.660177265    Fax: +34.96.3543385  
[Ernesto.Lopez@uv.es](mailto:Ernesto.Lopez@uv.es)  
<http://www.uv.es/anchors>



# VICARIOUS CALIBRATION OF ADEOS-2 GLI AND TERRA/AQUA MODIS USING GLOBAL DATA SET FOR MULTI-SENSOR OCEAN-COLOR APPLICATIONS

*Hiroshi Murakami, Earth Observation Research and Application Center, JAXA,*

*Mayumi Yoshida, Remote Sensing Technology Center of Japan,*

*Akihiko Tanaka, Nagasaki Industrial Promotion Foundation*

*Hajime Fukushima, and Mitsuhiro Toratani, School of High-Technology for Human Welfare, Tokai Univ.*

**Abstract** We improved consistency among ocean-color products by GLI, Terra MODIS, and Aqua MODIS through the same vicarious calibration scheme and ocean-color algorithms. We found characteristics of the global vicarious calibration coefficients; scan-angle and temporal dependency of GLI UV and blue channels, and temporal change of Terra MODIS visible channels. We still need further investigation about GLI near infrared calibration and dependency on the sun-glint location of Terra MODIS visible channels to make the consistent data sets enough for the combined applications.

## 1. Introduction

Several large-scale ocean-color sensors have been in orbit in these years. Consistent data sets from these sensors are important for effective data analysis improving temporal and spatial coverage and resolution for the ocean-color application study and monitoring. However, inter-sensor differences often reach in a comparable degree to variability of natural phenomena (e.g., short-time change in chlorophyll-a distribution) due to sensor and algorithm characteristics.

Vicarious calibration is an effective way to improve the consistency. The vicarious calibration coefficients ( $K_{vc}$ ) are derived using in-situ observations generally. However, we cannot obtain enough number of in-situ match-ups in the early phase of satellite mission and the in-situ measurement error and sub-pixel structure can be a serious problem. In addition, the in-situ observation sites can not cover all conditions of the satellite observation (scan geometry, time, latitudes and so on). The global vicarious calibration scheme proposed by Murakami et al. [1] does not need the in-situ observations and can derive scan angle, temporal, and latitudinal characteristics of  $K_{vc}$ . We processed GLI and MODIS ocean-color products using the  $K_{vc}$ , and evaluated their consistency.

A part of the product differences may be caused by characteristics of ocean-color algorithms. GLI standard atmospheric correction algorithm [2] is used for both GLI and MODIS processing in this study. Look up tables (LUTs) in the atmospheric correction algorithm are calculated considering GLI and MODIS channel responses using the same radiative transfer code, RSTER5b [3] [4] [5]. In-water algorithm for MODIS data is derived as same way as GLI standard algorithm ([6] a kind of empirical equation) using consistent in-situ data set provided by GLI ocean validation group.

## 2. Vicarious Calibration using Global Datasets

### 2.1 Procedure

Figure 1 shows the operation flow of the global vicarious calibration. We simulated  $L_{TOA}$  for all GLI (MODIS) visible, near-infrared (NIR), and short-wave infrared channels using the LUTs. GLI (MODIS) geometries, SeaWiFS nLw (level-3 Bin 8-day mean

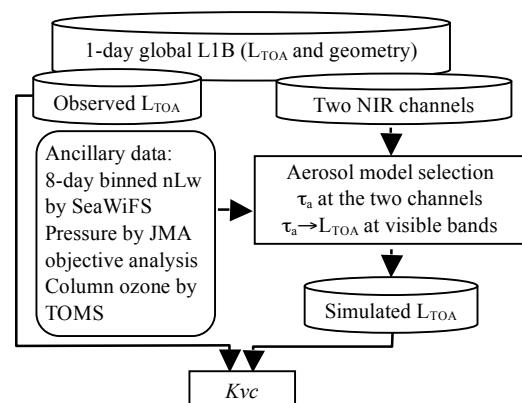


Figure 1 Operation flow of the global vicarious calibration

data), aerosol optical thickness ( $\tau_a$ ) and aerosol-type model ( $M_{select}$ ) from two NIR channels 13 and 19 of GLI (15 and 16 of MODIS), objective analysis pressure, and TOMS ozone data are used as ancillary and boundary condition. We used an in-water optical model [7] to extent the nLw at SeaWiFS channels (6 channels from 412nm to 670nm) to GLI (13 channels from 380nm to 710nm) and MODIS ocean-color channels (10 including 500m channels, see Table 1). The  $K_{vc}$  means a kind of relative calibration

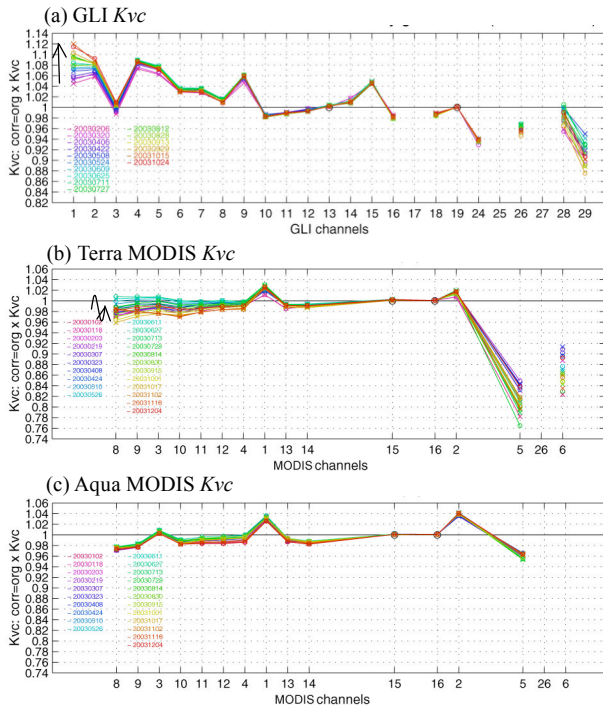


Figure 2  $K_{vc}$  for GLI (a), Terra MODIS (b), and (c) Aqua MODIS channels. Processed dates (15 days for GLI, 26 days for MODIS) are listed in each panel. Arrows show temporal change (see text).

TABLE 1  
GLI AND MODIS VN AND SW CHANNELS

GLI		MODIS	
CH (IFOV m)	band [width] nm	CH (IFOV m)	Band [width] nm
1	380 [10]		
2	400 [10]		
3	412 [10]	8	415 [15]
4	443 [10]	9	443 [10]
20 (250)	460 [70]	3 (500)	470 [20]
5	460 [10]		
6	490 [10]	10	490 [10]
7	520 [10]	11	531 [10]
8	545 [10]	12	551 [10]
21 (250)	545 [50]	4 (500)	555 [20]
9	565 [10]		
10	625 [10]		
11	666 [10]	13	667 [10]
12	680 [10]	14	681 [10]
22 (250)	660 [60]	1 (250)	659 [50]
13	678 [10]		
14	710 [10]		
15	710 [10]		
16	749 [10]	15	750 [10]
17	763 [8]		
18	865 [20]	16	865 [15]
23 (250)	825 [110]	2 (250)	865 [35]
19	865 [10]		
24	1050 [20]		
25	1135 [70]		
26	1240 [20]	5 (500)	1240 [20]
27	1380 [40]	26	1375 [30]
28 (250)	1640 [200]	6 (500)	1640 [24]
29 (250)	2210 [220]	7 (500)	2130 [50]

coefficients based on the fixed two NIR channels (i.e., set  $K_{vc}$  to 1.0 for the channels).

### 2.2 Global Averages of $K_{vc}$

Global averages of  $K_{vc}$  are shown in Fig. 2. Almost of the  $K_{vc}$  were stable during the 2003 except that GLI  $K_{vc}$  at channels 1, 2 and 3 increased about 7%, 4%, and 2% respectively (arrow in Fig, 2a), and Terra MODIS  $K_{vc}$  in channels 8 to 12 changed about 3% (arrow in Fig, 2b). Aqua MODIS  $K_{vc}$  looks more stable than Terra MODIS and GLI.

### 2.3 Latitude and Scan-mirror Incident Angle Dependencies of $K_{vc}$

Distributions of  $K_{vc}$  on latitude ( $Lat$ ) and scan mirror incident angle ( $\varphi$ ) are shown in Fig. 3. GLI  $K_{vc}$  at channel 1 changes with  $\varphi$  (arrow in Fig.3a).  $K_{vc}$  of Terra MODIS show a pattern related with sunglint position (broken curve in Fig. 3c). We found that the  $K_{vc}$  pattern changed according to seasonal movement of the sunglint location.

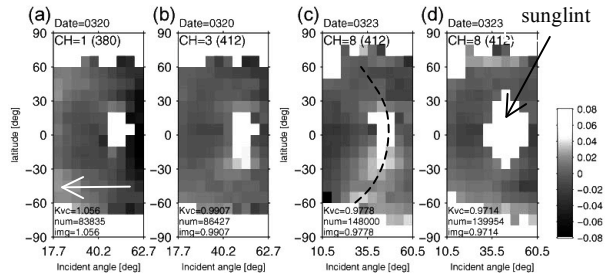


Figure 3 Lat and  $\varphi$  dependencies of  $K_{vc}$  (a) GLI CH1 (380nm) in 20 March 2003, (b) GLI CH3 (412nm) in 20 March 2003, (c) Terra MODIS CH8 (412nm) in 23 March 2003, and Aqua MODIS CH8 in 23 March 2003.

### 3. Comparison among GLI, MODIS and SeaWiFS chlorophyll-a products

We processed chlorophyll-a concentration (CHLA) using GLI, Terra MODIS and Aqua MODIS L1B data by the same ocean-color algorithm (GLI standard algorithm) and the  $K_{vc}$  which considers  $\varphi$  and observation days. CHLA histograms of Terra MODIS (NASA V004, solid line in Fig. 4a) and Aqua MODIS (NASA V003, broken line) are different from one of SeaWiFS (gray area) in high and low CHLA ranges. After using the  $K_{vc}$ , they agree well (Fig. 4b). GLI CHLA seems to be too high in low CHLA range (dotted broken line in Fig 4b), which may be caused from the fixed  $K_{vc}$  at two NIR channels or wavelength difference used in the in-water algorithm. Aqua MODIS by IOCCG (*OceanColor Web*) agrees with SeaWiFS very well (dotted broken line in Fig. 4a).

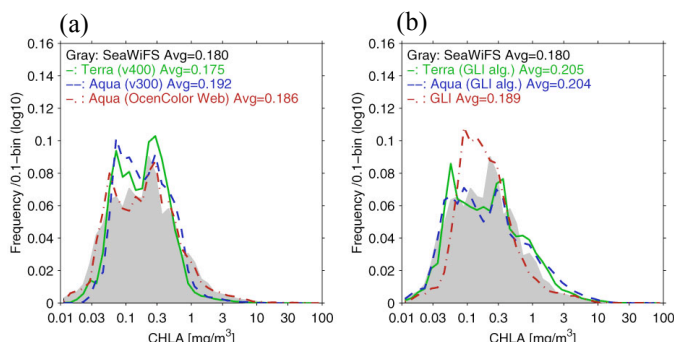


Figure 4 Histograms of SeaWiFS, MODIS and GLI CHLA. Left panel (a) shows NASA MODIS product, right (b), ones using  $K_{vc}$  and the same ocean-color algorithms (basing GLI standard algorithms).

### 4. Conclusion and Remarks

The vicarious calibration results and data comparisons show that GLI has scan-angle dependency and its temporal change in UV and blue channels. We fixed  $K_{vc}$  at two NIR channels to 1.0; however, we should better to know the  $K_{vc}$  of the NIR channels by some independent ways, e.g., in-situ aerosol observation, moon calibration, or in-orbit calibrations. Terra MODIS  $K_{vc}$  showed temporal changes and dependency on the sun-glint location. They may include characteristics of our  $L_{TOA}$  simulation; however difference among the results is assumed to indicate characteristics of each sensor and L1B product.

Consistency could be improved among ocean-color products of SeaWiFS, GLI, Terra MODIS and Aqua MODIS by the vicarious calibration and consistent ocean-color algorithms; attained to a level for rough or pattern comparison. However, we need to investigate the remaining issues to make the consistent data sets enough for the combined use.

### Reference

- [1] H. Murakami, M. Yoshida, K. Tanaka, H. Fukushima, M. Toratani, A. Tanaka, and Y. Senga, Vicarious calibration of ADEOS-2 GLI visible to shortwave infrared bands using global datasets, *IEEE Trans. Geosci. Remote Sensing*, submitted, 2004
- [2] H. Fukushima and R. Frouin, GLI algorithm description (ATBD), Atmospheric Correction for Ocean Color, [Online]. Available: <http://suzaku.eorc.jaxa.jp/GLI/ocean/algorithm/index.html>.
- [3] T. Nakajima, and M. Tanaka, Matrix formulation for the transfer of solar radiation in a plane-parallel scattering atmosphere, *J. Quant. Spectrosc. Radiat. Transfer*, 35, 13-21, 1986.
- [4] T. Nakajima, and M. Tanaka, Algorithms for radiative intensity calculations in moderately thick atmospheres using a truncation approximation, *J. Quant. Spectrosc. Radiat. Transfer*, 40, 51-69, 1988.
- [5] K. Stamnes, S.-C. Tsay, W. Wiscombe, and K. Jayaweera, Numerically stable algorithm for discrete-ordinate-method radiative transfer in multiple scattering and emitting layered media, *Appl. Opt.*, 27, 2502-2509, 1988.
- [6] B. G. Mitchell and M. Kishino, *GLI algorithm description (ATBD) GLI in-water algorithms*. [Online]. Available: <http://suzaku.eorc.jaxa.jp/GLI/ocean/algorithm/index.html>.
- [7] A. Tanaka, M. Kishino, R. Doerffer, H. Schiller, T. Oishi and T. Kubota, Development of a Neural Network Algorithm for Retrieving Concentrations of Chlorophyll, Suspended Matter and Yellow Substance from Radiance Data of the Ocean Color and Temperature Scanner, *Journal of Oceanogr.*, Vol. 60 (No. 3), pp. 519-530, 2004.

# A satellite cross-calibration experiment

Jens Nieke<sup>#a, e</sup>, Teruo Aoki<sup>b</sup>, Tomonori Tanikawa<sup>c</sup>, Hiroki Motoyoshi<sup>d</sup>, Masahiro Hori<sup>e</sup>

<sup>a</sup> Remote Sensing Laboratories, University of Zurich, CH-8057 Zürich, Switzerland

<sup>b</sup> Meteorological Research Institute, Tsukuba, Ibaraki 305-0052, Japan

<sup>c</sup> University of Tsukuba, Tsukuba, Ibaraki, 305-8572, Japan

<sup>d</sup> Space Service, Tsukuba, Ibaraki, 305-0028, Japan

<sup>e</sup> JAXA, Earth Observation Research Center (EORC), Tokyo 104-6023, Japan

## ABSTRACT

ADEOS-2 was launched (Dec 14<sup>th</sup> 2002) successfully and the Global Imager (GLI) onboard the ADEOS-2 satellite became operational from April 2003. In a first calibration check-up, the radiometric performance of GLI was compared relatively to that of other sensors on different satellites with different calibration backgrounds. As calibration site a large snowfield near Barrow (Alaska, USA) was used, where space sensors in polar orbits view the same ground target on the same day with small differences in the local crossing times. This is why GLI, MODIS (Terra, Aqua), SeaWiFS, AHVRR (N16, N17), MERIS and AATSR data sets were selected for the following clear-sky condition days: April 14<sup>th</sup> and 26<sup>th</sup> 2003. At the same time ground-truth experiments, e.g., measurements of ground reflectance, BRDF, aerosol optical thickness (AOT), were carried out. Thereinafter, top-of-atmosphere (TOA) radiance/reflectance was forward calculated by means of radiative transfer code (RTC) for each sensor, each band and each day. Finally, the vicariously retrieved TOA signal was compared to TOA sensor Level 1B (L1B) data. As a result, GLI's performance is encouraging at that time of the mission. GLI and the other 7 sensors deliver similar sensor output in the range of about 5-7 % around the expected vicariously calculated TOA signal.

## 1. INTRODUCTION

The multi-channel optical whiskbroom scanner GLI [1,2] was launched successfully on ADEOS-2 satellite in December 2002. GLI provided highly needed data of the Earth surface in the spectral region from 0.38–12  $\mu\text{m}$  for a better understanding of the environment in global and regional scale.

Earth observation data require a careful calibration of the sensor and validation of the algorithms to demonstrate the reliability of the data products at the required accuracy, such as described in [3]. Consequently the calibration of the GLI is one of the key parts in the sensor design, and efforts are made to check the sensor before launch (pre-launch calibration) and during mission duration time (on-board and vicarious and cross calibration methods). From launch until the failure of the ADEOS-2 satellite (Oct 24 2003), GLI was in the Calibration and Validation (CalVal) phase. In the CalVal phase, which generally ends 12 months after launch, the sensor output have to be checked rigorously using different CalVal techniques before the GLI data will be made available to the remote sensing user community. Besides on-board e.g., solar, lamp, blackbody) and vicarious (e.g., desert sites, ocean sites) calibration, the comparison with other space sensors delivers a better understanding of GLI's performance. In the following an approach in described to make use of simultaneous observations of space sensors on different satellites combined with ground-truth experiments performed during the satellites overflights. The selected space sensors have some similarity with GLI in respect of the spectral, spatial, and radiometric characteristics. These sensors were observing almost at the same time a ground target, where simultaneous ground-truth measurements are performed.

The capability of this cross-calibration approach over snowfields has been demonstrated recently in a case study for a SeaWiFS-MERIS inter-comparison [4]. At that time only ground-truth data was taken into account, which describe the

---

<sup>#</sup> corresponding author: nieke@geo.unizh.ch; phone/fax: +41 1 635 5260/6846

Please note, parts of this paper were recently published in Nieke et al., IEEE GRSL, 1, 3, 2004

atmospheric conditions.

In this paper the cross-calibration approach was improved performing additional ground-truth reflectance measurements. For April 14<sup>th</sup> and 26<sup>th</sup> 2003, GLI L1B data sets were successfully compared with L1B data sets of MODIS (Terra, Aqua), SeaWiFS, AHVRR (N16, N17), MERIS and AATSR over a large snowfield close to Barrow, Alaska, USA. At the same time a ground-truth campaign at Barrow delivered a good in-situ site description during the overflights of the satellites.

## 2. GROUND-TRUTH EXPERIMENT AT BARROW, ALASKA (APRIL 14th / 26th 2003)

### 2.1 Basic approach

The data sets from different sensors, such as GLI, MODIS, SeaWiFS, AHVRR (N16, N17) and MERIS/AATSR were used for this inter-comparison. These sensors are onboard different spacecrafts (ADEOS-2, Terra, Aqua, ENVISAT, Orbview-2/SeaStar, NOAA-16, NOAA-17) and passed the CalVal site at Barrow, Alaska, at least once during the ongoing ground-truth experiment. During the ground-truth campaign, various measurements were carried out, such as spectral ground reflectance, BRDF and AOT measurements.

Both, ground and satellite data were input data in a Radiance Transfer Code (RTC). As RTC a slightly modified version of the 6S code [5] was used. The modifications in the 6S code consist mainly of supplementary subroutines to account for updated solar irradiance [6] and spectral response functions, such as those of the above mentioned space sensors.

Using the ground-truth data the TOA radiance and reflectance for each sensor and each channel was calculated forwardly for each overpass. The resulting calculated TOA data were compared with the measured satellite sensor data.

### 2.2 Satellite data

Satellite sensor data of the following 7 space sensors were inter-compared:

- (1) GLI onboard ADEOS-2; pre-launch calibrated (launched Dec. 2002),
- (2) MODIS onboard Terra; operational L1B TOA reflectance/radiance data (launched Dec. 1999),
- (3) MODIS onboard Aqua; operational L1B TOA reflectance/radiance (launched May 2002),
- (4) AVHRR/3 onboard NOAA-16; L1B using MODIS-based calibration coefficients [7] (launched Sep. 2000),
- (5) SeaWiFS onboard Orbview-2/SeaStar; L1B retrieved from L1A with SeaDAS 4.4 (launched Aug. 1997),
- (6) AVHRR/3 onboard NOAA-17; pre-launch calibration (launched May 2002),
- (7) MERIS and AATSR onboard ENVISAT; operational L1B TOA radiance/reflectance (launched Mar. 2002).

### 2.3 Geometric Information

For the analysis the period from 22:35 – 23:33 (14<sup>th</sup>) and 21:41 – 23:19 (26<sup>th</sup>) was selected. Unfortunately, there was no MODIS (Terra) data set available for the 14<sup>th</sup>, same for the 26<sup>th</sup> SeaWiFS data set. On April 14<sup>th</sup> 2003, the apparent sunrise was at 14:17, the sunset at 6:40 (April 15<sup>th</sup>), solar noon at 22:26. For the 26<sup>th</sup>, these values change slightly to 14:08 (apparent sunrise), 22:24 (solar noon) and 6:45 sunset at April 27<sup>th</sup>. Note, that the 6S RTC is limited to 60° for viewing and 70° for solar zenith angles. Larger zenith or viewing angles may cause additional uncertainties due to plane parallel approximation of the atmosphere in the 6S code.

The CalVal site is located close to the Barrow observation site from NOAA. It is a horizontal field at the north slope of Alaska. For this approach a site with a size of 2 x 2 km<sup>2</sup> was selected having the center point at 71.31° N and 156.63° W. Additionally a macro site of 5.6 x 5.6 km<sup>2</sup> was used for uniformity check of the L1B data.

### 2.4 Calibration Coefficients

The comparison was mainly performed on the basis of TOA radiance or reflectance, depending on what kind of product was delivered by the different projects:

**GLI** was in operational mode from April until October 2003. For the comparison L1B data with pre-launch calibration factors were used. No further correction factors were applied, such as differences of the mirror sites or any degradation factors. Note, it was the objective of this analysis to check the radiometric performance of GLI in comparison with other space sensors.

**MODIS (Terra)** was launched in Dec. 1999 and the data was calibrated and validated recently. An overview of the performance is given in [8]. Whereas the Terra satellite is flown on a descending node during daytime, a similar instrument, **MODIS (Aqua)**, delivers daytime observation data in the ascending node. The Aqua satellite was

launched in May 2002 [9] .

**MERIS/AATSR** are onboard the ENVISAT, which was launched in Mar. 2002. At the time of the previous cross-calibration MERIS was in the commissioning phase. Now, MERIS and AATSR data products are considered to be calibrated and validated [10, 11].

**SeaWiFS** has a much longer and rigorous calibration history, such as described in [12] for the direct methods and in [13] for the vicarious methods. SeaWiFS is an ocean color mission and the calibration for ocean targets (dark signals) are retrieved vicariously over the MOBY site close to Hawaii. The vicarious calibration at MOBY is not applied to SeaWiFS's land and cloud measurements. The calibration for these bright targets is retrieved via direct calibration methods, i.e. not vicariously. The SeaWiFS project does not deliver Level 1B data as a standard product. This is why Level 1A data were processed using the code SEADAS 4.4 [14]. It delivers the required L1B data format as an optional output in TOA radiance.

Also for the **AHVR** sensors, there exists a long calibration history from early NOAA missions to the most recent NOAA-16 and NOAA-17 missions. The TOA reflectance and radiance for NOAA-16 were calculated using updated calibration coefficients provided by [7] recently. For NOAA-17 the pre-launch calibration factors were used [15]. For the TOA radiance representation the visible channel information for effective wavelengths, equivalent width and solar irradiance based on [16] were used.

## 2.5 Ground-Truth Data

The CalVal site is a large snow field in Alaskan tundra located about 5 km northeast of Barrow town and 2 km south of the NOAA's Climate Monitoring & Diagnostics Laboratory (CMDL).

From April 11<sup>th</sup> until April 27<sup>th</sup> a CalVal campaign in the scope of the ADEOS-2 project was carried out. The site and the type of measurements performed at the site were described in detail recently [17,18]. The results of this campaign are summarized in the following for parameters, which are relevant for this cross-calibration approach:

The CalVal site is a large horizontal flat snow field of 2 x 2 km<sup>2</sup>. The center point of the field is located at 71.31° N and 156.63° W, additionally a larger macro site (5.6 x 5.6 km<sup>2</sup>) around the CalVal site was selected to perform uniformity checks of the satellite signal by comparing the TOA L1B of the CalVal site with those signal (and its deviation) retrieved from the macro site.

The spectral reflectance measurements were performed using an FieldSpec FR (ASD Inc.). The reflectances of the selected days (April 14<sup>th</sup> and 26<sup>th</sup>) differ slightly, caused by differences in the snow grain size. An average spectrum for each day's CalVal period was used as RTC input.

For the aerosol optical thickness was retrieved using the measurements of a Prede 'Skyradiometer'. The AOT varies between the days, since the atmospheric conditions were different. Additionally, spectral reflectance and BRDF measurements on ground were carried out. As showed in [18], the characteristics of a snow site is not entirely Lambertian over the entire spectral range. For the sun-observer-viewing geometry during the satellite over flights no correction must be applied in the visible spectral range. In the NIR and short-wave infrared larger corrections must be taken under consideration, especially regarding large viewing angles.

Additional local weather information and data from the U.S. Department of Energy's Atmospheric Radiation Measurement Program (ARM) and CMDL site was taken into account to inter-compare and validate the measurement results performed at the CalVal site.

## 2.6 Algorithm

Both, satellite and ground-truth data are input data for radiative transfer modeling. As RTC, the inter-satellite calibration algorithm uses currently a slightly modified version of the 6S code [5]. From the satellite data the geolocation information, such as sun and viewing angles, is retrieved for each passing time of each satellite sensor.

The atmospheric input parameters for the RTC were defined using the AOT (measurements) and the aerosol components (assumptions) and taking additional atmospheric data into account (such as H<sub>2</sub>O, Ozone contents). For the aerosol components a typical composition of 2.85 % dust-like, 12.85 % oceanic, 70 % water-soluble components and 14.3 % soot components was assumed [19] for the 26<sup>th</sup> April. This composition could be confirmed with skyradiometer measurements at scattering angles of 5°, 7°, 10°, 15°, 20°, 25°, and 30°. However, measurements performed during 14<sup>th</sup> April showed a lower imaginary part of the refraction index indicating that less absorbing aerosols could be found in the boundary layer. Using additional information from ARM Mircopulse Lidar (MPL) measurements, a thin homogenous cirrus layer could be identified [20]. This non-visible cirrus layer caused higher AOT, but since placed on the top of the boundary layer, the cirrus results in an offset in the TOA reflectance. However, the influence on the results for relative

cross-calibration is considered to be small, since the AOT measurements and MPL response (ARM measurements) were homogeneous during the observation time from 21:41 to 23:19. Also the spectral influence of the cirrus is small assuming constant spectral reflectance in the visible (ice cloud).

## **2.7 Results and error estimation**

To provide an inter-satellite comparison relatively to the space sensors under consideration, the ratio of L1B TOA to ground-truth modeled TOA data was calculated and plotted versus the center wavelength of each sensor channel.

Keeping in mind that the error budget for each of the sensors is in the range of 5 % and that the method has an inherent error of 5 % for a single comparison, all satellite sensor L1B data are in the limits of the error bars.

However, the following tendency becomes obvious:

GLI's performance is encouraging at this early point of the mission (GLI was operational from April 2003). There is an excellent agreement in the visible (channel 7/8 and 13). Chan-1 and Chan-19 seem to be too low, however the deviation between the calibration days is significant.

For the other space sensors, the following tendency becomes "interesting", when looking at the results for MODIS Aqua, AATSR and AVHRR chan-1 are located at the upper limit of the range and MODIS Terra (together with GLI) are at the lower limit. MERIS and SeaWiFS seem to have a similar performance (with MERIS a bit higher than SeaWiFS) and are located in the center of the range. AVHRR chan-2 is more difficult to assess, since this channel has a broad spectral bandwidth ( $\Delta\lambda > 200$  nm) in a spectral region where snow reflectance is decreasing.

## **2.8 Accuracy of the method:**

The accuracy of a single satellite inter-calibration depends mainly on the accuracy of the space sensor (4 – 5 %), which will be used as a reference calibration source. Further uncertainties are the measurement accuracy (e.g., uniformity of the site, positioning accuracy) and uncertainties from atmospheric modeling and assumptions (e.g., change of atmospheric conditions, atmospheric characterization, and correction for viewing angle differences). Hence, the RMS error of a single inter-satellite comparison is in the range of 5 – 6.6 %. Assuming this error budget, all 12 L1B data sets used in this satellite inter-calibration are within the error bars of the sensors' calibration accuracies and the uncertainties of this vicarious calibration approach.

## **3. CONCLUSION**

For the 12 data sets this comparison showed, that all TOA radiances are within the error bars of the sensors' calibration accuracies and the uncertainties of this vicarious calibration approach. However, a tendency in the data sets was recognized: GLI and MODIS (Terra) seem slightly underestimate the snow site and AATSR, MODIS (Aqua) and AVHRR Chan-1 are slightly overestimating the same site. In the center SeaWiFS and MERIS are close to the predicted TOA values, whereas MERIS seems slightly higher than SeaWiFS. AVHRR chan-2 is difficult to assess since the channel has a broad spectral bandwidth of  $\Delta\lambda > 200$  nm.

Concluding, it was an encouraging result for GLI at that point of the mission: Using the pre-launch calibration factors GLI delivers comparable results to other space sensor in the visible and near infrared.

These results are currently compared with other CalVal technique results, such as the on-board (solar, lamp) and vicarious (e.g., desert sites, ocean sites) calibration, such as described in [21,22]. This ongoing comparison will deliver a better understanding of GLI's performance and the limitations of the various CalVal techniques.

## **ACKNOWLEDGEMENT**

The authors would like to thank NASA's SeaWiFS Project, Distributed Active Archive Center, Brent Holben (PI Aeronet site at Barrow), C.R. McClain (SeaDAS code), E. Vermote (6S code), ESA, Brockmann Consulting, U.S. Department of Energy (DOE) and NOAA's Satellite Active Archive and Climate Monitoring and Diagnostics Laboratory for the production and distribution of data and codes used in this paper, respectively.

The authors want also to express their appreciation for considerable help of the GLI calibration-working group (leader: Prof. Y. Senga) and the ADEOS-2 project team. Last but not least the authors would like to acknowledge the support and help from various collaborators, such as Rune Stovold, Hans Eide, Yasuko Iizuka, and Yukinori Nakajima.

## REFERENCES

- [1] T.Y. Nakajima, T. Nakajima, M. Nakajima, H. Fukushima, M. Kuji, A. Uchiyama, M. Kishino, "Optimization of the Advanced Earth Observing Satellite (ADEOS) II Global Imager (GLI) channels by use of radiative transfer calculations", *Appl. Opt.* 37, 15, pp. 3149–3163 (1998)
- [2] <http://sharaku.eorc.nasda.go.jp/GLI/> (JAXA's GLI homepage at the EORC server)
- [3] IOCCG Report Number 3, "Remote Sensing of the ocean colour in coastal, and other optically-complex waters", edited by S. Sathyendranath, in reports of the international ocean-colour coordinating group (2000)
- [4] J. Nieke, M. Hori, R. Höller, I. Asanuma, T. Aoki, "Satellite sensor inter-calibration; A case study", ENVISAT Validation Workshop, 9<sup>th</sup> – 13<sup>th</sup> Dec. 2002 in Frascati, Italy; and published in Workshop proceedings [URL: [envisat.esa.int/workshops/validation\\_12\\_02/proceedings/meris/06\\_nieke.pdf](http://envisat.esa.int/workshops/validation_12_02/proceedings/meris/06_nieke.pdf)], pp. 1-10 (2003)
- [5] E. Vermote, D. Tanre, J.L. Deuze, M. Herman, J.J. Morcrette, "Second simulation of the satellite signal in the solar spectrum '6S': An overview", *IEEE Trans. Geosci. Remote Sens.*, Vol. 35, pp. 675-686 (1997)
- [6] G. Thuillier, M. Herse, D. Labs, T. Foujols, W. Peetermans, D. Gillotay, P. C. Simon, and H. Mandel, "The solar spectral irradiance from 200 to 2400 nm as measured by the SOLSPEC spectrometer from the ATLAS and EURECA missions", *Solar Physics* 214, pp. 1-22 (2003)
- [7] A. Heidinger, C. Cao, J. Sullivan, "Using MODIS to calibrate AVHRR reflectance channels", *Journal of Geophysical Research*, Vol. 107, No. D23, 4702 (2002)
- [8] B. Guenther, X. Xiong, V. Salomonson, W. Barnes, J. Young, "On-orbit Performance of the Earth Observing System Moderate Resolution Imaging Spectroradiometer; First Year of Data", *Remote Sensing of the Environment*, Vol. 83, pp. 16-30 (2002)
- [9] X. Xiong, V. Chiang, J. Sun, W. Barnes, "Aqua MODIS first year on-orbit calibration and performance", *SPIE*; Vol. 5234 (2003)
- [10] D. Smith, "AATSR 1st Year calibration results", Working meeting on MERIS and AATSR Calibration and Geophysical Validation (MAVT-2003) ESRIN, Frascati, Italy, 20-24 October 2003 (2003)
- [11] S. Delwart, L. Bourg, J. Huot, "MERIS 1<sup>st</sup> Year: early calibration results", *SPIE*, Vol. 5234 (2003)
- [12] R.A. Barnes, R.E. Eplee, G.M. Schmidt, F.S. Patt, C.R. McClain, "The calibration of SeaWiFS. I direct techniques", *Appl. Opt.* 40, pp. 6682-6700 (2001)
- [13] R.E. Eplee, W.D. Robinson, S.W. Bailey, D.K. Clark, P.J. Werdell, M. Wang, R.A. Barnes, C.R. McClain, "The calibration of SeaWiFS. II vicarious techniques", *Appl. Opt.* 40, 6701-6718 (2001)
- [14] SeaDAS homepage at URL: <http://seadas.gsfc.nasa.gov> (last visit: May 2003)
- [15] NOAA Meteorological Satellite Page at URL: [http://orbit-net.nesdis.noaa.gov/crad/sit/page\\_of\\_pages.html](http://orbit-net.nesdis.noaa.gov/crad/sit/page_of_pages.html) (last visit: May 2003)
- [16] H. Neckel and D. Labs, "The solar radiation between 3300 and 12500 Å", *Sol. Phys.* 90; pp. 205-258 (1984)
- [17] Te. Aoki, Ta. Aoki, M. Fukabori, Y. Tachibana, Y. Zaizen, F. Nishio, T. Oishi, "Spectral Albedo Observation on the snow field at Barrow, Alaska", *Polar Meteorol. Glaciol.*, 12, pp. 1-9 (1998)
- [18] Te. Aoki, Ta. Aoki, M. Fukabori, A. Hachikubo, Y. Tachibana, F. Nishio, Effects of snow physical parameters on spectral albedo and bidirectional reflectance of snow surface, *Journal of geophysical research*, 105, D8, pp. 10219-10236 (2000)
- [19] S. Ohta, personnel communication (2003)
- [20] ARM at URL: [http://nanuma.gi.alaska.edu/qlview.html?qlurl=products/nsa/gif/nsamplhrC1.a1/mpl\\_tz/20030426.gif](http://nanuma.gi.alaska.edu/qlview.html?qlurl=products/nsa/gif/nsamplhrC1.a1/mpl_tz/20030426.gif) (last visit: July 2003)
- [21] H. Murakami, K. Tanaka, S. Kurihara, Y. Okamura, J. Inoue, J. Nieke, I. Asanuma, H. Yatagai, Y. Mitomi, M. Yoshida, R. Higuchi, S. Kawamoto, K. Isono, and Y. Senga; GLI early calibration results for oceanographic applications, to be published in *SPIE* Vol. 5155 (2003)
- [22] M. Yoshida, Y. Mitomi, Y. Senga, Murakami, I. Asanuma, H., S. Kurihara, K. Sasaoka, K. Sato, Early phase evaluations of GLI vicarious calibration factors for ocean color channels, to be published in *SPIE* Vol. 5155 (2003)

## Abstract Sheet - Abstract number: 6

Author Name: Nieke, Jens  
Organisation: University of Zurich  
Country: SWITZERLAND  
Authors: Nieke, Jens, University of Zurich, SWITZERLAND (P)  
Kaiser, Johannes, University of Zurich, SWITZERLAND  
Schlaepfer, Daniel, University of Zurich, SWITZERLAND  
Itten, Klaus, University of Zurich, SWITZERLAND  
Schaeppman, Michael, University Wageningen, NETHERLANDS  
Topic: 2 Hyperspectral imaging instruments calibration an

### Advanced Calibration Concept of APEX

APEX is a dispersive pushbroom imaging spectrometer operating in the spectral range between 380 - 2500 nm. The spectral resolution will be better than 10 nm in the SWIR and < 5 nm in the VNIR range of the solar reflected range of the spectrum. The total FOV will be  $\pm 14$  deg, recording 1000 pixels across track with max. 300 spectral bands simultaneously.

A large variety of characterisation measurements will be performed in the scope of the APEX project, e.g., on-board characterisation, frequent calibration home base, and vicarious calibration.

These characterisation measurements are combined in the Processing and Archiving Facility (PAF) of APEX. It performs the transformation of raw data to calibrated Level1 products. This includes the radiometric, spectral and geometric data calibration and the calculation of the required, time-dependent calibration coefficients from the calibration measurements. Because of the heterogeneity of the characterisation measurements, the optimal calibration for each data set can not be achieved using standard methods.

In the paper the different characterization measurements, the PAF and the new data assimilation algorithm will be outlined.

# Inter-comparison of atmospheric data using the Basic Envisat Atmospheric Toolbox

S.V. Niemeijer<sup>(1)</sup>

<sup>(1)</sup>Science and Technology BV  
Mijnbouwplein 11  
2628 RT Delft - The Netherlands  
Email:niemeijer@science-and-technology.nl

*The Basic Envisat Atmospheric Toolbox (BEAT) is a software toolbox funded by ESA that considerably simplifies the analysis and comparison of atmospheric earth observation data. Due to the complex data contents and wide variety of formats, researchers usually have to spend a large amount of time writing and testing routines for reading data from product files. By using the ingestion functionality from BEAT these efforts can be greatly reduced. BEAT provides the user with a single abstract interface that is able to ingest data from a wide range of different product files. Through user-defined selection criteria (on e.g. time, earth location, altitude, etc.) the data ingestion process can be further tuned to read only a subset of the available data. BEAT currently supports access to product files ranging from level 0 to level 4 and for instruments such as GOMOS, MIPAS, SCIAMACHY, GOME, TOMS, and OMI. Support for even more types of product files will be added in the future. The BEAT functionality is accessible via traditional programming languages such as C and Fortran but can also be used directly from within well-known applications such as IDL and MATLAB. The toolbox runs on a wide variety of platforms and is provided free of charge. Furthermore, BEAT is distributed as open source software, which makes it possible for users to reuse and extend the source code for their own applications.*

## INTRODUCTION

In the field of earth observation one of the primary focus areas is the research into the composition and dynamics of the atmosphere. Over the past years, several atmospheric measurement instruments have been constructed to this end. Some of these instruments measure from the ground, others from balloons or airplanes, but the most popular – because they can cover a large area of the world – are the ones that are hosted on satellites. Each of these instruments provides measurement data that can be used to retrieve the concentration of constituents in the atmosphere at a certain time and location. In order to get a full global view of the state of the atmosphere, one cannot just rely on atmospheric instrument data. There is simply not enough instrument data available to look up the concentration for each constituent at every location and point in time. Therefore, scientists use a combination of models and atmospheric instrument data to construct a view of the state of the atmosphere. Of course, the quality of the measurement data provided by the atmospheric instruments highly influences the final results. Therefore it is important to get a good characterization of the quality of the data coming from such an instrument.

Furthermore, for most methods that assimilate measurement data into the models, error estimates on measured data play a crucial role. Thus, when determining the quality of instrument data the error information should also be taken into account.

One of the ways to get an indication of the quality of the data is by comparing the retrieved data with data obtained from other atmospheric instruments. In order for a scientist to exercise such a comparison, usually some pre-processing steps have to be performed. These pre-processing steps consist of reading the required data from one or more product files and converting the data into a form that can be used to compare it with data from the other instrument (and for this other data usually similar pre-processing steps have to be performed). Because of the complexity of some data product formats this pre-processing can be a time consuming and error prone activity. In this article we will show how the Basic Envisat Atmospheric Toolbox (BEAT) [1] can be used to dramatically reduce the effort required to perform these reading and data restructuring steps.

## THE BASIC ENVISAT ATMOSPHERIC TOOLBOX

The Basic Envisat Atmospheric Toolbox is an ESA funded software toolbox that provides a series of functional components that help scientists read, analyze, and visualize data from any of the atmospheric instruments on board the Envisat satellite [2]. There are three atmospheric instruments flying on Envisat: the star occultation instrument GOMOS, the limb sounding Michelson interferometer MIPAS, and SCIAMACHY, a limb/nadir viewing spectrometer.

One of the primary reasons for the development of BEAT was to provide easy access to the data products for each of the atmospheric instruments. ESA provides both Level 1 data products containing annotated – and often calibrated – spectral readouts, and Level 2 products containing total column and/or profile retrievals for one or more species. The data format for these products was a totally new format and therefore there was a lack of a direct product reading library (such as available for other data formats, e.g. HDF [3] and netCDF [4]). To fill this gap, the first functionality that was included in BEAT was such a direct product interface, which also forms the heart of the toolbox. On top of this direct product interface a data abstraction layer was implemented. This layer provides advanced data ingestion functionality, such as reading from multiple files using a single operation and applying basic selection criteria to limit the range of data that should be read. This second layer also provides a means to more easily compare data coming from different instruments. Because of this two-layer approach, the direct product interface is sometimes also referred to as Layer 1 or BEAT-I and the data abstraction interface as Layer 2 or BEAT-II. Both layers are implemented as libraries using the C programming language. On top of these C libraries interfaces were developed to access the BEAT functionality from other programming languages such as Fortran and Python [5], and from popular commercial data analysis applications such as IDL [6] and MATLAB [7].

The Basic Envisat Atmospheric Toolbox also comprises an analysis and visualization application called VISAN. This application can be seen as the third layer of BEAT. The VISAN application is provided to users as a free and very basic alternative to commercial data analysis applications such as IDL and MATLAB. Just as its commercial big brothers, VISAN is also based around a command language (the Python scripting language). Using this language one can ingest product data, perform analysis, and create visualisations.

An important feature of BEAT (including VISAN) is that it is provided as open source software. This has several advantages for scientists: they will be able to inspect and verify the source code of the toolbox in case they suspect erroneous behaviour, they can borrow parts of the toolbox source code in order to use it in their own applications, or, in case they find some functionality missing, they can extend the toolbox with source code of their own. Furthermore, BEAT is a cross-platform toolbox. Even though it already works on a wide range of platforms, its open source nature makes it possible to adapt it so it can be run on even the most specialized platforms (such as supercomputer systems).

In this paper we will discuss all three layers of BEAT. However, since BEAT-II is the layer that contains the most interesting facilities to simplify the process of instrument inter-comparison, we will primarily focus on this abstract data layer.

## **DIRECT PRODUCT INTERFACE**

The data products for the Envisat satellite are distributed as files using a hybrid ASCII/binary data storage format. Each data file contains a header section with annotation data in ASCII format, followed by one or more data sets (DS) in a raw (i.e. uncompressed) binary format. Each data set contains one or more data set records (DSR) and can contain measurement data, geolocation information, or annotation data.

Data files are categorized by their product type, each of which has a 10 character identifier. The first 3 of these characters indicate which instrument the data comes from (or AUX in case of auxiliary data products). Examples are MIP\_NL\_\_1P (MIPAS nominal level 1 product), GOM\_NL\_\_2P (GOMOS nominal level 2 product), and SCI\_OL\_\_2P (SCIAMACHY offline level 2 product). For each product type there exists a fixed product format definition that the data files should follow. The structural layout of an Envisat data file is not included in the files itself (as is the case for self-describing data formats such as HDF or XML [8]). This means that, in order to be able to read data from a file, a reading routine needs to have knowledge of this data storage definition. This aspect has been the basis of the BEAT direct product interface. In order to interpret each data file, the BEAT-I library consists of a built-in database of over 70 product file descriptions. This database, called the Data Dictionary, uses a tree-like structure to describe a product where compound types, such as arrays and records form the branches, and basic types, such as doubles, integers, etc. form the leaves. Since arrays (such as data sets, which can be considered arrays of DSRs) can have a variable size, some steps are usually necessary to calculate the array sizes and file offsets of data elements. These calculations can be based on other data inside the product (that contains information about e.g. number of DSRs, number of measurements, number of retrieved species, number of retrieval heights, etc.). Instead of hard-coding these calculations and dependencies in the source code, this information is included in the Data Dictionary in the form of expressions that can be evaluated at runtime. This approach has made it possible to keep the product reading code of the BEAT-I library very generic. This in turn had another advantage, which was that it made it possible to support all 60+ level 0, level 1, level 2 and auxiliary product files for GOMOS, MIPAS, and SCIAMACHY with a relatively moderate implementation effort (only Data Dictionary descriptions had to be constructed, no product specific source code was needed). Furthermore, the generic approach also makes it possible to support non-Envisat products in BEAT as long as these files are stored in either a raw binary format or a structured ASCII format. For example the current version of BEAT

also supports both the binary and ASCII versions of the GOME level-1 and level-2 products (which are stored in a format very different from the Envisat data files).

Another advantage of the Data Dictionary approach is that it allows for automatically generated product format specification documentation. This functionality has also been included in BEAT, and the result is that the Data Dictionary documentation in HTML that comes with the BEAT package is, because it is generated, always 100% consistent with the reading functionality provided by the library.

Finally, the Data Dictionary also contains meta-data such as unit information and descriptions about each data element. This information is included in the generated Data Dictionary documentation but can also be retrieved at runtime using one of the BEAT interfaces.

The example below shows how one can read the ozone profile and tangent altitude values for a single GOMOS level 2 profile using the BEAT-I interface of MATLAB (this is almost identical to the way it is done in IDL):

```
>> pf = beat_open('GOM_NL_2P...');  
>> tangent_alt = beat_fetch(pf, 'NL_GEOLOCATION', -1, 'tangent_alt');  
>> o3 = beat_fetch(pf, 'NL_LOCAL_SPECIES_DENSITY', -1, 'o3');  
>> beat_close(pf);
```

There are some remarks to be made based on this example. First of all, the *beat\_open* function only needs a filename and doesn't require a hint about the type of file that is to be opened. This is because BEAT is able to automatically recognize the type of a product file. Furthermore, a user will – for most cases – just need to remember only three functions, *beat\_open*, *beat\_fetch*, and *beat\_close*, in order to read data from a product file. There is also no need to keep track of many handles and pointers in order to get to the data that is required (as is sometimes the case with direct product access libraries for other file formats). The *beat\_fetch* function is also a very powerful function: through its arguments one can descend into the structural hierarchy of a product file and point directly to the data element that one wants to read. The parameter '-1' in the example indicates that the specified data element for all DSRs of the data set is requested (it is an array range specifier). Both 'tangent\_alt' and 'o3' will thus become one-dimensional arrays.

## ABSTRACT DATA INTERFACE

Even though the BEAT direct product interface solves some essential problems, there are still certain cases it does not cover. First of all, the data storage structure for some products (with the SCIAMACHY Level 1b file being the most notorious) can be quite complex. This means that BEAT-I users will first have to get acquainted with the product file format by studying the appropriate entry in the Data Dictionary documentation and in this way find out what series of parameters need to be passed to *beat\_fetch* in order to get to the data they need. Especially for scientists who are new to the product this can be rather tedious. And usually most scientists are only interested in some primary data from a product (e.g. as in the GOMOS example: just the ozone profile with some annotation data such as time, geolocation, altitude, etc.). For these cases the abstract data interface BEAT-II was developed. The BEAT-II interface is, just like BEAT-I, a data ingestion interface for product data, but on a higher level. Besides hiding the sometimes complex structure of the product files from the user, BEAT-II also provides some powerful functionality to filter and/or convert data during ingestion. And although BEAT-II uses the BEAT direct product interface to read data from the Envisat atmospheric instruments and GOME instrument, it is not limited to BEAT-I. BEAT-II is also able to provide an abstraction for data products that are stored using other file formats and require a different direct product reading library. BEAT-II, for instance, also supports ingesting data from OMI level 2 products which are stored in HDF5-EOS.

In the sections that follow we will discuss several of the aspects that lie at the foundation of BEAT-II.

## COMMON DATA STRUCTURE

In order to shield the user from the complex structure of a product, a simpler structure is needed to return the data in. To this end the types of data that can be returned are divided into five main classes:

1. spectral readout data: this is level 1 measurement data.
2. reference spectra data: reference spectra are similar to level 1 measurement data, but do not have a time dimension.
3. profile data: level 2 vertical profiles.
4. swath/ground pixel data: level 2 total column data.
5. geo-map data: level 3/4 worldly averages.

In order to facilitate instrument inter-comparison it is important to remove as many differences as possible between the data types within a certain class. For example, GOMOS level 2 profile data should be retrieved in a similar structure as MIPAS level 2 data, and this should again be similar to profile data retrieved from a SCIAMACHY level 2 product.

field name	type	dimension
type	string	
species	string	
time	double	[measurements]
corner_latitude	double	[measurements, 4]
corner_longitude	double	[measurements, 4]
latitude	double	[measurements]
longitude	double	[measurements]
value	double	[measurements]
value_unit	string	
error	double	[measurements]
error_unit	string	
integration_time	double	[measurements]
solar_zenith_angle	double	[measurements]
los_zenith_angle	double	[measurements]
relative_azimuth_angle	double	[measurements]
backscan_pixel	int32	[measurements]

Table 1. BEAT-II record for SCIAMACHY level 2 total column data

On the other hand, since instruments are different, there will be differences in what type of annotation data is interesting (or even available) and should be returned. Furthermore, another requirement was to keep the data structures in BEAT-II as simple as possible, which means that the data structures should be as flat as possible.

These design considerations combined have led to a common data structure for all classes called the BEAT-II record. A BEAT-II record is a one level deep data structure, meaning that each field of a BEAT-II record can contain a single data element or an array of data elements, but it cannot, for instance, contain another record. For each class a set of mandatory fields is defined (these are the data elements that are common to all instruments). This list of fields can be extended on a per product type basis with fields containing instrument specific annotation data. Table 1 shows an example of a BEAT-II record definition for the total column data from a nominal SCIAMACHY level 2 (SCI\_NL\_2P) file. In this example the first 11 fields (*type - error\_unit*) are mandatory for all ground pixel data and the last 5 fields (*integration\_time - backscan\_pixel*) were specifically added for the nominal SCIAMACHY level 2 file.

All BEAT-II records have a *type* field that contains the name of the record type. This name is a combination of the product type and the name of the class that the data falls in (in the example of Table 1 the value of the *type* field would be “SCI\_NL\_2P\_ground\_pixel”).

To keep it simple there are only three basic storage types that can be used for each field: string (for character data), double (for floating point values), and int32 (for integers). Each field can be an n-dimensional array (with n=0 corresponding to a scalar). Dimensions of arrays are usually named (the arrays in the example in Table 1 all have a dimension with the name “measurements”). Naming dimensions makes it possible to couple the sizes of certain dimensions for different fields (this is used for size verification, record appending algorithms, etc.).

After an ingestion, the user will receive the BEAT-II record in the form of a ‘native’ record (in MATLAB and IDL you will receive a *struct* type), which means that the data will be fully manipulatable afterwards (fields can be changed, added and removed as one would normally do within these applications). The BEAT-II interface also contains some special operations that can be used to manipulate BEAT-II records, such as sorting (using a specific named dimension), appending, slicing, exporting, importing, etc.

## DATA CONVERSIONS

In order to return the product data in a BEAT-II record, the ingest function needs to perform a certain set of data conversion operations. In this section we show some examples of data conversions that can be applied.

The easiest form of conversion is unit conversion. This usually only requires a linear scaling of the values. In BEAT-I there already is a form of unit conversion available (this feature is enabled by default in BEAT-I, but can be disabled). Data disseminators usually try to keep the data products as small as possible. To this end floating point values are often stored as integers if the values are all of the same magnitude. For example, latitude and longitude values in Envisat products are stored as integers with a multiplication factor of  $10^6$  (i.e.  $69.125368^\circ$  is stored as 69125368). This saves 4 bytes per value, while still keeping a high number of significant digits. With the automatic conversion functionality in BEAT-I these values are converted back to their original floating point values when they are read.

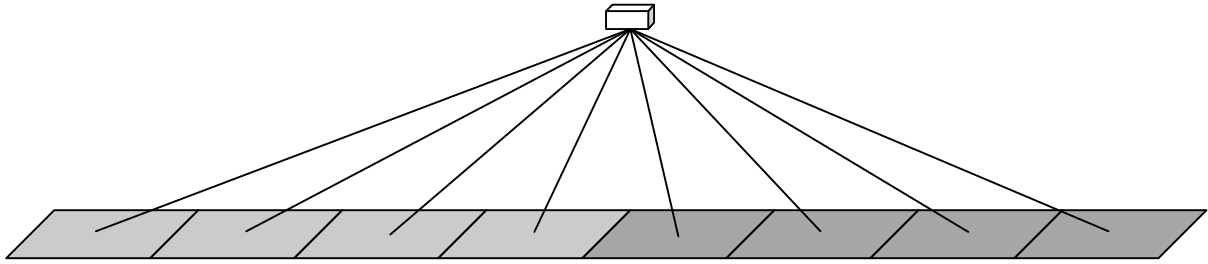


Figure 1. Co-adding of ground pixels

BEAT-II also uses this conversion functionality of BEAT-I, but goes one step further. For some of the fields BEAT-II will always return the value using a pre-defined unit, which is independent of the product type that the value came from. For instance, altitude is always returned in 'km', geolocation always in degrees (latitude from -90 up to 90 and longitude from -180 to 180), and time as a floating point value giving the number of seconds since January 1<sup>st</sup> 2000 00:00:00. For some products this does not require any conversions, but for other products (such as time values for GOME products) it does.

A more complex conversion operation is co-adding. For SCIAMACHY level 2 products, for instance, the total column data for a certain species is often given using a lower temporal resolution than the ground pixels (this comes from the fact that the integration time for the measurements that were used for the retrieval was higher than the swath integration time). So in order to provide the proper ground pixel coordinates for a vertical column measurement, some ground pixels need to be co-added. For example, if we have a scan of eight swaths with an integration time of 0.25 seconds each, and two measurements with a 1 second integration time each then we need to co-add four swaths to retrieve the ground pixel for each measurement (see the two different coloured areas in Fig. 1). This co-adding is done automatically by BEAT-II. In these cases BEAT-II also takes appropriate averages for other geolocation properties such as centre latitude/longitude, solar and line of sight zenith/azimuth angles, etc.

Sometimes data is structured in such a way that it is very difficult to map it on a BEAT-II record. A good example in this case is the SCIAMACHY level 1b product. Spectral readout data in BEAT-II is represented by a two dimensional array [*number of measurements, number of detector pixels*], but with SCIAMACHY the detector array is divided into eight bands, where each band is again divided into a series of clusters. Each cluster can have its own integration time during a series of measurements. To make matters even more complex, during a single orbit the SCIAMACHY instrument can switch between different states where each state can have its own separate cluster configuration (i.e. different segmentation in clusters and different integration times for each cluster). We will not go into detail and explain how the conversion to a two-dimensional spectral readout array is done, but suffice to say that BEAT-II is able to handle such cases and can often eliminate complex data structures by mapping them onto simpler (although sometimes a bit more memory-consuming) structures.

It should be noted that within BEAT-II no 'scientific' conversion algorithms are performed, only structural conversions. This is mainly because scientific algorithms (such as calibration/correction operations) can be disputable and each scientist may wish to use his own version of the algorithm.

## FILTERING AND SELECTION

One of the most powerful features of the BEAT-II interface is the filtering and selection mechanism. When ingesting data from a product it is possible to provide a string with comma-separated options that can limit the types and amount of data that will be read. All filter options take the form 'variable=value', which makes them very easy to use. We will give some examples below of the types of filter options that can be used and also give an example of an ingestion.

As can be seen from the BEAT-II record example in Table 1 a record can contain only data for the retrieval of a single species, but often level 2 products contain retrievals for far more than one species. BEAT-II handles this by requiring the user to provide a mandatory filter option that selects the species for which the data should be ingested (e.g. 'species=o3'). Most of the selection decisions are handled in this fashion. For instance to select the type of state (nadir, limb, occultation, monitoring) from which to read data for a SCIAMACHY product, the user will provide a 'state\_type' filter option with one of the values 'nadir', 'limb', 'occultation', or 'monitoring'. Most selection filter options are mandatory, but if a sensible default is available (e.g. the default species for a GOME level 2 file is ozone) then it is possible to omit the filter option.

Another category of filter options is the one that limits the range of data that will be ingested (i.e. it influences the array ranges of the data that is returned). If a user is interested in just a small time range of data or only a certain geographical area then BEAT-II is able to provide you just the data for this range. All time-based products, for instance, have 'time\_min' and 'time\_max' options that allow the placement of lower and upper boundaries to the measurement time of the data. Similar ranges are available for geographically based data: 'latitude\_min', 'latitude\_max', 'longitude\_min', 'longitude\_max', 'altitude\_min', and 'altitude\_max'.

The BEAT-II ingestion function is optimized to handle range-limiting options efficiently. When range options are provided, first the data on which the limitation is placed is read from a product. Then the values are matched against the range limits and a list of array indices is created for which data should be ingested. Finally the BEAT-II record is ingested, but BEAT will now only read the data for which the array index was included. This means that the ingestion can become much faster if small time, geolocation, or wavelength ranges are used.

Finally we provide an example (again in MATLAB) of an ingestion of GOME level 2 data using BEAT-II:

```
>> files = dir('*.lv2'); filenames = strvcat(files.name);
>> data = beatl2_ingest(filenames,'time_min=30-SEP-2000,time_max=01-OCT-2000,backward_scan=0')
```

```
data =
      type : 'GOME_L2_ground_pixel'
    species : 'o3'
      time : [19239x1 double]
  corner_latitude : [19239x4 double]
  corner_longitude : [19239x4 double]
    latitude : [19239x1 double]
    longitude : [19239x1 double]
     value : [19239x1 double]
  value_unit : 'DU'
    error : [19239x1 double]
  error_unit : '%'
  solar_zenith_angle : [19239x1 double]
    los_zenith_angle : [19239x1 double]
  relative_azimuth_angle : [19239x1 double]
  subset_counter : [19239x1 int32]
```

As can be seen the ingestion with BEAT-II only requires a single command and is able to handle multiple files at once. The filter options that are provided limit the range of data that is returned to data from 30 September 2000 and the 'backward\_scan=0' option assures that we only retrieve data for forward scans.

## VISAN

Where BEAT-II is able to reduce the ingestion procedure to a single command, within VISAN the capability has been added to do the same for creating visualizations. Usually, when data is ingested one still needs to perform several steps before the data can be visualized on screen. Since VISAN knows about the several classes of BEAT-II records, it knows how to set up appropriate visualizations for each class, and is thus able to hide this behind a single command.

Below is an example in VISAN that performs an ingestion and creates a visualization from this data. The visualization is shown in Fig. 2. Note that, since VISAN is based on Python, the syntax of the BEAT-II ingest in VISAN is a bit different from MATLAB and IDL.

```
>>> data = beatl2.ingest('*.lv2', 'time_min=30-SEP-2000,time_max=01-OCT-2000,latitude_min=30,
      latitude_max=60,longitude_min=-25,longitude_max=25,backward_scan=0')
>>> wplot(data, colortable='blacktowhite', colorrange=[250,300], projection='Plate Carree')
```

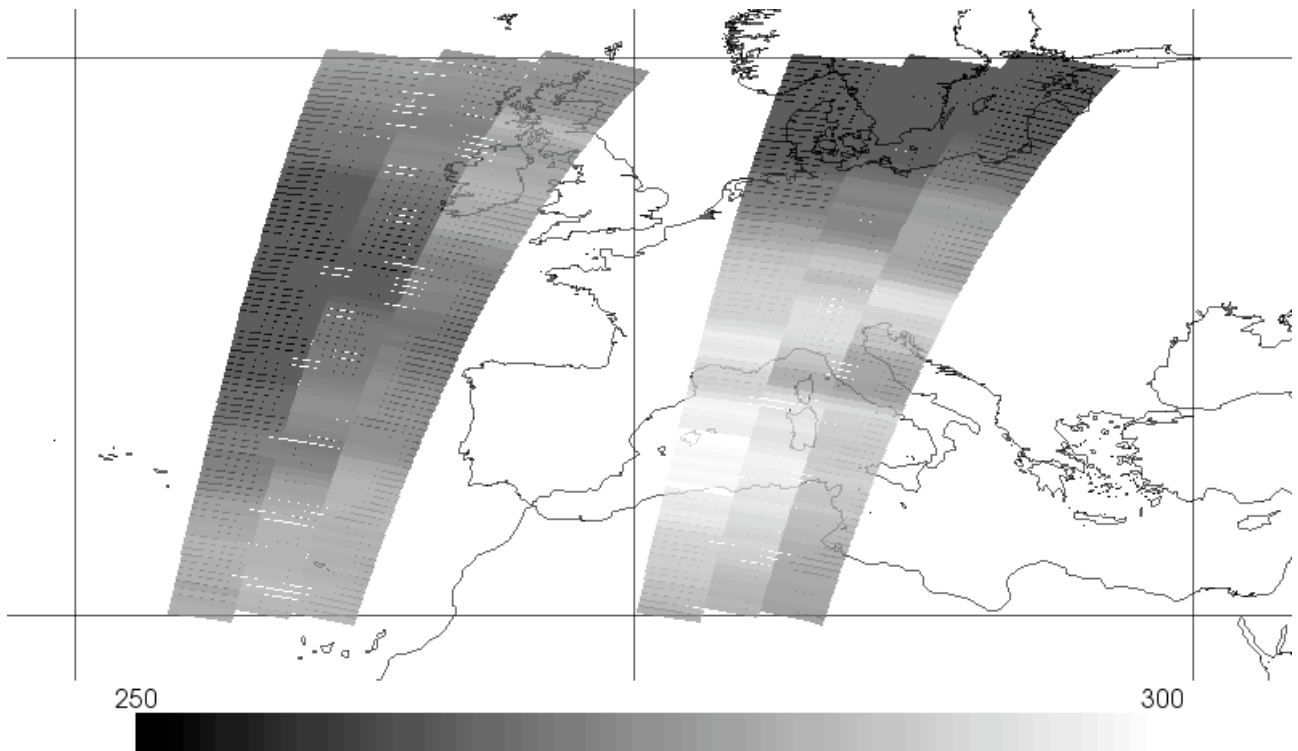


Figure 2. GOME level 2 data ingested with BEAT-II and visualized with VISAN

## REFERENCES

- [1] Basic Envisat Atmospheric Toolbox website, 2004. <http://www.science-and-technology/beat/>.
- [2] Envisat website, 2004. <http://envisat.esa.int/>.
- [3] HDF website, 2004. <http://hdf.nsa.uiuc.edu/>.
- [4] NetCDF website, 2004. <http://my.unidata.ucar.edu/content/software/netcdf/>.
- [5] Python website, 2004. <http://www.python.org/>.
- [6] IDL website, 2004. <http://www.rsinc.com/idl/>.
- [7] MATLAB website, 1994-2004. <http://www.mathworks.com/products/matlab/>.
- [8] XML website, 1996-2004. <http://www.w3.org/XML/>.

## **Abstract Sheet - Abstract number: 22**

Author Name: PINTY, Bernard  
Organisation: Joint Research Centre  
Country: ITALY  
Authors: PINTY, Bernard, Joint Research Centre, ITALY (P)  
Taberner, Malcolm, EC-JRC, IES, ITALY  
Lattanzio, A, Makalumedia gmbh, GERMANY  
Liang, S., University of Maryland, UNITED STATES  
Martonchik, J. V., NASA-JPL, Caltech, UNITED STATES  
Verstraete, M. M., EC-JRC, ITALY  
Dickinson, R. E., SEAC, Georgia Tech., UNITED STATES  
Gobron, N., EC-JRC, ITALY  
Widlowski, J.-L., EC-JRC, ITALY  
Govaerts, Y., EUMETSAT, GERMANY

### **Intercomparison of Surface Albedo Products from Various Spaceborne Sensors**

Satellite instruments have been delivering a wealth of information regarding land surface albedo. However, the so-called albedo products delivered by various space agencies may correspond to different physical quantities, depending on the level of sophistication adopted to account for the coupling between the bidirectional properties of the surface and the diffuse irradiance available at the bottom of the atmosphere. This presentation will first describe albedo in terms of this radiative transfer coupling and highlight simple schemes that permit us to link the various meanings of albedo. Second, we will present an application of this investigation based on the analysis of one year of surface albedo products derived from MODIS, MISR and Meteosat.

# Eight Years MOS-IRS – Summary of Calibration Activities

Horst Schwarzer, DLR Optical Information Systems\*)  
Andreas Neumann, DLR Remote Sensing Technology Institute\*)  
Thomas Walzel, DLR Remote Sensing Technology Institute\*)  
\*) 12489 Berlin, Rutherfordstr. 2, Germany

## ABSTRACT

After eight successful years of operation in orbit the mission of the Modular Optoelectronic Scanner (MOS) on board the Indian Remote Sensing Satellite (IRS-P3) ended in May 2004. Being the first imaging spectrometer in the Earth's orbit and due to the long lifetime it allowed extensive calibration and inter-calibration studies. The paper will give a summary on the results of in-orbit calibrations (internal lamps, sun, vicarious and moon) and inter-comparisons with other missions using ground targets and derived geophysical products. Conclusions are drawn for future improvements of inter-calibration strategies.

**Keywords:** In-orbit calibration, ground target based calibration, inter-calibration, imaging push broom scanner, VIS/NIR remote sensing, earth observation

## 1. INTRODUCTION

For the last 8 years the Modular Optoelectronic Scanner MOS has been delivering valuable findings of the qualitative and quantitative determination of characteristic parameters to determine the ecological changes of the oceans, especially of the coastal zones. The MOS mission is the longest and the most successful environmental remote sensing mission of the German Aerospace Center (DLR), where the MOS VIS/NIR imaging spectrometer was developed and built. The satellite orbited the earth about 42,000 times on its 820 km sun synchronous orbit. Fundamental problems did not occur during this long term mission, all detector elements are still working now. Some difficulties and the failure of the on board calibration equipment caused by the failure of its power supply could be overcome only by using alternative methods and the instrument performance data that had been established by the lab measurements as well as by the in orbit calibrations.

Only in this way it was possible to maintain the high data quality which is necessary for deriving the desired ecological parameters and their time trends. About 4,700 lamp calibrations, 70 sun calibrations, 36 ground target based (vicarious) calibrations and 9 moon calibrations are the basis for the knowledge of the behaviour and the changes of the MOS sensor components and the total time trend of the responsivity of the different spectral channels during the last 8 years in orbit.

Table 1 gives an overview of the performance data of the MOS sensor and fig. 1 shows the optical design of MOS-B.

**Performance data: Modular Optoelectronic Scanner MOS-IRS**  
(orbit: altitude 817 km; 10:45 AM equator crossing time, descending node,  
sun synchronous polar)

Parameter	MOS-A	MOS-B	MOS-C
Spectral range [nm]	755 - 768	408 - 1010	1550-1650
No. of channels	4	13	1
Centre wavelengths [nm]	756.7; 760.6; 763.5; 766.4	408; 443; 485; 520; 570; 615; 650; 685; 750; 815; 870; 945; 1010	1600
Spectral FWHM [nm]	1.4	10	93
Swath width [km]	187	200	192
No. of pixels	420	384	299
Pixel size x-y [km <sup>2</sup> ]	4.9 x 0.45	1.34 x 0.52	0.74 x 0.74
Measuring range $L_{min}...L_{max}$ [ $\mu Wcm^{-2}nm^{-1}sr^{-1}$ ]	0.1 .. 40	0.2 .. 48	0.5 .. 8
Accuracy $\Delta L/L$ at $L_{min}$ [%]	0.3	1.0	2.0
Dynamic range [bit]	16	16	16

Tab. 1: MOS Performance data

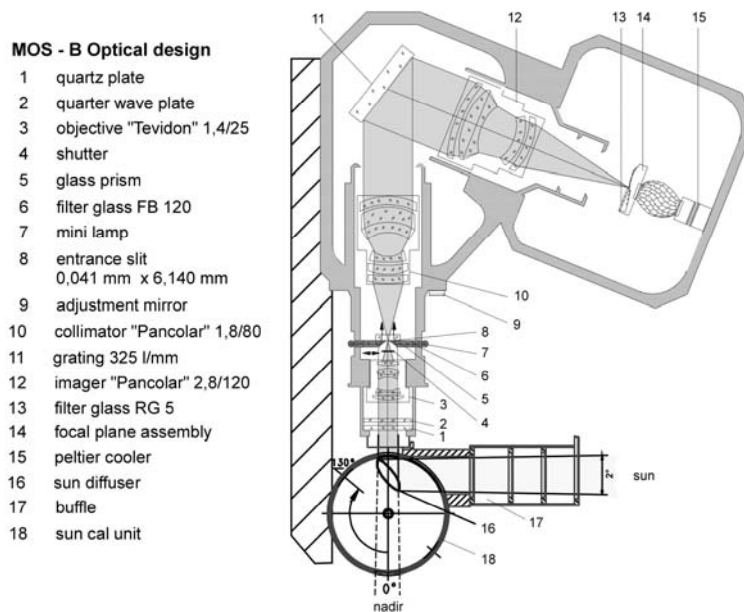


Fig. 1: Optical design and in-orbit calibration equipment MOS-B

## 2. IN-ORBIT CALIBRATION

The data quality during the mission time has been checked by different methods and also different equipment for each of the three MOS instruments.

The **internal lamp calibration** is a relative check. It was done at the beginning of each measuring cycle in 4 different radiation levels. The light of the two mini lamps (7) passed the glass prisms (5) and entered the spectrometer via two separate slits beneath the spectrometer slit. Only the following opto-electronical components could be checked by the internal lamps: The collimator (10), the grating (11), the imager (12), filter glass for second order spectrum suppression (13), CCD focal plane (14) and the sensor electronics.

The **sun calibration** permitted an absolute radiometric recalibration of the instruments. It was done periodically every 14 days when the satellite passed the terminator. Then the spectralon sun diffuser (16) was turned into the FOV of the spectrometer. The sun light passed the baffle (17) and fell under an angle of  $40^\circ$  onto the diffuser. The diffused sun light illuminated the TFOV of the instrument and now all opto-electronical components could be checked. That means we could check the quartz plate (1), the quarter wave plate (2), the entrance optics (3), the spectrometer slit (8) and additionally we could check the same components as the internal lamps but in a different way. This enabled us also to check the internal lamps and to find out in many cases which optical component generates observed changes in the response of the instrument.

For the **ground target based or vicarious calibrations** we have chosen a region near the border between Tunisia and Algeria south of Chott el Djerid, part of the Great Eastern Erg, a largely sandy desert. This is an area with good homogeneity, high reflection degree and with stable surface and atmospheric conditions which lies in the receiving area of the DLR satellite ground station Neustrelitz.

The vicarious calibration data have been corrected with respect to sun zenith angle at the centre of the test site and the distance between sun and earth. Atmospheric corrections were not taken into account. But we selected from the received spectrometer data of the test site only those which were taken at cloudless conditions also in the surrounding area and at sun zenith distance angles smaller than  $50^\circ$ . That means that we did not use measurements in wintertime and thus we can also exclude hoar frost effects at the surface.

The **moon calibration** served as a relative check of the calibration of the MOS sensors without atmospheric effects. It was evident especially for comparison between the different MOS-A channels inside and outside the  $O_2A$ -absorption band and the 750nm channel of MOS-B.

The history of MOS in orbit calibration started shortly after the launch on 21<sup>st</sup> March, 1996. The first what we found were some small changes in the internal lamp calibration data<sup>1</sup>. The internal lamps, for example, showed changes of the data taken before and after launch in the order of 2 to 4%. The in orbit sun calibration data indicated changes of the vignetting curves in the same order especially at one end of the CCD lines. Some of these effects were obviously caused by mechanical manoeuvres of the satellite. That means small particles seem to have been transported into the spectrometer slit plane and into the calibration slit plane where they changed the transmission of these slits. But after this time in the middle of April 1996 the instruments reached a new stable state for some years.

The next event was a small change of the vignetting curves of MOS-B in February 1999. Approximately the last 40 pixels of all spectral channels suffered a wavelength dependent decrease of responsivity up to 4%, the longer the wavelength the smaller the decrease. We found this effect only in the sun calibration data and in the ground target based calibration data, but not in the internal lamp calibration data. Taking into account the design of the on board calibration equipment the only explanation for this behaviour was a shadowing effect in front of the entrance optics. This change of the vignetting was a stable effect without variations up to the mission end.

In September 2000 the most dramatic occurrence during the whole mission time happened: the power supply of the internal lamp calibration and of the complete sun calibration equipment dropped out. That means also the dark signal measurement by using the shutter failed. Fortunately the nadir looking remote sensing measurements could be continued and were not affected in any way. The in orbit calibration based on lamp and sun calibration could be replaced and continued by the ground target based calibration using our test site of the Great Eastern Erg in the Sahara.

The dark signals needed for all measurements and for the calibration data too as from now were obtained by nadir measurements at the night side of the earth over the dark ocean during new moon.

The next two years mission time was without any problem. But in November 2002 we had to meet a new challenge. The thermo-electrical cooling of the CCD sensors did not work. Normally the detectors were stabilised to 5.0°C. But as from now the temperature decreased up to 20°C when the satellite moved from the dark to the illuminated side of the earth. To get accurately calibrated data we had to take into account the temperature dependence of the dark signals on the one hand and the temperature dependence of the responsivity on the other hand.

Fig. 2...4 show the data and the trend curves of the internal lamp calibration, the sun calibration and the ground target based calibration for 3 typical examples: the 408nm, the 685nm and the 1010nm channel. The last four data points of the ground target based calibration (bij\_vic) after November 2002 are shown for two cases: a) the temperature correction is applied for 15°C (◆) and b) without temperature correction (○). From the 500...700nm spectral channels, which are unaffected by temperature variations practically (see fig. 3), we can see that the time trend must be a continuous function for all channels. The best indicator for the right temperature correction of the data is the 1010nm channel 13 because of its strong responsivity variation with temperature (see fig.4).

In spite of all the different events in orbit we always were able to derive actual recalibration data of high accuracy from the ground target based calibrations during the whole mission time without any break.

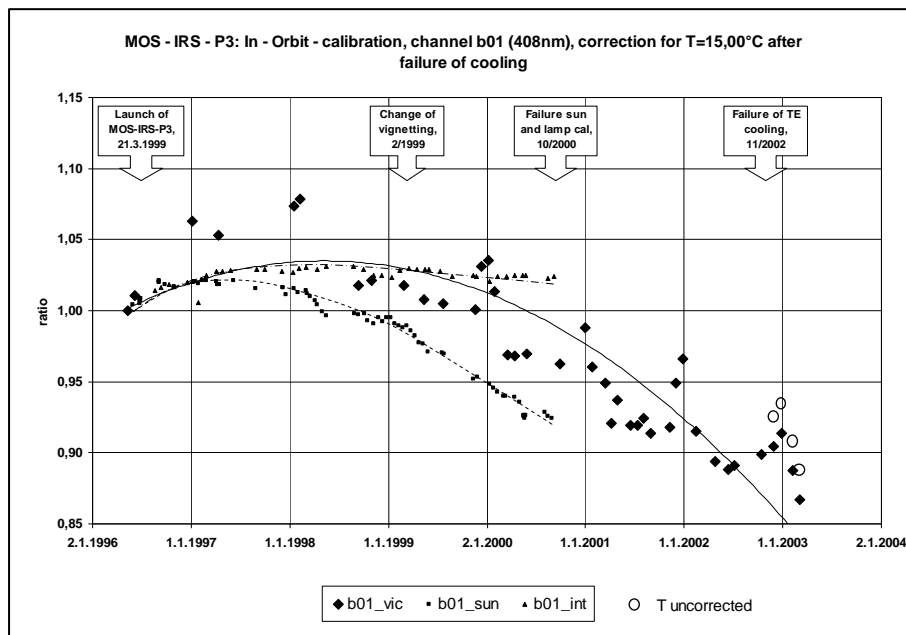


Fig. 2: Time trend of MOS in-orbit calibrations (vic: ground target based calibration, sun: sun calibration, int: internal lamp calibration), channel 01 (408nm)

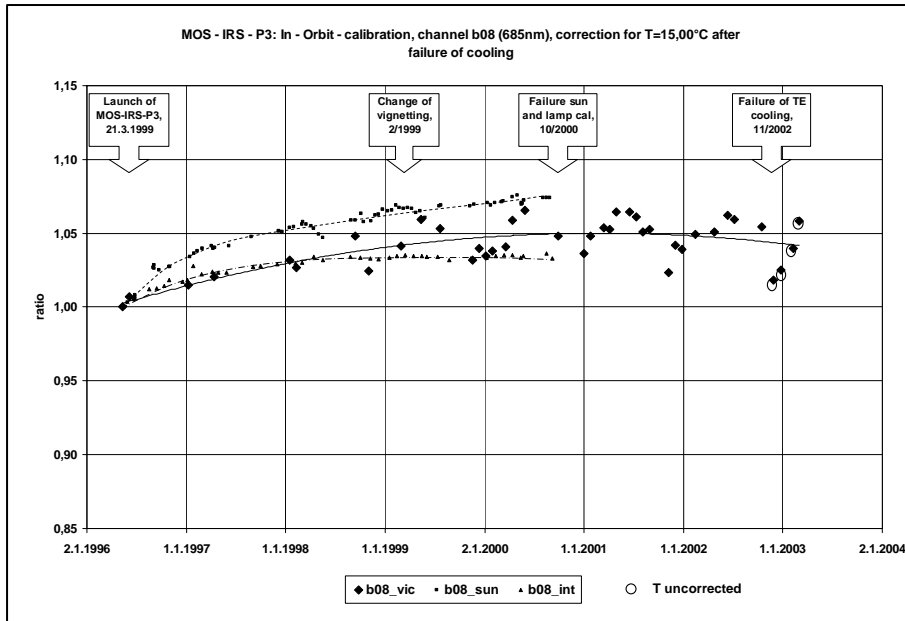


Fig. 3: Time trend of MOS in-orbit calibrations (vic: ground target based calibration, sun: sun calibration, int: internal lamp calibration), channel 08 (685nm)

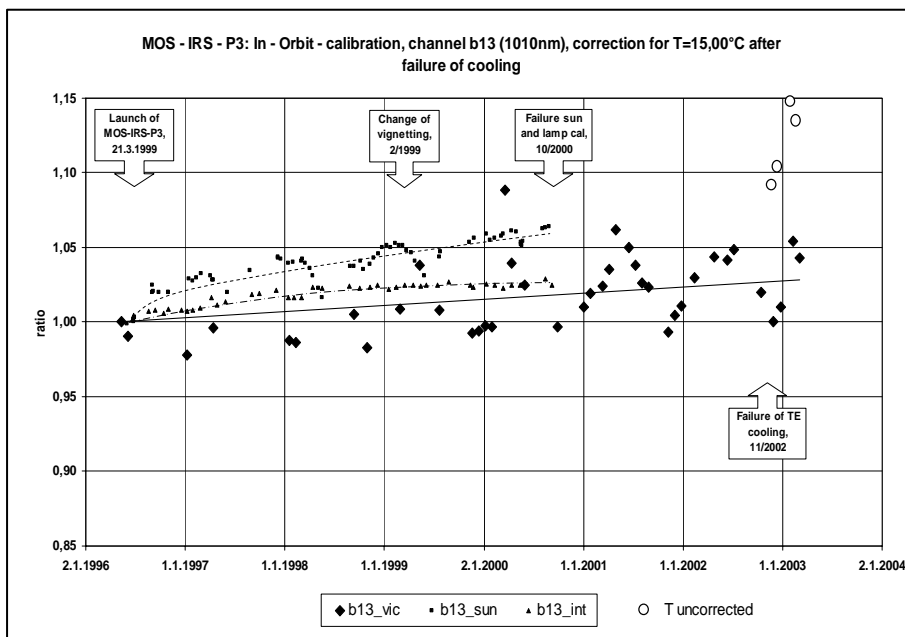


Fig. 4: Time trend of MOS in-orbit calibrations (vic: ground target based calibration, sun: sun calibration, int: internal lamp calibration), channel 13 (1010nm)

The different contributions of different MOS opto-electronical components to the total change of spectral responsivity of the MOS channels 7 years after launch are shown in fig.5. These results could be obtained by an intensive analysis of the different in-orbit calibration methods.

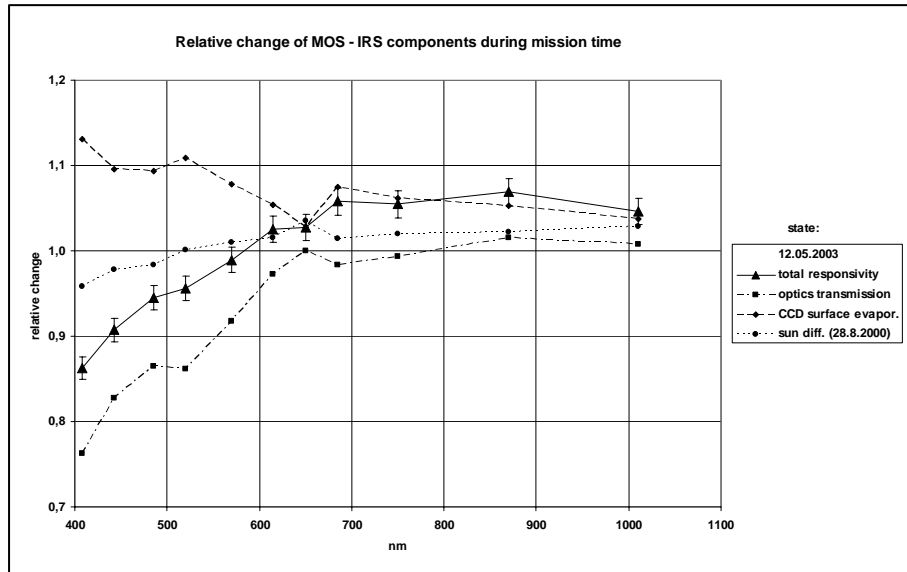


Fig. 5: Wavelength dependent change of optical and electronic MOS components in orbit

For the reason of an independent check of the calibration of MOS sensors some moon measurements were carried out in the year 1999. They were realised in the full moon phase at three different dates in August, October and December in 1999. Within 1 or 2 orbits per night the moon was scanned by the MOS instruments. Therefore it was necessary to carry out a manoeuvre with the satellite IRS-P3 to orientate MOS to the moon. While passing the moon, the pitch angle of the satellite was changed to get an image of the moon. With help of this operation it was possible to get 2-3 scans of the moon in one orbit.

The objective of the moon measurements was relative check of the calibration of the MOS instrument. It was assumed, that the spectral reflectivity of the moon surface is a smooth function over the wavelength interval of MOS instrument (400 – 1020 nm).

A mean value of selected pixels (bright pixels, not at the border of the moon) of each moon scan was determined and normalized to the wavelength of MOS-B-channel 8 (685 nm) after a resampling of the measured data (because of different scan velocities at different scans).

A definite difference of the smoothed function of normalized reflectivity could be used to derive a correction factor. Knowing, that the PRNU (Photo Response Non Uniformity) within one wavelength channel didn't change significantly, this correction factor is to apply to all pixels of a wavelength channel.

In the scatterplots of MOS-A channels (758, 760, 763 and 766 nm) in fig. 6 the correct calibration of MOS-A is confirmed (no O<sub>2</sub>-absorption like on earth). The comparison of MOS-B-channel 9 (750 nm) and MOS-A-channel 1 (758 nm) confirmed corrections, which were derived from earlier sun calibration measurements for MOS-B instrument (see fig. 8).

So the moon measurements gave an additional approval for MOS calibration derived from sun measurements

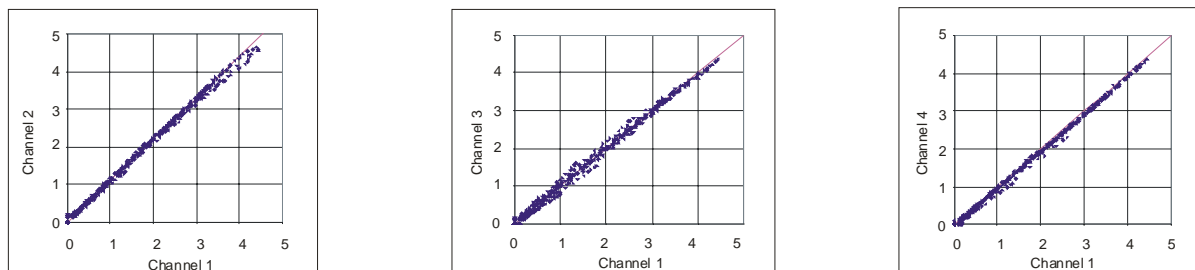


Fig. 6: Scatterplots of MOS-A channels (all radiances in  $\mu\text{W}/\text{cm}^2 \text{ nm sr}$ )

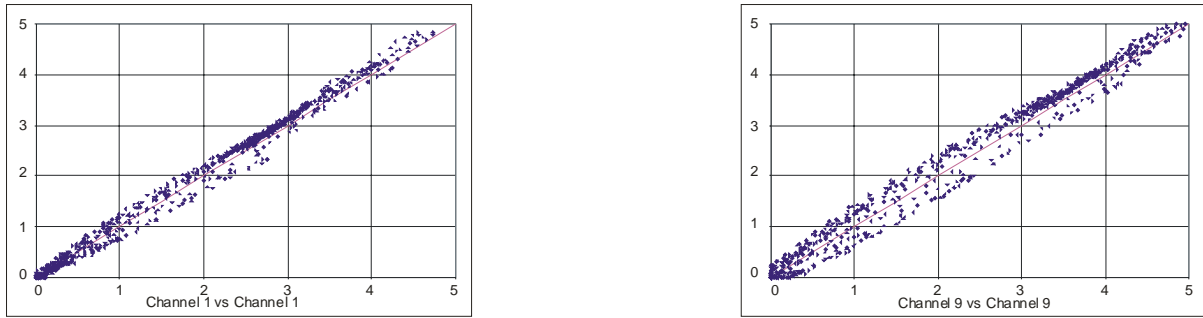


Fig. 7: MOS-B Scatterplots of different records and same channels (all radiances in  $\mu\text{W}/\text{cm}^2 \text{ nm sr}$ )

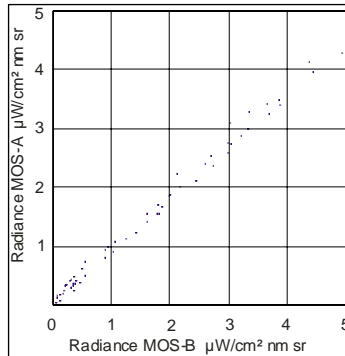


Fig. 8: Scatterplot of MOS-B vs MOS-A at 750nm

### 3. INTERCOMPARISON OF DERIVED PRODUCTS

Having different instruments in orbit for similar applications raises the question of intercomparison of derived products. For MOS an algorithm using Principal Component Inversion (PCI) was developed to compute water constituents directly from top-of-atmosphere radiances<sup>2</sup>. The inversion scheme accounts for aerosols internally and generates also a map of aerosol-optical thickness. The existing algorithm has been modified for SeaWiFS and MODIS respectively. Due to some reasons no intercomparison was made for large amounts of data. However, several samples of (nearly) synchronous overpasses of MOS, SeaWiFS and MODIS were processed, mainly in the North Sea, Baltic Sea, Black Sea and the Mediterranean. The results were analysed with respect to:

- intercomparison of SeaWiFS chlorophyll computed by SeaDAS with PCI-derived MOS chlorophyll
- intercomparison of PCI-derived chlorophyll, suspended sediment and aerosol-optical thickness both for SeaWiFS and MOS.

The analysis showed:

- good agreement for chlorophyll and aerosol-optical thickness in general, with clear differences for very small and very large values
- for most cases the PCI-derived values for all instruments agreed very good
- in turbid case-2 waters the better spectral resolution of MOS allowed a better distinction between chlorophyll, sediment and aerosol, the derived SeaWiFS products still show cross-influence between single parameters.

The latter is illustrated in Fig. 9, showing PCI-derived parameters for MOS and SeaWiFS over the German Bight.

Additional, very detailed intercomparisons have been made by the SIMBIOS project<sup>3</sup>.

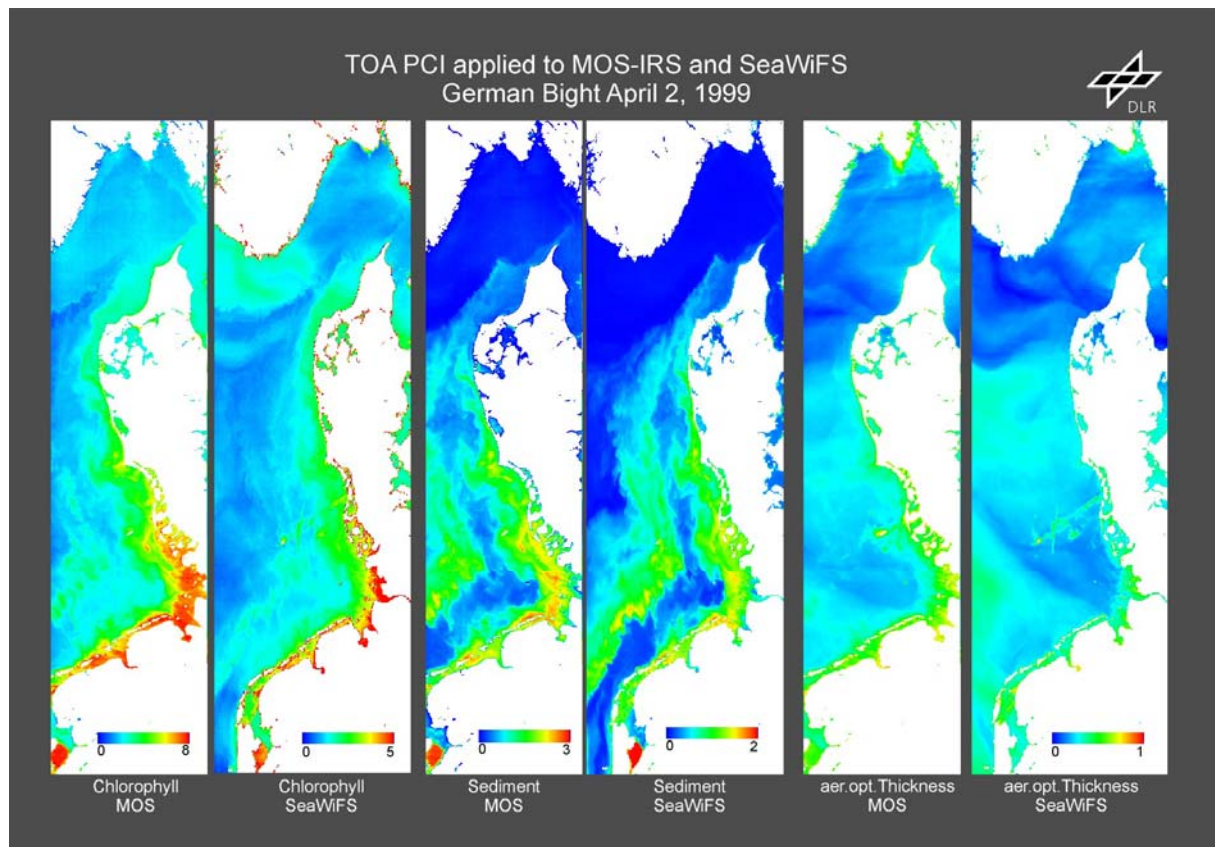


Fig. 9: PCI-derived parameters for MOS and SeaWiFS over the German Bight

#### 4. CONCLUSIONS

The 8 years of in-orbit calibration of MOS was a very successful story. In spite of some critical events with respect to the in-orbit calibration such as changes of the vignetting, the failure of the sun and lamp calibration equipment after 4 years and the failure of the TE cooling of the detectors in 2002, we found solutions to continue the relative in-orbit calibration with very high accuracy without any break during the whole mission time. The changes of the relative calibration factors were caused by the aging of some opto-electronical components under the hard orbit conditions and by evaporation effects of the CCD surfaces. The changes of vignetting may have been caused by satellite manoeuvres especially at the beginning of the mission.

The good results of the in-orbit calibration based on the appropriate calibration concept, on the precise lab calibration and adjustment and on the precise knowledge of the instrument behaviour under different environmental conditions.

Using different and independent methods of in-orbit calibration often affords to get continuously recalibration data in spite of failure of instrument components. This also gives the possibility of discrimination and identification of different sources and reasons for changes in the calibration data.

Relative accuracy of about 1...2% for the recalibration data is achievable.

#### ACKNOWLEDGEMENTS

The authors would like to thank all the colleagues who have supported this work.

#### REFERENCES

1. K.-H. Sümnick, A. Neumann, G. Zimmermann, H. Schwarzer, 1996, Calibration of the Modular Optoelectronic Scanner MOS flight models, SPIE Proceedings, Volume **2819**, pp 218 – 223
2. Krawczyk H. et. al., Investigation of interpretation possibilities of spectral high dimensional measurements by means of principal component analysis - a concept for physical interpretation of those measurements, SPIE Intern. Symposium on Aerospace Sensing 1993, SPIE Proceedings Vol. 1938 (1993), pp 401-411
3. Wang M. and Bryan A. Franz, Comparing The Ocean Color Measurements Between MOS & SeaWiFS: A Vicarious Intercalibration Approach for MOS, IEEE TGARS, 38 (1), 184-197, Part 1, January 2000

## **Abstract Sheet - Abstract number: 26**

Author Name: Smith, David  
Organisation: CCLRC Rutherford Appleton Laboratory  
Country: UNITED KINGDOM  
Authors: Smith, David, CCLRC Rutherford Appleton Laboratory, UNITED KINGDOM (P)

### **The calibration of the short-wavelength channels of the ATSR series of Instruments**

The Along-Track-Scanning-Radiometer (ATSR) instruments have been built to measure Sea Surface Temperatures (SSTs) to an accuracy of 0.3K over a 15+ year timeframe. ATSR-2 and the Advanced ATSR (AATSR) are equipped with visible/near infrared (VNIR) channels at 0.56 $\mu$ m, 0.67 $\mu$ m and 0.87 $\mu$ m as well as a 1.6 $\mu$ m channel already present on ATSR-1. To allow calibration of the VNIR channels a novel visible calibration system (VISCAL) was developed.

The author presents a summary of the calibration activities that were carried out on the instruments, including pre-launch measurements and in-orbit calibration using vicarious methods. The results and lessons learned will be discussed.

# COMPARISON OF THE EARTH'S SHORTWAVE RADIATION MEASURED BY ERB INSTRUMENTS (CERES/GERB)

**Z. Peter Szewczyk** (Science Applications International Corp., Hampton, VA),  
**G. Louis Smith** (Institute for Aerospace at NASA LaRC, Hampton, VA),  
**Pamela E. Mlynczak** (Science Applications International Corp., Hampton, VA),  
**Kory J. Priestley** (NASA Langley Research Center; Hampton, VA)

## EXTENDED ABSTRACT

There exists a consistent, two-decades-long Earth Radiation Budget (ERB) dataset established based on measurements obtained from various instruments (Smith, 2004). By carefully validating instruments with respect to each other, such a set can be used for long-term climate studies. CERES measurements have been part of this dataset since 1998 by establishing the consistency between instruments operating on the TRMM, Terra, and Aqua satellites. A launch of the GERB instrument in 2002 aboard Meteosat-8 (Harris, 2004) offers unprecedented information about the diurnal cycle of heating and cooling of the Earth; however, it is important that radiances measured by the GERB are also consistent with the ERB dataset. Comparison of CERES shortwave radiances measured by FM1 and FM4 on Terra and Aqua, respectively, is shown here as a backdrop for comparing FM2 on Terra and GERB on Meteosat-8. This work presents a methodology for comparing ERB instruments with a focus on shortwave radiation as there are several challenges (Smith, 2000) to the comparison of remote sensing instruments: (a) time constraints, (b) viewing geometry constraints, (c) observation site constraints, and also (d) presence of spatial noise.

In dealing with time constraints, it is usually assumed that an Earth's scene does not change significantly within 15-20 minute time span. Since Terra and Aqua satellites are in sun-synchronous polar orbits, with their respective equatorial crossing times at 10:30AM and 1:30PM, they arrive at the nodes (approximately 70°N and 70°S latitude) of their intersecting orbits about 15 minutes apart. The vicinity of orbital crossings presents then an opportunity for comparisons between instruments on both satellites. The GERB instrument on the other hand, produces radiation images every 5 minutes; therefore it offers almost simultaneous observations with FM2 on Terra. To compare the shortwave channels of FM1 and FM4, it is best to use the maximum insolation occurring around the northern summer solstice on June 20. Summer and winter solstice campaigns are needed to collect data for the CERES/GERB comparison, as eventually all GERB detectors get strong signals.

Comparison of shortwave radiation requires that measurements are taken from the same direction. In other words, viewing zenith and relative azimuth angles of an observation have to be within a prescribed tolerance. A CERES scanner offers an opportunity to satisfy these conditions by scanning in a predefined plane, and a special mode, referred to as Programmable Azimuth Plane Scan (PAPS), has been developed for that purpose. In the case of the FM1/FM4 comparison, the scan plane of each instrument is orthogonal to the solar plane at the nodes. For the CERES/GERB comparison, the scan plane is adjusted so that it always contains the Meteosat-8 sub-satellite point. In both cases, footprints with matched viewing zenith angles are found on processing each scan; there is always a match between CERES and GERB.

In comparing measurements by remote sensing instruments, selecting the ideal source of radiation and ideal experiment conditions is nearly impossible. Therefore, using the best setup available is the only practical approach. For the FM1 and FM4 comparison data collection, Greenland is identified as having the most homogenous and uniform scenes. Although its surface is more complex than a thick sheet of ice, it still offers the best conditions for comparison, particularly in the plane orthogonal to the solar plane. In addition to measurements collected over Greenland, shortwave radiation is also collected for other scene types according to the ERBE-like classification. In the CERES/GERB experiment, data are collected for various scene types, with the focus on the clear sky condition.

Daytime scenes are very dynamic in their nature, affected by cloud cover, terrain, and the direction and time of observations. Measurements of even seemingly homogeneous scenes may have a wide range. In order to reduce the dependence of radiance measurements on the spatial noise, averaging over a  $1^\circ \times 1^\circ$  grid-box is performed. For a gridded average to be valid, it is required that at least 20 CERES or 4 GERB footprints lie in it or that at least 75% of its area is covered by footprints. To increase statistical independence of averaging, an assembly of grid-boxes for a specific scene type and a given time is formed and averaged. A difference of these averages is computed, and their distribution is analyzed for equivalence.

There were several campaigns for collecting comparison data. Each campaign was 3-4 weeks long to collect a sufficient amount of data for statistical analysis. Data for comparing FM1 and FM4 were collected during summer solstices of 2002 and 2003, and for FM2 and GERB during the winter solstice of 2003. Results are provided for comparing shortwave radiances based on the ERBE-like CERES data product, and unfiltered, non-averaged, and non-rectified GERB shortwave images provided by the Royal Meteorological Institute of Belgium. The GERB data are based on SEVIRI improved geolocation. It is shown that the CERES instruments provide shortwave radiances with 1% consistency (complete results for CERES are in Szewczyk, Smith and Priestley 2004), and also that the SEVIRI enhanced GERB geolocation produces improved correlation with the FM2 shortwave radiances. It is important to note that only preliminary results exist for comparing CERES and GERB, and it is an on-going effort to establish the correlation between these two instruments.

**References:**

- G.L. Smith, Z.P. Szewczyk, D.A. Rutan, R.B. Lee III: "Comparison of measurements from satellites radiation budget instruments", Proc. 13-Sat. Met. Conf., 2004
- J.E. Harris et al.: "The geostationary Earth Radiation Budget (GERB) project", Bull. AMS, 2004
- G.L. Smith: "Critical Overview of Radiation Budget Estimates from Satellites," *Adv. Space Res.*, 24, 887-895, 2000
- Z.P. Szewczyk, G.L. Smith, K.J. Priestley: "Validation of CERES instruments aboard the Terra and Aqua satellites", JGR, 2004

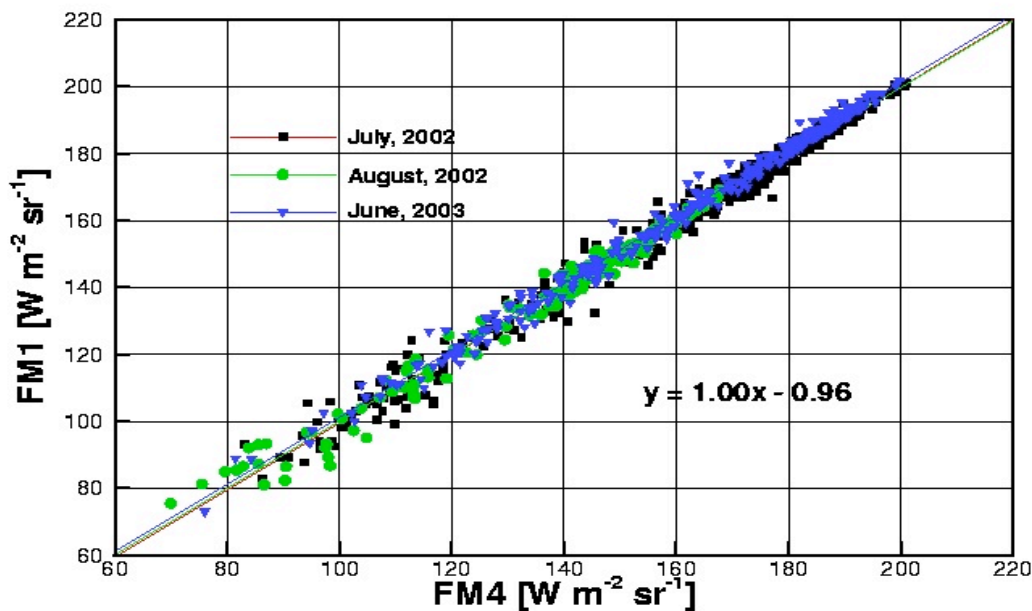


Figure 1. Scatter plot of shortwave radiances measured by FM1 and FM4 over Greenland. Linear fits indicate that both instruments' measurements are consistent. A confidence test for  $\alpha$  of 95% indicates a significant difference between instruments of less than 1%.

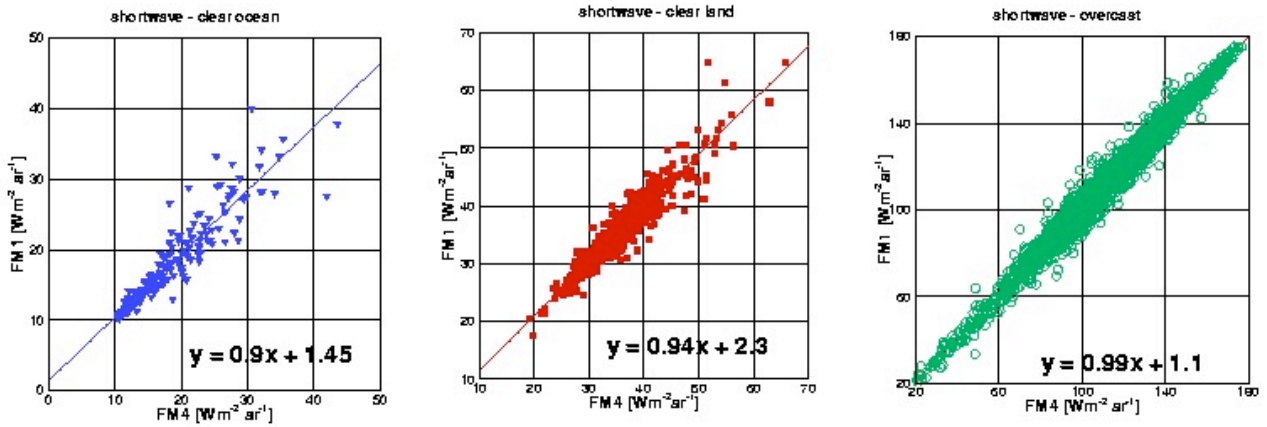


Figure 2. Scatter plots of shortwave radiance measured by FM1 and FM4 for different scene types. For clear ocean and clear land scene types, there is more scatter and bias attributable to possible scene misclassification (increased cloud cover).

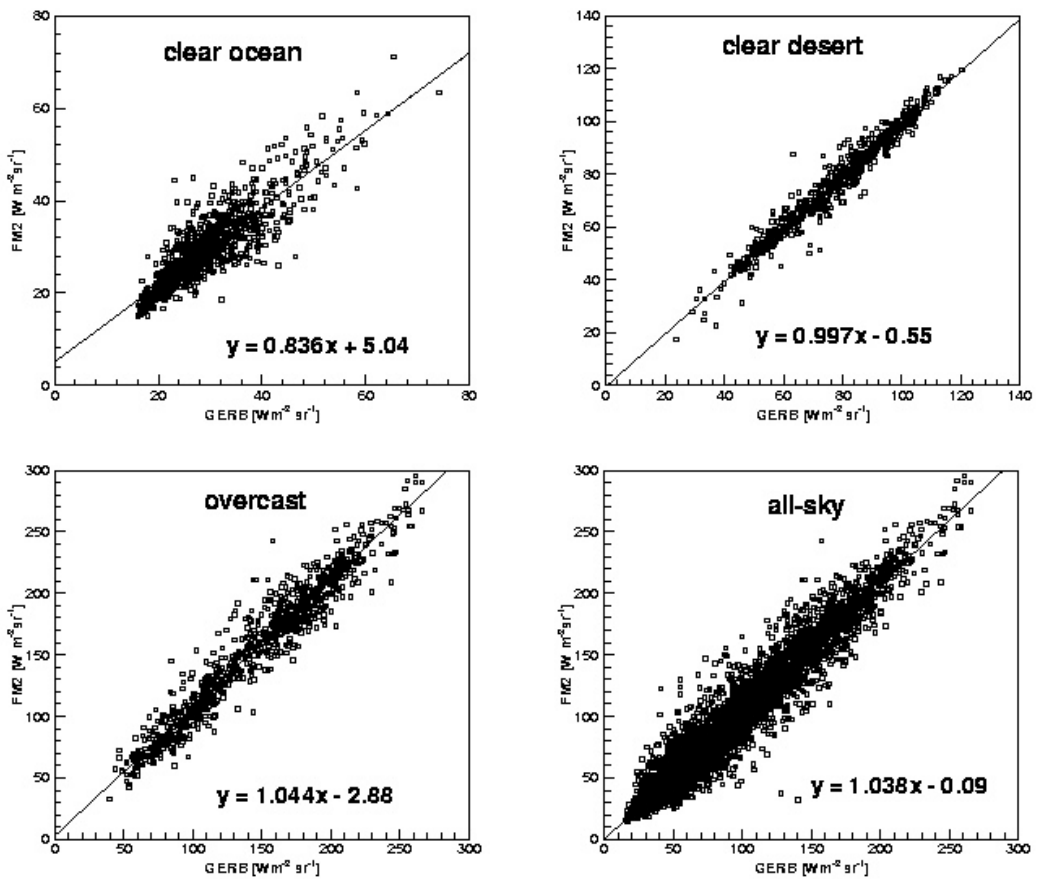


Figure 3. Scatter plots of shortwave radiances for different scene types as measured by GERB and FM2. Each sample shown on a plot represents a gridded average computed based on at least 20 CERES footprints and 4 GERB footprints. Both instruments show excellent correlation for a clear desert scene type. There is more bias for the overcast and clear ocean. As the plot for all-sky data indicates, differences of averages are well placed along the 45-degree line partly due to improved pointing accuracy of the GERB instrument based on SEVIRI data.

# Railroad Valley Playa for use in vicarious calibration of large footprint sensors

K.Thome, J. Czapla-Myers, S. Biggar

Remote Sensing Group, Optical Sciences Center, University of Arizona, Tucson AZ 85721

**Abstract** - The Remote Sensing Group at the University of Arizona has been successfully using the Railroad Valley Playa for the calibration of both large and small footprint sensors since 1999. This paper presents the results of this work for the EO-1, Terra, and Landsat platform sensors. The paper also describes work currently underway to overcome the limitation that Railroad Valley Playa requires on-site personnel for high-accuracy results. This work presents the design and implementation of a set of ground-based, ground-viewing radiometers based on LED detectors. The LED approach allows the radiometers to be robust and inexpensive. The goal is to combine these ground-look data with atmospheric data that are also autonomously collected to develop a model of the playa's surface for arbitrary sun-sensor geometries. This model is both spatial and spectral allowing the playa to be used for the reflectance-based calibration of any sensor viewing the playa with spatial resolutions up to the kilometer scale. Early results from this autonomous approach are presented for the Landsat ETM+ and MODIS sensors giving results of the same order of accuracy as those with on-site personnel. In addition, the results show that the intercomparison of sensors can occur using this ground test site without the need for coincident viewing of the site.

## I. INTRODUCTION

The reflectance-based approach relies on ground-based measurements of surface reflectance and atmospheric conditions to obtain inputs to a radiative transfer code.<sup>1</sup> The approach has been used more recently for both high resolution and low resolution sensors.<sup>2,3</sup> Examples of the results from ETM+ and the MODIS sensor on the Terra and Aqua platforms are shown in Figures 1 and 2 for the near-infrared bands of each sensor. The agreement with RSG results are typically in the +/-5% range and this is true for both large and small footprint sensors. Also, the number of points for MODIS is fewer than for ETM+ due to the larger footprint of MODIS. This limits the available

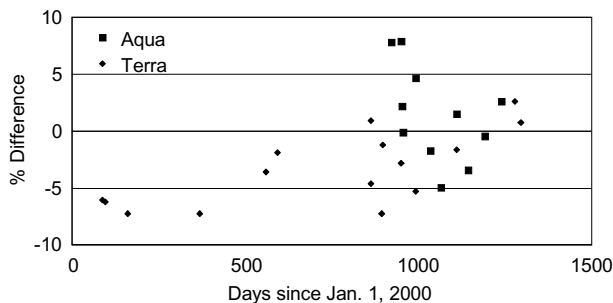


**Figure 1.** Reflectance-based results for MODIS NIR band (band 2). Percent difference is relative to Level 1B radiance reported by Aqua and Terra MODIS.

test sites for the RSG and increases the difficulty of collecting ground-based data for the reflectance-based approach.

A primary effort of MODIS is to develop synergy between morning and afternoon data sets from Aqua and Terra. This synergistic approach is also one purpose of the multi-sensor Terra platform and coordinated orbit with Landsat 7. This clearly requires that data from the sensors are radiometrically consistent necessitating an accurate radiometric calibration of the sensors.<sup>4</sup> Recent terrestrial imaging programs such as NASA's EOS program have taken great care during the preflight phase of the sensor characterization to ensure accurate calibration and consistency of laboratory calibrations across multiple national standards and individual vendor calibration facilities.<sup>5,6</sup> Preflight efforts are supplemented in flight by onboard calibrators.<sup>7,8,9</sup> It is also useful to supplement the onboard calibrator data with vicarious approaches. The reflectance-based approach provides such an accurate calibration and cross calibration.

## II. METHOD AND TEST SITE

The reflectance-based approach and Railroad Valley Playa have been described in detail in previous work.<sup>1,2,3</sup> Briefly, the RRV site used in this work on Bureau of Land Management land in central Nevada. It is approximately 15 km by 15 km in size at an elevation of 1.5 km elevation located in a region with typically clear weather. Typical atmospheric conditions at the site include an aerosol optical depth at 550 nm that is less than 0.05. The reflectance of the playa is generally greater than 0.3 and relatively flat spectrally. Ground-based measurements of the directional reflectance characteristics of the playa show it to be nearly lambertian out to view angles of 30 degrees for incident solar zenith angles seen for overpasses of Terra.

The reflectance-based method characterizes the surface of a test site and the atmosphere over that test site. The results of these characterizations are inputs to a radiative transfer code to

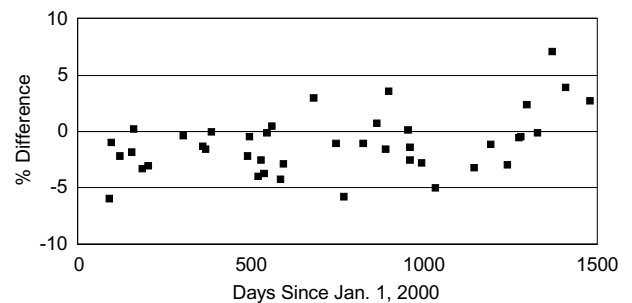


**Figure 2.** Reflectance-based results for ETM+ NIR band (band 4). Percent difference is relative to preflight calibration.

predict at-sensor radiance. The surface reflectance retrieval relies on transporting a spectroradiometer across a selected area. The approach adopted for large footprint sensors is to cover a 1-km by 1-km area with eight 500-m paths in a cross-like pattern. The site used for smaller footprint sensors is much smaller with the goal to collect 8-10 samples within a linear path through a given spatial pixel. A total of 30 to 64 pixels are sampled depending on the sensor. The other primary input to the radiative transfer code is the atmospheric conditions at the time of sensor overpass and these are obtained from solar extinction measurements.

### III. RECENT RESULTS AND INTERCOMPARISONS

Figure 3 shows the results of the VNIR bands of Terra, EO-1, and Landsat-7 sensors. This graph shows the average percent difference between predicted radiance from the reflectance-based approach to those reported by each sensor. The results do not use identical dates, but have similar numbers of total dates. All results for MODIS and MISR come from Railroad Valley Playa while the other sensors include results from the smaller Ivanpah Playa. Excluding the Ivanpah data sets does not impact strongly the results. In addition, data from Railroad Valley Playa for ASTER, ALI, Hyperion, and ETM+ are from measurements of a smaller test site that is approximately 700 m north of the site measured for MODIS and MISR.

Figure 3 shows good agreement between the sensors in the VNIR and the all sensors show similar standard deviations of the average with MISR showing the smallest standard deviations and ASTER the largest. MISR and MODIS agree to better than 4% in all bands and better than 2% in equivalent MISR bands 1 and 2. It should be noted that the larger difference in band 4 appears to be consistent with the behavior of MODIS bands 2 and 17 and the band 17 behavior of Terra MODIS is similar to Hyperion and MODIS on Aqua. The agreement between ASTER and the other two sensors is also reasonably with band 1 showing a difference of more than 6% with MODIS band 4 and ASTER band 2 has a 7% difference with MISR band 3. This is a significant difference when considering the expected accuracy of the vicarious results is 3% and the precision is

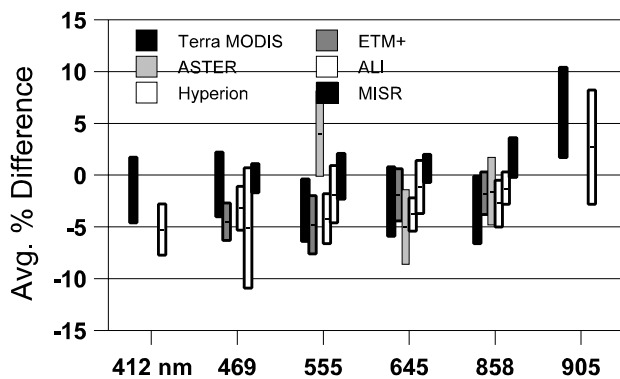


Figure 3 Intercomparison results of Terra, EO-1, and Landsat-7 sensors using the reflectance-based results as reference.

better than this. This example illustrates the utility of the reflectance-based approach as an intercomparison method.

### IV. AUTONOMOUS MEASUREMENTS

A difficulty with the reflectance-based approach is a lack of data points making it difficult to detect sensor degradation. One approach to improve this problem is to collect more ground-based data sets. This is not feasible due to personnel and budgetary constraints. Another method is to use invariant sites. Unfortunately, this RRV is not an invariant site. A combination of the invariant-scene approach with periodic ground-based collections to provide information about the spectral nature of the test site is then desired. A combination of ground-based monitoring instrumentation provides the necessary data for applying the reflectance-based approach whenever clear-sky conditions and an appropriate sensor overpass permits. The cornerstone is an LED-based detector package to characterize temporal changes in surface reflectance and instrumentation to provide atmospheric information.

Measurements of the spectral reflectance of RRV playa indicate that the surface maintains a basic spectral shape across the entire playa. Thus, placing an instrument that can monitor several spectral bands should provide enough spectral information regarding the spectral reflectance of the surface. Lightweight, inexpensive, and robust LED-based radiometers similar to those developed for the GLOBE project provide the basis of the ground reflectance collection.<sup>9</sup> The advantage to these “detectors” is their low cost, robust behavior, and built in spectral selection.<sup>10</sup> The first multispectral system deployed at Railroad Valley relies on four radiometer tubes with LEDs in the blue, green, red, and near infrared portion of the spectrum. Figure 4 shows typical radiometer output at Railroad Valley. from March 18-20. The current approach for converting these data to reflectance is to reference the data to a panel of known reflectance. This is similar to that of the standard reflectance-

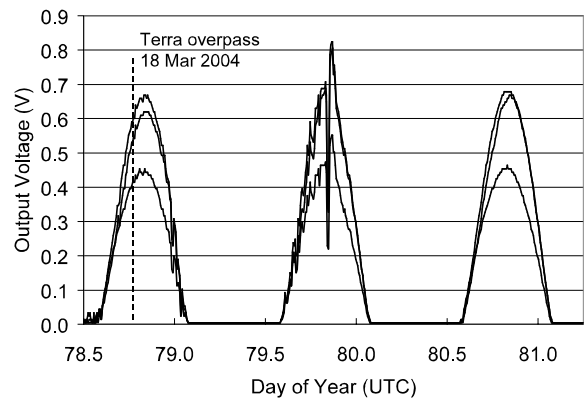
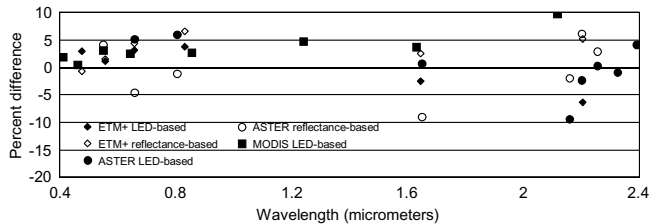


Figure 4. LED radiometer output for green, red, and near-infrared bands for March 18, 19, and 20 at Railroad Valley Playa. Also indicated in the figure is the Terra overpass time on March 18.



**Figure 5.** Percent differences between predicted at-sensor radiance and those reported by the ASTER, ETM+, and MODIS sensors. Solid symbols are based on LED-based approach while open symbols correspond to typical reflectance-based results

based approach except that the reference data are not collected at the time of the site measurements. The scattering and absorbing properties of the atmosphere are obtained from a Cimel CE318 sun photometer that is part of Goddard Space Flight Center's Aeronet.<sup>11</sup> An onsite meteorological station provides ancillary information for the sun photometer giving further indications of the atmospheric conditions.

Data collected on March 18, 2004 have been processed and compared to on-site data collected on the same date. The results for wavelengths less than 2  $\mu\text{m}$  show good agreement between the predicted and measured radiance. Wavelengths longer than 2  $\mu\text{m}$  show larger disagreements due to the lack of spectral bands in the LEDs at these wavelengths (see figure 5).

The ultimate goal of this work is to develop a ground-based system to increase the number of available calibrations for a given sensor using Railroad Valley Playa. One approach under study is to combine the LED data with ETM+ imagery and ground-based characterizations. This combined data set allows production of an image of Railroad Valley Playa at 10-nm spectral resolution and 30-m spatial resolution for any given date, time, and view angle. The LED ground-based data and the MODIS data will be used to derive BRDF of the playa. MODIS and ETM+ data combined with hyperspatial data from commercial sensors to evaluate the temporal variability.

The atmospheric data from the sun photometer are used to atmospherically correct the Landsat-7 ETM+ data to derive the surface reflectance on a 30-m spatial scale. These data are extended to hyperspectral reflectance using ground-based hyperspectral measurements at high spectral resolution. This gives the surface reflectance required for the radiative transfer code to produce an at-sensor radiance and combined with the atmospheric data provides the at-sensor radiance for a selected view geometry and solar geometry (based on date and time). The LED data, coupled with rainfall information, are used to fill the temporal gap between the Landsat overpasses.

## V. CONCLUSIONS

Much of the future work for this effort will focus on improving the LED radiometers so that they provide temporally accurate

data. It is important to place the radiometers to allow accurate characterization of the playa surface while keeping the number of radiometers to a minimum for logistical and cost reasons.

The overall conclusions of this work are that vicarious methods are proving to be an excellent approach for cross-comparing the radiometric response of remote sensing systems and the use of a well-understood test site such as Railroad Valley Playa is helpful in applying these vicarious approaches. Such results will have ever increasing importance as the possibility of data gaps in such data sets as the Landsat-series of data increases. Vicarious methods can now provide a method for closing these possible data gaps allowing for the long-term records to be extended even without overlap.

## REFERENCES

1. P. N. Slater, S. F. Biggar, R. G. Holm, R. D. Jackson, Y. Mao, M. S. Moran, J. M. Palmer, and B. Yuan, "Reflectance- and radiance-based methods for the in-flight absolute calibration of multispectral sensors," *Rem. Sens. Env.*, Vol. 22, pp 11-37, 1987.
2. Thome K. J., J. Czapla-Myers, S. F. Biggar, "Vicarious calibration of Aqua and Terra MODIS," *Proc. SPIE Conf. #5151*, pp. 395-405, San Diego, Calif., 2003.
3. Thome, K. J., "Absolute radiometric calibration of Landsat-7 ETM+ using the reflectance-based method," *Remote Sensing of Environment*, 78, pp. 27-38, 2001.
4. J. J. Butler and R. A. Barnes, "Calibration strategy for the Earth Observing System (EOS)-AM1 platform," *IEEE Trans. On Geoscience and Remote Sensing*, Vol. 36, pp. 1056-1061, 1998.
5. Butler, J. J., S. W. Brown, ..., "Radiometric measurement comparison on the integrating sphere source used to calibrate the Moderate Resolution Imaging Spectroradiometer (MODIS) and the Landsat-7 Enhanced Thematic Mapper Plus," *J. of Res. Of the Nat'l Inst. of Standards and Technology*, 108, pp. 199-228, 2003.
6. Butler, J. J., B. C. Johnson, and R. A. Barnes, "Radiometric measurement comparisons at NASA's Goddard Space Flight Center: Part 1. The GSFC sphere sources," *The Earth Observer*, 14, pp. 3-7, 2002.
7. A. Ono, F. Sakuma, K. Arai, Y. Yamaguchi, H. Fujisada, P. N. Slater, K. J. Thome, F. D. Palluconi, and H.H. Kieffer, "Preflight and In-flight calibration plan for ASTER," *J. of Atmos. and Oceanic Tech.*, Vol. 13, pp. 322-335, 1996.
8. C.J. Bruegge, B.G. Chafin, N.C.L. Chrien, D.J. Diner, R. Ando, "In-flight calibration of the EOS/ Multi-angle Imaging SpectroRadiometer (MISR)," *Sensors, Systems, and Next Generation Satellites*, Vol. 4169-08, 2000.
9. Mims III, Forrest M., "Sun photometer with light-emitting diodes as spectrally selective detectors", *Applied Optics*, Vol. 31, No. 33, pp. 6965-6967, 1992.
10. Mims III, Forrest M., "An inexpensive and stable LED Sun photometer for measuring the water vapor column over South Texas from 1990 to 2001", *Geophysical Research Letters*, Vol. 29, pp. 20-1 - 20-4, 2002.
11. B. N. Holben, T. F. Eck, I. Slutsker, D. Tanre, J. P. Buis, A. Setzer, E. Vermote, J. A. Reagan, Y. Kaufman, T. Nakajima, F. Lavenu, I. Jankowiak, and A. Smirnov, "AERONET - A federated instrument network and data archive for aerosol characterization," *Rem. Sens. Environ.*, 66, 1-16, 1998.

# Investigation of Spectral Effects On Radiometric Cross-Calibration Between Multiple Satellite Sensors

P.M. Teillet<sup>\* a</sup>, G. Fedosejevs<sup>a</sup>, and K.J. Thome<sup>b</sup>

<sup>a</sup> Canada Centre for Remote Sensing, 588 Booth Street, Ottawa, Ontario, K1A 0Y7

<sup>b</sup> Remote Sensing Group, Optical Sciences Center, University of Arizona,  
1630 E. University Blvd, Tucson, Arizona, USA 85721-0094

**ABSTRACT:** Spectral band difference effects have been investigated in the context of radiometric cross-calibration between five Earth observation satellite sensors in the Landsat solar-reflective spectral domain. Modelling results are presented in the form of spectral band adjustment factors for all sensor spectral band combinations for two test sites.

**Keywords:** spectral response functions, radiometric calibration, satellite sensors, optical remote sensing.

## 1. INTRODUCTION

This paper reports on an investigation of radiometric calibration errors due to differences in spectral response functions between satellite sensors when attempting cross-calibration based on near-simultaneous imaging of common ground targets in analogous spectral bands. Given that the Landsat-7 Enhanced Thematic Mapper Plus (ETM+) is well-calibrated radiometrically, cross-calibration between the ETM+ and several other sensors was the starting point for the study. In particular, five Earth observation sensors on three satellite platforms were included on the basis of their overpass times being within 45 minutes of each other on the same day (Landsat-7 ETM+; Earth Observing-1 Advanced Land Imager (EO-1 ALI); Terra MODIS; Terra Advanced Spaceborne Thermal Emission and Reflection (ASTER); Terra Multi-angle Imaging Spectro-Radiometer (MISR)) (Table 1). Scene content was simulated using ground target spectra for the calibration test sites at Railroad Valley Playa, Nevada (RVPN) and Niobrara Grassland, Nebraska (NIOB). With SBDEs on cross calibration between ETM+ and other sensors in hand, it was straightforward to examine all other combinations between sensors (in spectral bands with analogs to one or more of the six solar-reflective Landsat bands). Results were obtained as a function of calibration test site, satellite sensor, and spectral region. The paper also makes recommendations on spectral data and tools that would facilitate cross-calibration between multiple satellite sensors.

Satellite	Sensor	Blue Band	Green Band	Red Band	NIR Band	SWIR Band I	SWIR Band II
Landsat-7	ETM+	1	2	3	4	5	7
Earth Observing 1	ALI	1	2	3	4p	5	7
Terra	MODIS	3	4	1	2	6	7
Terra	MODIS	10	12	13	16	-	-
Terra	ASTER	-	1	2	3	4	6
Terra	MISR	1	2	3	4	-	-

Table 1. Satellite sensors and analogous spectral band numbers, where NIR = near infrared; SWIR = shortwave-infrared.

## 2. METHODOLOGY

The cross-calibration radiometric formulation developed by Teillet et al. (2001) yields a spectral band adjustment factor,  $B_i$ , for the two sensors being compared, reference sensor ("R") and another sensor ("X") whose calibration is to be checked via cross-calibration with respect to sensor R in analogous spectral band i:

$$B_i = \rho_{iR}^* / \rho_{iX}^* . \quad (1)$$

$\rho^*$  is top-of-atmosphere (TOA) at-sensor reflectance.  $\rho_{iX}^*$  and  $\rho_{iR}^*$  are not the same because of the differences in relative spectral response profiles between corresponding (analogous) spectral bands. Figure 1 illustrates these differences for the green band for the satellite sensors involved. Thus, one of the keys to this method of cross-calibration is to have sufficient knowledge of the spectral band adjustment factor  $B_i$ , since uncertainty in the cross-calibration due to this effect is directly proportional to the uncertainty in  $B_i$ . The surface reflectance spectra for both ground targets were used as inputs to an atmospheric radiative transfer (RT) code to calculate the TOA reflectances in corresponding solar reflective spectral bands for all five sensors under consideration. The RT code is the Canadian Advanced Modified

\* [phil.teillet@ccrs.nrcan.gc.ca](mailto:phil.teillet@ccrs.nrcan.gc.ca); phone 1-613-947-1251; fax 1-613-947-1408; <http://www.ccrs.nrcan.gc.ca/ccrs/>

5S (CAM5S) code (O’Neill et al., 1996). Inputs consisted of the aforementioned surface reflectance spectra plus standard choices for the atmospheric models (US62 atmospheric profile and continental aerosol model). The aerosol optical depth was set at 0.05 at 0.55 micrometers and the solar zenith angle was set at 60 degrees. An Earth-Sun distance of 1 A.U. and nadir viewing geometry were also assumed. Actual terrain elevations were used (1.425 km and 0.760 km for RVPN and NIOB, respectively). Given that the NIOB test site is a grassland area, it was meaningful to generate results for NDVI, which can be defined as a function of TOA reflectance in the red and NIR bands and

$$B_N = NDVI_R / NDVI_X \quad (2)$$

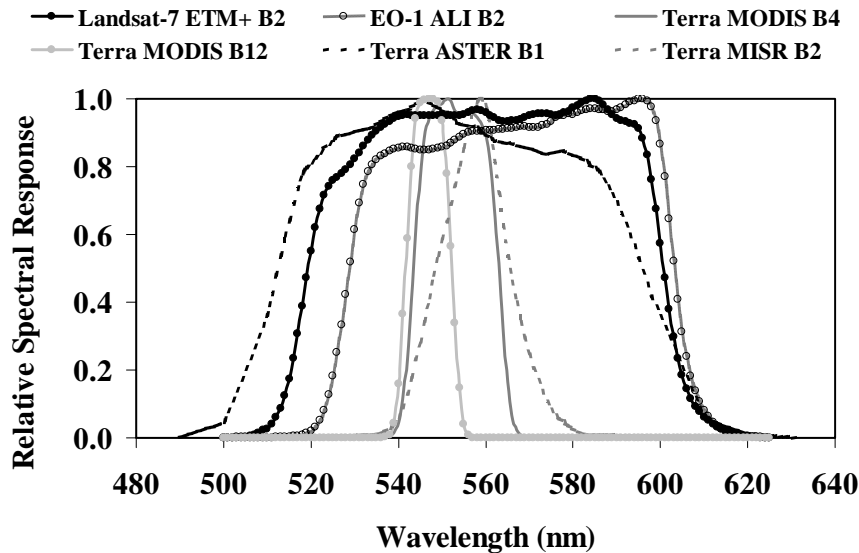


Figure 1. Satellite sensor spectral bands analogous to Landsat ETM+ band 2.

### 3. RESULTS

The modeling results are presented in the form of matrices of the spectral band adjustment factors  $B_i$  for all sensor spectral band combinations for both test sites (Table 2). Because SBDEs are but one of many sources of sensor Xcal uncertainty, one would like them to be as small as possible. Hence, “very good” cases are considered to be those where the  $B_i$  spectral band adjustment factors (equation 1) are within  $\pm 1\%$  of  $B_i = 1$  (i.e., 0.99 – 1.01). In such cases, uncertainty or lack of knowledge about the spectral content of the scene should not significantly compromise the cross-calibration. Similarly, “good” results are defined as those that are  $\pm 1\%$  to  $3\%$  off  $B_i = 1$  (i.e., in the range of 0.97-0.99 and 1.01-1.03), whereas “poor” results are those off by  $\pm 3\%$  to  $7\%$  (i.e., in the ranges of 0.93-0.97 and 1.03-1.07). “Bad” cases are those with spectral adjustment factors off by greater than  $7\%$  (i.e., in the ranges of  $< 0.93$  and  $> 1.07$ ). It is clear from Table 2 that the RVPN calibration site is less susceptible to SBDEs than the NIOB site in almost all sensor Xcal combinations examined. For the NIOB site and for the sensors involved, with few exceptions, the spectral content of the scene must be known for accurate cross-calibration based on near-simultaneous imaging. The green spectral region for the RVPN site is the best overall in that two-thirds of the Xcal combinations are “very good” and the remaining third are all “good”. The “poorest” spectral region overall is the NIR for both test sites. For the NIOB site, there are no spectral regions that can be considered “very good” and only the green and red spectral regions have more than a few “good” Xcal combinations. For the RVPN site, the ETM+ band 7 analog spectral region is also to be avoided in the absence of SBDE corrections. Sensor Xcal combinations involving ETM+, ALI, ASTER and one MODIS band set (bands 3, 4, and 1) are “very good” in the blue, green and red spectral regions for RVPN (the one exception is the band 2 analog band combination of ASTER band 1 and MODIS band 4 where  $B_i = 0.985$ ). Sensor combinations involving MISR are the most susceptible to SBDEs, with generally “poor” results. Overall, there are no sensor Xcal combinations for which the entire Landsat solar-reflective spectral domain yields “good” results in the absence of SBDE corrections. While there are a few “very good” cases, the NDVI is generally highly susceptible to SBDEs (Table 3), with a percent root mean square difference in  $B_N$  (equation 2) from unity of  $9.4\%$  across the set of 15 comparisons.

Sensor Spectral Bands	Railroad Valley Playa						Niobrara Grassland					
ETM+ Band 1 Analogs	A	B	C	D	E	F	A	B	C	D	E	F
A: Landsat-7 ETM+ B1	1	0.995		1.005	0.990	1.025	1	1.032		0.967	1.076	0.844
B: EO-1 ALI B1		1		1.010	0.995	1.030		1		0.937	1.043	0.818
C: Terra ASTER N/A												
D: Terra MODIS B3				1	0.985	1.020				1	1.113	0.873
E: Terra MODIS B10					1	1.035					1	0.784
F: Terra MISR B1						1						1
ETM+ Band 2 Analogs	A	B	C	D	E	F	A	B	C	D	E	F
A: Landsat-7 ETM+ B2	1	0.996	1.005	0.990	0.988	0.989	1	1.018	0.982	0.956	1.005	0.966
B: EO-1 ALI B2		1	1.009	0.994	0.992	0.993		1	0.965	0.939	0.987	0.949
C: Terra ASTER B1			1	0.985	0.983	0.984			1	0.974	1.023	0.984
D: Terra MODIS B4				1	0.998	0.999				1	1.051	1.010
E: Terra MODIS B12					1	1.001					1	0.961
F: Terra MISR B2						1						1
ETM+ Band 3 Analogs	A	B	C	D	E	F	A	B	C	D	E	F
A: Landsat-7 ETM+ B3	1	0.998	1.001	0.997	1.016	0.950	1	1.004	0.962	0.983	1.017	1.015
B: EO-1 ALI B3		1	1.003	0.999	1.018	0.952		1	0.958	0.979	1.013	1.011
C: Terra ASTER B2			1	0.996	1.015	0.949			1	1.022	1.057	1.055
D: Terra MODIS B1				1	1.019	0.953				1	1.035	1.033
E: Terra MODIS B13					1	0.935					1	0.998
F: Terra MISR B3						1						1
ETM+ Band 4 Analogs	A	B	C	D	E	F	A	B	C	D	E	F
A: Landsat-7 ETM+ B4	1	0.947	1.037	0.961	0.942	0.948	1	0.911	1.069	0.926	0.906	0.911
B: EO-1 ALI B4p		1	1.095	1.015	0.995	1.001		1	1.173	1.016	0.995	1.000
C: Terra ASTER B3			1	0.927	0.908	0.914			1	0.866	0.848	0.852
D: Terra MODIS B2				1	0.980	0.986				1	0.978	0.984
E: Terra MODIS B16					1	1.006					1	1.006
F: Terra MISR B4						1						1
ETM+ Band 5 Analogs	A	B	C	D	E	F	A	B	C	D	E	F
A: Landsat-7 ETM+ B5	1	0.989	0.976	0.972			1	0.992	0.931	0.920		
B: EO-1 ALI B5		1	0.987	0.983				1	0.939	0.927		
C: Terra ASTER B4			1	0.996					1	0.988		
D: Terra MODIS B6				1						1		
E: Terra MODIS N/A												
F: Terra MISR N/A												
ETM+ Band 7 Analogs	A	B	C	D	E	F	A	B	C	D	E	F
A: Landsat-7 ETM+ B7	1	0.957	0.938	0.795			1	0.947	0.804	0.846		
B: EO-1 ALI B7		1	0.980	0.831				1	0.849	0.893		
C: Terra ASTER B6			1	0.848					1	1.052		
D: Terra MODIS B7				1						1		
E: Terra MODIS N/A												
F: Terra MISR N/A												

Table 2. Results for spectral band adjustment factors  $B_i$ . Relative to  $B_i = 1$ , cells for factors within  $\pm 1\%$  (i.e., 0.99 – 1.01) are white, factors within  $\pm 1\%$  to  $3\%$  (i.e., 0.97-0.99 and 1.01-1.03) are light grey, factors within  $\pm 3\%$  to  $7\%$  (i.e., 0.93-0.97 and 1.03-1.07) are medium grey, and factors greater than  $7\%$  (i.e.,  $< 0.93$  and  $> 1.07$ ) are dark grey.

Sensor	Niobrara Grassland					
	A	B	C	D	E	F
<b>ETM+ NDVI Analogs</b>						
<b>A: Landsat-7 ETM+</b>	1	1.068	0.923	1.080	1.080	1.076
<b>B: EO-1 ALI</b>		1	0.864	1.011	1.011	1.007
<b>C: Terra ASTER</b>			1	1.170	1.170	1.166
<b>D: Terra MODIS B1B2</b>				1	1.000	0.996
<b>E: Terra MODIS B13B16</b>					1	0.996
<b>F: Terra MISR</b>						1

Table 3. Results for spectral band effects on NDVI  $B_N$ . Relative to  $B_N = 1$ , cells for factors within  $\pm 1\%$  (i.e., 0.99 – 1.01) are white, factors within  $\pm 1\%$  to  $3\%$  (i.e., 0.97-0.99 and 1.01-1.03) are light grey, factors within  $\pm 3\%$  to  $7\%$  (i.e., 0.93-0.97 and 1.03-1.07) are medium grey, and factors greater than  $7\%$  (i.e.,  $< 0.93$  and  $> 1.07$ ) are dark grey.

#### 4. CONCLUDING REMARKS

Overall, in the absence of corrections for SBDE, the Railroad Valley Playa site is a “good” to “very good” ground target for cross-calibration between most but not all satellite sensors considered in most but not all spectral regions investigated. “Good” and “very good” are defined as SBDEs within  $\pm 3\%$  and  $\pm 1\%$ , respectively. Without SBDE corrections, the Niobrara test site is only “good” for cross-calibration between certain sensor combinations in some spectral regions. It is clear from the results that, except for a limited number of cases, sound Xcal requires that the spectral characteristics of the common ground targets used be known. Indeed, even for the Railroad Valley Playa test site, a target that has relatively low spectral variability across most wavelength regions of interest, one can only do without SBDE corrections in selected cases: primarily sensor Xcal combinations involving ETM+, ALI, ASTER, and MODIS in the blue, green, and red spectral regions. Thus, low-cost Xcal methodologies that seek to complement the more accurate calibrations that often (but not always) result from costly field campaigns should somehow take SBDEs into account. The following spectral data and tools are recommended to facilitate cross-calibration between satellite sensors.

- An on-line repository of relative spectral response profiles for as many Earth observation sensors as possible.
- An on-line repository of well-documented ground spectra for key calibration test sites.
- Tools for easy transformations between different wavelength grids to facilitate comparisons.

Agencies that assume responsibility for one or more of these repositories should coordinate their activities with the Committee on Earth Observation Satellites (CEOS) Working Group on Calibration and Validation (WGCV).

#### REFERENCES

- Teillet, P. M., Barker, J., Markham, B. L., Irish, R. R., Fedosejevs, G., and Storey, J. C., “Radiometric Cross-Calibration of the Landsat-7 ETM+ and Landsat-5 TM Sensors Based on Tandem Data Sets”. *Remote Sensing of*
- O’Neill, N.T., Royer, A., and Nguyen, M.N., “Scientific and Technical Report on the Development of a Modified Version of the H5S Code which Incorporates Major Features of the 6S Code”, CARTEL Internal Report CARTEL-1996-020, CARTEL, Department de géographie et télédétection, 2500, boul. de l’Université, Université de Sherbrooke, Sherbrooke, Québec, Canada J1K 2R1, 62 p (1996).

# SCIAMACHY inflight calibration issues: instrument monitoring and calibration two years after launch

Manfred W. Wuttke, Stefan Noël, Jochen Skupin, Konstantin Gerilowski,  
Heinrich Bovensmann and John P. Burrows,  
Institute of Environmental Physics and Remote Sensing,  
University of Bremen, FB1 Physik,  
P. O. Box 3304,D28334 Bremen, Germany

October 12, 2004

## 1 Introduction

### 1.1 The SCIAMACHY instrument

The Scanning Imaging Absorption Spectrometer for Atmospheric Chartography[1] (SCIAMACHY) is one of 10 scientific instruments on the European environmental research satellite ENVISAT, which has been launched into a sun-synchronous polar orbit on 2002-03-01. SCIAMACHY comprises light collection optics, spectrometer, electrical, thermal and calibration subsystems. Electromagnetic radiation, reaching the instrument, is collected by a scan mirror and telescope. After passing through the spectrometer entrance slit, the light is dispersed. A small part of this spectrum is sent to the broad band polarization monitoring devices (PMDs). The majority of the light is directed to 8 channels, each containing a grating lens and linear diode array detectors (see Fig. 1). In this manner the entire spectrum between 220 and 2380 nm is recorded simultaneously having channel dependent spectral resolution of 0.2 to 1.4 nm (see Tbl. 1) .

Thus the instrument consists mainly of two parts: the optical bench module (OBM) which basically divides the incoming light into the 8 channels and a scanner module used to perform different viewing geometries, i. e. observations are made in nadir, limb and solar and lunar occultation modes[2] (see Figs. 2 and 4). By combining nadir and limb measurements it is possible to observe the same volume of air in two different geometries in the same orbit. Inversion of these measurements provides the amount and global distribution of a large number of atmospheric constituents, such as O<sub>3</sub>, BrO, OClO, ClO, SO<sub>2</sub>, H<sub>2</sub>CO, NO<sub>2</sub>, CO, CO<sub>2</sub>, CH<sub>4</sub>, H<sub>2</sub>O, N<sub>2</sub>O, metals, clouds, and aerosols (see Fig. 3).

channel	spectral range [nm]	spectral resolution [nm]	Detector material	operating temperature [K]
1	240 - 314	0.24	Si	185 - 215
2	309 - 405	0.26	Si	185 - 215
3	394 - 620	0.44	Si	215 - 235
4	604 - 805	0.48	Si	215 - 235
5	785 - 1050	0.54	Si	225 - 235
6	1000 - 1750	1.48	InGaAs	190 - 210
7	1940 - 2040	0.22	InGaAs	130 - 160
8	265 - 2380	0.26	InGaAs	130 - 160

Table 1: SCIAMACHY Detector characteristics

### 1.2 Instrument calibration

The absolute radiometric calibration of the SCIAMACHY detector readouts is defined in detail in the SCIAMACHY Algorithm Theoretical Basis Document [3]. The calibration includes the following steps:

- Memory effect correction
- Dark signal correction
- Pixel-to-pixel gain (PPG) correction
- Etalon correction
- Spectral calibration

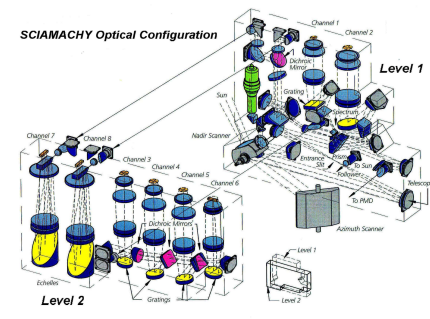


Figure 1: SCIAMACHY optical configuration.

- Correction of internal straylight
- Polarization correction (not needed for unpolarized solar irradiance)
- Absolute radiometric calibration

Additional corrections that are necessary to compare the SCIAMACHY solar irradiance with validation sources include:

- Doppler shift correction
- Sun-earth distance correction

The calibration depends on the calibration key-data obtained from measurements of a number of onground calibration campaigns before launch. A correct consistent set of key-data is yet to be delivered to the operational data processor.

### 1.3 Monitoring concept

Health and performance of the SCIAMACHY instrument are regularly monitored by the Sciamachy Operations Support Team (SOST) located at DLR-Oberpfaffenhofen and the University of Bremen. Monitoring activities are essential to detect and possibly correct for the degradation of instrument components. Therefore operational long-term monitoring (OLTM) is a prerequisite for a high data product quality throughout the lifetime of SCIAMACHY. One part of the long-term monitoring activities is the trend analysis of measurements with the internal White Light Source (WLS) and of observations of the unobscured Sun above the atmosphere. A more detailed description of the SCIAMACHY monitoring concept including some results from early WLS measurements can be found in the references.[4, 5, 6]

SCIAMACHY comprises two scanner systems: The Azimuth Scanner Module (ASM) and the Elevation Scanner Module (ESM). Both modules contain a mirror and a diffuser which is mounted on the backside of the mirror.[7, 8, 5] In order to monitor the different SCIAMACHY light paths solar measurements are taken in various viewing geometries: In

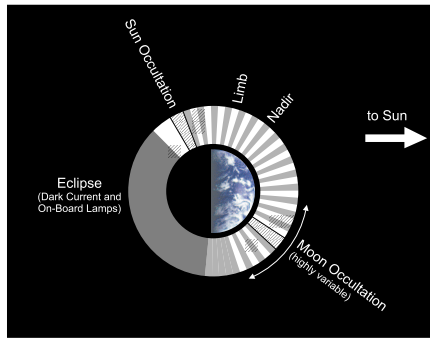


Figure 2: Typical SCIAMACHY orbital sequence of measurements.

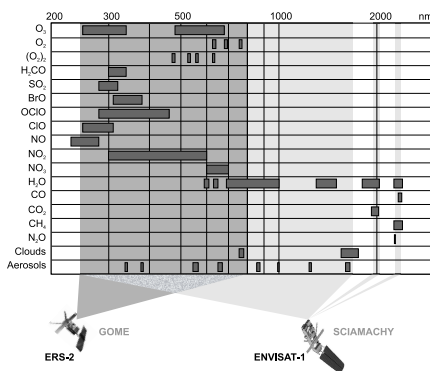


Figure 3: Products to be retrieved from different SCIAMACHY wavelength ranges and comparison with GOME

limb/occultation geometry (via ASM and ESM mirrors), in nadir geometry (via the ESM mirror through the subsolar port), and via the so-called calibration light path involving the ASM mirror and the ESM diffuser. SCIAMACHY long-term monitoring comprises a regular analysis of these measurements.

So called m-factors are used in the 0-1b processor to compensate for the radiometric degradation of SCIAMACHY's optical components. In general, a m-factor is defined as the ratio between a measured solar spectrum at the time  $t$  to a reference spectrum obtained for the same optical path at the instrument's begin of life.[6]

Ideally, these reference spectra should be taken on-ground, but in practice this is not possible because measurements of the unobscured sun cannot be performed on-ground. Therefore, an early in-flight measurement is taken as reference. These m-factors provide an end-to-end monitoring of the different light paths under the assumptions, that the relative sensitivity to polarized light parallel and perpendicular to the entrance slit does not change and that there is no change in the instrument performance between the last on-ground and the first in-flight measurements. The m-factors are fed back into the operational Level 0 to 1b processing and must therefore be based on operationally calibrated Level 1b spectra to avoid double correction of instrumental effects.

## 2 Instrument status: First Results of the Long Term Monitoring

It is a task of the OLTM to compute the m-factors and to provide them as input for the operational 0-1b processor. This OLTM m-factor function shall be activated once a month. Shorter timescales or different timescales for each m-factor will be required when the m-factors show a higher temporal variability.

Due to the fact that up to now the operational calibration of the Level 1b products is not sufficient, the m-factor function and the operational monitoring based on Level 1b products[6] are not active. Instead, Level 0 data are used to monitor the instrument status.

The plots displayed on the website [9] show the results of these monitoring activities for all SCIAMACHY channels. All measured signals have been averaged over the entire channel and then divided by the corresponding

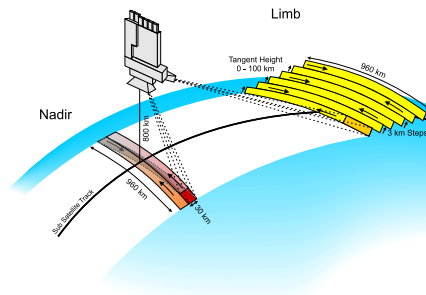


Figure 4: SCIAMACHY Nadir and limb scans.

measurement at a reference time (currently 2 August 2002, at about orbit 2200), yielding an effective instrument throughput for the considered light paths, i. e.

1. White Light Source via ESM Mirror
2. Sun via ASM Mirror and ESM Diffuser
3. Sun via ASM mirror and ESM Mirror
4. Sun via ESM Mirror through subsolar port

These instrument throughputs are plotted for each channel as function of time since 2002-08-02.

Note that measurements performed during times of reduced instrument performance (e.g. switchoffs or decontamination periods) have been omitted. The results presented here are based on the analysis of uncalibrated Level 0 data, which have been corrected for dead/bad pixels, dark current, scan angle dependencies, quantum efficiency changes, and the seasonally varying distance to the Sun. Additional calibration steps, like for example a stray-light correction, have not been performed. Therefore, variations smaller than about 1 % may not be due to instrumental effects and require careful investigation. However, some features in the plots require additional explanation:

- The timing of subsolar measurements before 30 November 2002 (about orbit 3922) did not consider the known yaw misalignment of SCIAMACHY on ENVISAT. This is the reason for the deviations of the average subsolar signal from the other light paths before this time. The timing has been corrected in the final flight settings. To take this change into account, all subsolar measurements after 30 November 2002 have been referred to orbit 4519 (10 January 2003, just after a long decontamination phase).
- Between 21 and 27 February 2003 the detector temperature settings have been slightly changed. This explains small jumps in the average signals at about orbit 5140 (especially visible in channel 1 for subsolar measurements).
- The WLS has proven to be radiometrically very stable except for a degradation in the UV which is correlated with the burn time (This correlation was confirmed during the commissioning phase before the period shown here, where the WLS was extensively used).
- Variations of the measured average solar signal are often correlated with solar activity. Especially, this can be seen in the "Sun via ASM Mirror and ESM Mirror" data, which have the best temporal resolution.
- The (end of the) partial solar eclipse of 31 July 2003 shows up in the monitoring plots as a slight decrease of the "Sun via ASM Mirror and ESM Mirror" signal. This signal drop is not visible in the other data, because there were no corresponding measurements for the other light paths at the time of the eclipse.
- The "Sun via ASM Mirror and ESM Mirror" data for 9 and 10 December 2003 are affected by the reduced ENVISAT pointing performance during this time.

The results show that SCIAMACHY is degrading much less than expected from the experience with GOME [10, 11], in the UV at a rate of approximately 3 % per year. In the visible and near-infrared wavelength region - i. e. in channels 3 to 6 - SCIAMACHY is stable on a sub-percent level. These results are permanently displayed on the website <http://www.iup.physik.uni-bremen.de/sciamachy/LTM/LTM.html> and updated on a daily base.

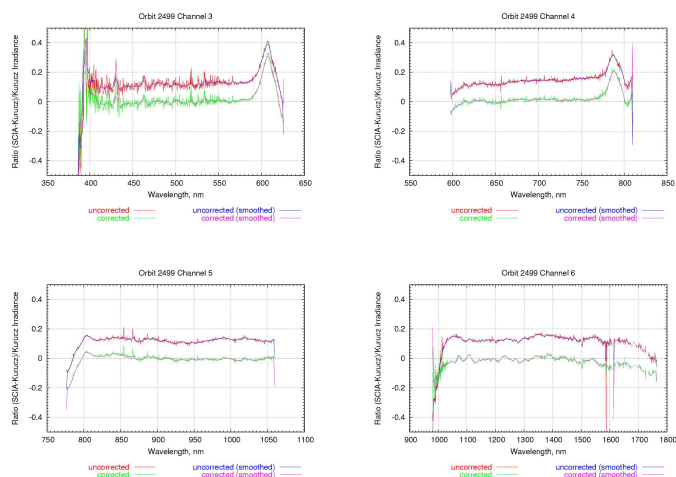


Figure 5: Comparison of SCIAMACHY irradiances with a Kurucz solar reference spectrum for orbit 2499, channels 3 – 6. For each channel the upper curves are data calibrated with uncorrected, the lower curves with corrected key-data.

## 3 In-Orbit Calibration issues

### 3.1 Radiometric calibration

Optical bench module (OBM) and scanner mechanism were calibrated extensively on-ground using internal and external light sources but already first in-flight validation results showed inconsistencies in this initial radiometric calibration of SCIAMACHY.[12] First comparisons of radiances and irradiances measured by SCIAMACHY with independent sources indicate an error in the absolute radiometric calibration, which has a strong impact on the quality of most level-1 data products.[13] To overcome this problem, an extensive analysis of the radiometric on-ground calibration measurements of SCIAMACHY has been performed, and a new procedure has been developed to recalculate some of the radiometric key data from existing end-to-end measurements. These calculations were primarily based on a subset of NASA sphere measurements, performed for SCIAMACHY’s radiance and irradiance verification during the OPTEC-5 period in 1999/2000. This integrating sphere is a 20” diameter internally illuminated sphere coated with BaSO<sub>4</sub>. It has a long history of providing accurate absolute radiances for NASA’s SBUV2 and TOMS programs and has also been used for the validation of the GOME absolute radiance calibration. First tests with in-flight measurements show a significant improvement of the quality of the level-1 data products when using these new key data.[14]

In Fig. 5 as a result of this analysis a comparison of SCIAMACHY irradiances with a Kurucz solar reference spectrum for orbit 2499 and for the channels 3 – 6 is shown. The deviation of more than 10 % when using the old key-data is almost completely removed when using the corrected key-data.

Note that the newly derived correction factors and key data are based on only a subset of the available on-ground measured data. For this subset the most appropriate data of a certain type have been selected (e.g. NASA sphere radiance measurements at the largest distance and a FEL irradiance measurement close in time to that). Using other (also reasonable) data to compute the correction factors/key data may give slightly different results because of e.g. different thermal conditions of SCIAMACHY during the measurement. The deviations resulting from different data sets are expected to be in the order of 1 % for the absolute radiance/reflectance.

### 3.2 Icing

During in-flight operation an ice layer buildup is observed on the detectors of channels 7 and 8 of SCIAMACHY causing a loss of radiative sensitivity up to 80 % [12]. These ice layers can be removed by decontamination procedures, i. e. heating the instrument, originally only foreseen to decontaminate the radiative coolers. But the (presumably water) ice is coming back to different levels after some time after each decontamination period. The source of this contamination is probably water vapour carried into orbit by the spacecraft and contained in the instrument structure and under the MLI cover. The mechanism how the water vapour is contained in the structure of channels 7 and 8 and how it is distributed between them is not understood. A light leak in channel 7 and the covering of venting holes by the spacecraft MLI may play a role. Note that after the last decontamination end of June 2004

when one would have thought that channel 7 is almost free of water, the throughput loss is as bad as in October 2002.

In order to compensate this throughput loss it has been decided to include a throughput correction for these channels in the operational data processing. The correction shall be performed by multiplication of the radiances and irradiances with a spectral dependent throughput correction factor determined from regular measurements of the unobscured sun. The main purpose of the correction is to enhance the quality of the level 1 products. Since both radiances and irradiances are to be multiplied with the same throughput correction factor, the throughput correction should not affect sun- or earthshine-normalised radiances which are typically used in 1–2 processing. However, since the PMD detectors are – as far as it is known at the moment – not affected by icing, the throughput loss (and its correction) may affect the computation of the PMD virtual sum and thus the polarisation correction factor. This in turn may also influence the level 2 products.

## 4 Acknowledgments

SCIAMACHY is a national contribution to the ESA ENVISAT project, funded by Germany, The Netherlands, and Belgium. SCIAMACHY Level 0 Data have been provided by ESA. This work has been funded by the BMBF via GSF/PT-UKF, by DLR-Bonn, and by the University of Bremen.

## References

- [1] J. P. Burrows, E. Hölzle, A. P. H. Goede, H. Visser, and W. Fricke, “SCIAMACHY — Scanning Imaging Absorption Spectrometer For Atmospheric Cartography,” *Aas* **35**(7), pp. 445–451, 1995.
- [2] S. Noël, H. Bovensmann, M. W. Wuttke, J. P. Burrows, M. Gottwald, E. Krieg, A. P. H. Goede, and C. Muller, “Nadir, limb, and occultation measurements with SCIAMACHY,” *Adv. Space Res.* **29**(11), 2002.
- [3] S. Slijkhuys, “ENVISAT-1 SCIAMACHY Level 0 to 1c Processing Algorithm Theoretical Basis Document,” Tech. Rep. ENV-ATB-DLR-SCIA-0041, DLR, 2000. 2 edn.
- [4] J. Frerick, H. Bovensmann, S. Noël, J. P. Burrows, and M. Dobber, “SCIAMACHY on-ground/in-flight calibration, performance verification and monitoring concepts,” in *Earth Observing Systems II, Proc. SPIE* **3117**, pp. 176–187, 1997.
- [5] S. Noël, H. Bovensmann, J. Skupin, M. W. Wuttke, J. P. Burrows, M. Gottwald, and E. Krieg, “The SCIAMACHY calibration/monitoring concept and first results,” *Adv. Space Res.* **32**(11), pp. 2123–2128, 2003.
- [6] SCIAMACHY Operations Support Team, “PO-TN-DLR-SH-0004: SCIAMACHY operational long-term monitoring,” tech. rep., DLR, ife, 2002.
- [7] H. Bovensmann, J. P. Burrows, M. Buchwitz, J. Frerick, S. Noël, V. V. Rozanov, K. V. Chance, and A. H. P. Goede, “SCIAMACHY — mission objectives and measurement modes,” *Jas* **56**(2), pp. 127–150, 1999.
- [8] “<http://www.sciamachy.de>.”
- [9] “<http://www.iup.physik.uni-bremen.de/sciamachy/ltn/ltn.html>.”
- [10] J. P. Burrows, M. Weber, M. Buchwitz, V. Rozanov, A. Ladstädter-Weissenmayer, A. Richter, R. de Beek, R. Hoogen, K. Bramstedt, K.-U. Eichmann, M. Eisinger, and D. Perner, “The Global Ozone Monitoring Experiment (GOME): Mission concept and first scientific results,” *J. Atm. Sciences* **56**, pp. 151–175, 1999.
- [11] I. Aben, M. Eisinger, E. Hegels, R. Snel, and C. Tanzi, “GOME data quality improvement GDAQI final report,” Tech. Rep. TN-GDAQI-003SR/2000, SRON, DLR, AWI Potsdam, and ife, SRON Ruimteonderzoek, NL-3584 Utrecht, The Netherlands, 2000.
- [12] H. Bovensmann, M. Buchwitz, J. Frerick, R. Hoogeveen, Q. Kleipool, G. Lichtenberg, S. Noël, A. Richter, A. Rozanov, V. Rozanov, J. Skupin, C. v. Savigny, M. W. Wuttke, and J. P. Burrows, “SCIAMACHY on ENVISAT: In-flight optical performance and first results,” in *Remote Sensing of Clouds and the Atmosphere VIII*, K. P. Schäfer, A. Comeron, M. R. Carler, and R. H. Picard, eds., *Proc. of SPIE* **5235**, pp. 160–173, 2004.
- [13] H. Bovensmann, B. Ahlers, M. Buchwitz, J. Frerick, M. Gottwald, R. Hoogeveen, J. W. Kaiser, Q. Kleipool, E. Krieg, G. Lichtenberg, R. Mager, J. Meyer, S. Noël, A. Schlesier, C. Sioris, J. Skupin, C. v. Savigny, M. W. Wuttke, and J. P. Burrows, “SCIAMACHY in-flight instrument performance,” in *Proceedings of the Envisat Calibration Review (SP-520)*, ESA Publications Division, 2002.
- [14] S. Noël, “Determination of Correction Factors for SCIAMACHY Radiances and Irradiances,” Tech. Rep. IFE-SCIA-SN-20040712\_IrrRadCorrection, ife, July 2004. issue 4.

# INTER-COMPARISON OF TERRA AND AQUA MODIS

XIAOXIONG XIONG AND VINCE SALOMONSON

*Earth Sciences Directorate, NASA/Goddard Space Flight Center, Greenbelt, MD 20771*

JUNQIANG SUN AND AISHENG WU

*Science Systems and Applications, Inc., 10210 Greenbelt Road, Lanham, MD 20706*

WILLIAM BARNES AND BRUCE GUENTHER

*University of Maryland, Baltimore County, Baltimore, MD 21250*

Nearly identical copies of the Moderate Resolution Imaging Spectroradiometer (MODIS) have been operating on-board the NASA's Earth Observing System (EOS) Terra and Aqua satellites since their launches in December 1999 and May 2002 respectively. Each MODIS has 20 reflective solar bands (RSB) with center wavelengths from 0.41 to 2.1 $\mu$ m and 16 thermal emissive bands (TEB) from 3.7 to 14.4 $\mu$ m. The absolute radiometric calibration accuracy requirements (1 $\sigma$ ) at the top of atmosphere (TOA) typical scene radiances are  $\pm 2\%$  for the RSB reflectance factors and  $\pm 5\%$  for the RSB radiance products. With a few exceptions, the TEB radiance calibration requirements are  $\pm 1\%$ . In order to achieve and maintain its calibration accuracy, each MODIS is equipped with a set of on-board calibrators (OBCs), including a solar diffuser (SD) and a solar diffuser stability monitor (SDSM) for the RSB calibrations and a blackbody (BB) for the TEB calibrations<sup>1</sup>. The SDSM is used to track the SD reflectance changes on-orbit. In addition, lunar observations have been extensively used by both Terra and Aqua MODIS to support their on-orbit calibration and characterization<sup>2</sup>.

In principle, both Terra and Aqua MODIS should have the same calibration scale since their on-board calibrators were calibrated pre-launch against the same ground sources. For example, the SD bi-directional reflectance was characterized in a comparison mode using a reference sample traceable to NIST reflectance standard and the on-board BB was characterized using a laboratory blackbody calibration source (BCS) with high emissivity (0.9995) over the spectral range of the thermal emissive bands<sup>3,4</sup>. This paper describes MODIS lunar calibration methodology and its applications to the inter-comparison of Terra and Aqua MODIS RSB in the visible (VIS) and near-infrared (NIR) spectral regions and the inter-comparison of Terra and Aqua MODIS TEB on-orbit calibration consistency using closely matched thermal infrared (TIR) channels on the Advanced Very High Resolution Radiometer (AVHRR) at 11 $\mu$ m and 12 $\mu$ m. These two channels are primarily used for retrieving sea-surface temperature (SST) and land surface temperature (LST) and, therefore, have higher calibration accuracy requirements.

## *Inter-comparison of Terra and Aqua MODIS RSB calibration using the Moon*

One of the MODIS on-orbit operational activities is to plan and perform lunar observations. The primary objective of MODIS lunar observations is to support the RSB calibration by tracking their on-orbit radiometric

stability. The Moon is a very stable calibration source because of the intrinsic stability of its surface reflectance properties<sup>5,6</sup>. In order to reduce the uncertainty in the corrections, due to lunar viewing geometry differences, the lunar observations for both instruments are carefully scheduled to occur at nearly the same phase angle (55-56°) via spacecraft roll maneuvers with Terra viewing a waning Moon while Aqua views a waxing Moon.

Each MODIS views the Moon through its space view (SV) port, approximately 9 times a year. Depending on the observing time and viewing geometry, the sensor can view the Moon over multiple scans. For a given spectral band, we compute a quantity called the integrated lunar irradiance that depends on the calibration coefficients, lunar viewing geometry factors (the Sun-Moon-MODIS phase angle, the lunar libration angles, and the Sun-Moon and the Moon-MODIS distances), and the over-sampling factor when multi-scan observations are used.

Figure 1 presents an example of a time series of the measured lunar irradiance for Terra MODIS band 1 with a center wavelength at 647nm. The starting time is chosen to match the Aqua MODIS time series. The large annual oscillation is primarily due to the variations in viewing geometry of the lunar observations. For comparison purposes, the modeled lunar irradiance under the same viewing condition is also included in this plot. Clearly the modeled results have trending similar to that of the measurements. The modeling results are computed using Robotic Lunar Observatory (ROLO) program from the U.S. Geological Survey (USGS)<sup>7</sup>. Notice that there is a near-constant scaling factor between the measurements and modeling results that should include the errors in both the modeling and measurements. As one would expect, the difference is spectral band (wavelength) dependent. Similar time series or trending results for the Aqua MODIS bands 1 are shown in Figure 2. Because of the viewing geometry differences between the Terra and Aqua MODIS lunar observations, the overall shapes of their time series (trending) are not exactly the same. Like Terra MODIS, an approximately constant and spectral band dependent scaling factor between the modeling and measurements also exists in the Aqua MODIS lunar irradiance trending.

If this scaling factor for a given band is the same for both Terra and Aqua MODIS, then their on-orbit calibration is considered to be consistent. For MODIS band 1, the calibration difference between Terra and Aqua is about  $1\pm 0.5\%$ . This inter-comparison approach has been applied to all MODIS reflective solar bands that do not

saturate during lunar observations. Current results from Terra and Aqua MODIS lunar observations show that the overall calibration difference between the two sensors' reflective solar bands is less than  $\pm 1\%$ . We have also applied this approach of using the Moon for calibration inter-comparison of MODIS with other sensors, such as the MISR on the Terra spacecraft and the SeaWiFS<sup>8</sup>.

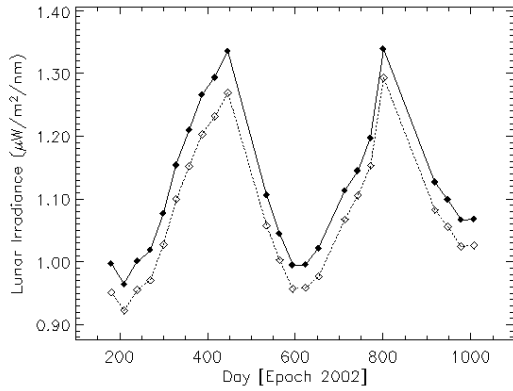


Figure 1 Measured (solid) and modeled lunar irradiance time series for Terra MODIS band 1.

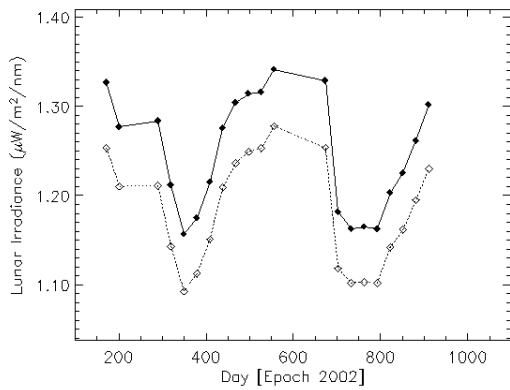


Figure 2 Measured (solid) and modeled lunar irradiance time series for Aqua MODIS band 1.

### Inter-comparison of Terra and Aqua MODIS TEB calibration using the AVHRR

The second part of this paper presents an approach that uses the NOAA-16/17 AVHRR channels at  $11\mu\text{m}$  and  $12\mu\text{m}$  to examine MODIS TEB on-orbit calibration consistency. This approach was developed from a method for comparing two sensors using nearly simultaneous nadir-viewing observations over relatively uniform Earth view (EV) scenes during orbit intersections<sup>9,10</sup>. First each MODIS (on Terra or Aqua) is compared with a selected AVHRR (on NOAA-16 or NOAA-17). Then the effective brightness temperature (BT) difference between the Terra MODIS and the selected AVHRR and that between the Aqua MODIS and the same AVHRR are determined. The difference between the two comparison results is used to determine the two MODIS sensors' calibration differences.

Though both Terra and Aqua MODIS cannot view the same ground target (nadir) at the same time, they do have orbit intersections with an AVHRR (NOAA-16/17). In this study, the AVHRR is used as an intermediate transfer device. This approach assumes that the AVHRR calibration is stable between each inter-comparison pair, one with Terra MODIS and the other with Aqua MODIS. Because of this, each inter-comparison pair is selected to be very close in time.

The MODIS TEB on-orbit calibration is performed using its on-board BB on a scan-by-scan basis. To a certain extent, the consistency of Terra and Aqua MODIS TEB on-orbit calibration is linked through the pre-launch characterization of the BB with the same ground reference source. The difference between the inter-comparison pair reflects the actual on-orbit calibration differences between Terra and Aqua MODIS. Figures 3 and 4 are examples of the inter-comparison time series of AVHRR (NOAA-17) with both Terra and Aqua MODIS at  $11\mu\text{m}$  and  $12\mu\text{m}$ . Each point in these plots is derived from many pixel-by-pixel matched near simultaneous observations at their orbit intersections.

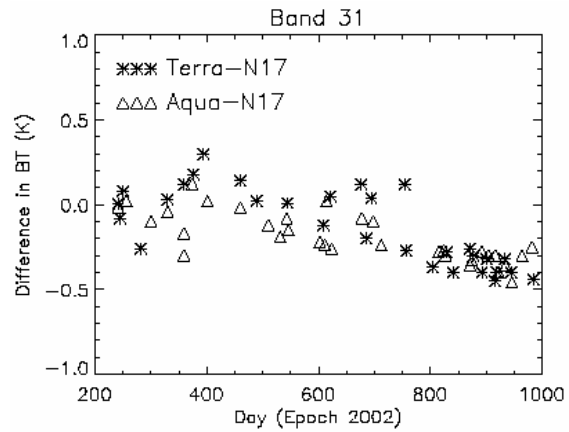


Figure 3 Brightness temperature differences between Terra/Aqua MODIS band 31 and NOAA-17 AVHRR channel 4 at  $11\mu\text{m}$ .

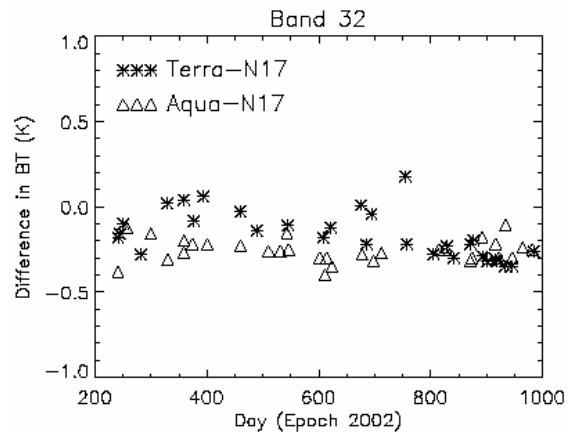


Figure 4 Brightness temperature differences between Terra/Aqua MODIS band 32 and NOAA-17 AVHRR channel 5 at  $12\mu\text{m}$ .

From Figures 3 and 4, the brightness temperature (BT) difference between Terra and Aqua MODIS, on average,

is less than  $0.10 \pm 0.15\text{K}$  for band 31 and  $0.15 \pm 0.12\text{K}$  for band 32. Similar results have also been derived by using the NOAA-16 AVHRR as an intermediate transfer device. Our investigations show that the observed differences between Terra and Aqua MODIS bands 31 and 32 are smaller than their calibration uncertainty requirements of  $0.35\text{K}$ . By plotting the temperature difference as a function of the EV scene temperature, shown in Figures 5-6, the impact of the sensors' non-linearity on the calibration can be quantified.

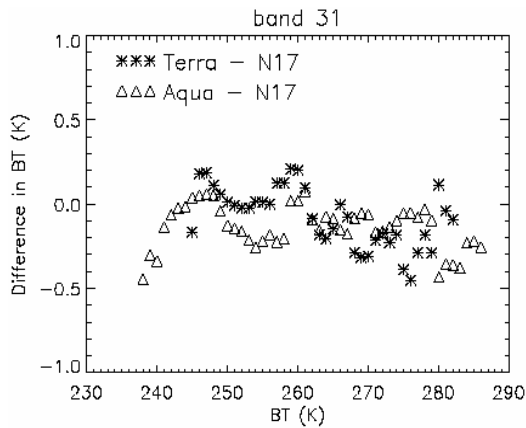


Figure 5 Brightness temperature differences between Terra/Aqua MODIS band 31 and NOAA-17 AVHRR channel 4 at  $11\mu\text{m}$  versus scene temperature.

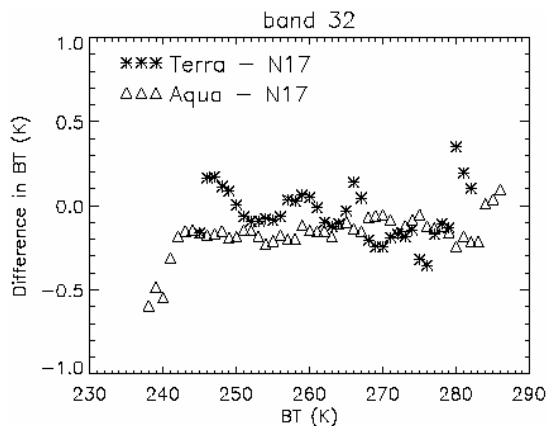


Figure 6 Brightness temperature differences between Terra/Aqua MODIS band 32 and NOAA-17 AVHRR channel 5 at  $12\mu\text{m}$  versus scene temperature.

The results presented above are part of our ongoing inter-comparison study of Terra and Aqua TEB calibration using AVHRR (NOAA-16 and -17). From the same data sets, we can also study the calibration difference between

NOAA-16 and -17 AVHRR TIR channels at  $11\mu\text{m}$  and  $12\mu\text{m}$ . Currently we are also applying the same method to observations from the ADEOS-II/GLI which has more thermal channels that match those of the MODIS TEBs.

The two approaches presented (orbit intersections and lunar observations) can be applied to many other sensors for calibration inter-comparisons and, no doubt, will benefit future remote sensing missions by contributing to the establishment of climate data records (CDRs).

## References

- [1] Xiong X, Chiang K, Esposito J, Guenther B, Barnes WL, (2003) MODIS on-orbit calibration and characterization, *Metrologia*, 40, 89-92
- [2] Xiong X, Sun J, Chiang K, Xiong S, Barnes WL, (2002) MODIS on-orbit characterization using the Moon, *Proceedings of SPIE*, 4881, 299-307
- [3] Barnes WL, Pagano TS, Salomonson VV, (1998) Pre-launch characteristics of the Moderate Resolution Imaging Spectroradiometer (MODIS) on EOS AM-1, *IEEE Transactions on Geoscience and Remote Sensing*, 36, 1088-1100
- [4] Guenther B, Godden GD, Xiong X, Knight EJ, Montgomery H, Hopkins MM, Khayat MG, Hao Z, (1998) Pre-launch algorithm and data format for the Level 1 calibration products for the EOS AM-1 Moderate Resolution Imaging Spectroradiometer (MODIS), *IEEE Transactions on Geoscience and Remote Sensing*, 36, 1142-1151
- [5] Sun J, Xiong X, Guenther B, Barnes WL, (2003) Radiometric stability monitoring of the MODIS reflective solar bands using the Moon, *Metrologia* 40, 85-88
- [6] Keiffer H and Wildey R, (1996) Establishing the Moon as a Spectral Radiance Standard, *J. of Atmos. Oceanic Tech*, 13, 360-375
- [7] Stone TC and Kieffer HH, (2002) An absolute irradiance of the Moon for on-orbit calibration, *Proceedings of SPIE – Earth Observing Systems VII* 4814, 211-221
- [8] Barnes W, Xiong X, Eplee R, Sun J, and Lyu C, (In Press) Use of the Moon for calibration and characterization of MODIS, SeaWiFS and VIRS, *Earth Science Satellite Remote Sensing*, J. Qu, W. Gao, M. Kafatos, R. Murphy, and V. Salomonson eds., Vol. 1, Springer-Verlag
- [9] Cao C. and Heidinger A., (2002) Inter-comparison of the longwave infrared channels of MODIS and AVHRR/NOAA-16 using simultaneous nadir observations at orbit intersections, *Proceedings of SPIE – Earth Observing Systems VII* 4814, 306-316
- [10] Wu A, Cao C, Xiong X, (2003) Inter-comparison of the  $11\mu\text{m}$  and  $12\mu\text{m}$  Bands of Terra and Aqua MODIS Using AVHRR/NOAA-16/17, *Proceedings of SPIE – Earth Observing Systems VIII*, 5151, 384-394

# MODIS IN-FLIGHT CALIBRATION METHODOLOGIES

XIAOXIONG XIONG

Earth Sciences Directorate, NASA/Goddard Space Flight Center, Greenbelt, MD 20771

WILLIAM BARNES

University of Maryland, Baltimore County, Baltimore, MD 21250

The Moderate Resolution Imaging Spectroradiometer (MODIS) is a cross-track scanning radiometer with a wide field-of-view (FOV), enabling complete global coverage of the Earth in less than 2 days. It is currently operating on both the Terra and Aqua satellites, two of the major contributors to the NASA's Earth Observing System (EOS), launched in December 1999 and May 2002, respectively. The sensor was developed based on the desire of the science community to extend existing global data sets from heritage sensors to enable studies of the Earth's land, oceans, and atmosphere and associated global environment and climate changes. Each MODIS has 36 spectral bands with wavelengths from 0.41 to 14.4 $\mu$ m, located on four focal plane assemblies (FPAs): visible (VIS), near infrared (NIR), short- and mid-wave infrared (SMIR), and long-wave infrared (LWIR). It makes observations at three spatial resolutions (bands 1-2 at 250m, bands 3-7 at 500m, and bands 8-36 at 1km). MODIS bands 1-19 and 26 are the reflective solar bands (RSB) and bands 20-25 and 27-36 are the thermal emissive bands (TEB). Table 1 provides a summary of key design specifications, such as spectral bandwidth, typical scene radiance, and the required signal-to-noise ratio (SNR) for the RSB or noise-equivalent temperature difference (NE $\Delta$ T) for the TEB. The MODIS Level 1B (L1B) algorithms provide calibrated top of the atmosphere (TOA) radiance (RSB and TEB) and reflectance factor (RSB only). From the L1B radiances and reflectance factors, nearly 40 science data products are generated for each MODIS instrument<sup>1</sup>.

MODIS radiometric calibration accuracy requirements at typical scene radiances are  $\pm 2\%$  ( $1\sigma$ ) for the RSB reflectance factors and  $\pm 5\%$  for the RSB radiance. For the TEB, the calibration requirements at typical scene radiances are  $\pm 1\%$  except  $\pm 0.75\%$  for band 20,  $\pm 10\%$  for band 21 (for fire detection with very low gain), and  $\pm 0.5\%$  for bands 31, and 32 (for sea-surface temperature). The MODIS pre-launch calibration and characterization included radiometric, spatial, and spectral measurements at both sub-system and system levels. Key calibration activities were performed in thermal vacuum (TV) at three different instrument temperatures (cold, nominal, and hot plateaus) and three different focal plane temperatures (TEB only). The RSB radiometric calibration source was a large aperture spherical integrating source (SIS) operated at various numbers of lamps and the TEB calibration source was a specially designed large aperture blackbody calibration source (BCS) operated at temperatures from 170 to 340K. An integration-and-alignment collimator (IAC) and a spectral measurement assembly (SpMA) were used for the sensor's spatial and spectral characterization. Other key parameters, such as the SD bi-directional

reflectance factor (BRF), the BB spectral emissivity, and the sensor's response versus scan-angle (RVS), were also derived from these measurements<sup>2</sup>.

Table 1 MODIS design specifications and its primary applications

Orbit:	705 km, 10:30 a.m. descending node or 1:30 p.m. ascending node, sun-synchronous, near-polar, circular			
Scan Rate:	20.3 rpm, cross track			
Swath Dimensions:	2330 km (across track) by 10 km (along track at nadir)			
Telescope:	17.78 cm diam. off-axis, afocal (collimated), with intermediate field stop			
Size:	1.0 x 1.6 x 1.0 m			
Weight:	250 kg			
Power:	225 W (orbital average)			
Data Rate:	11 Mbps (peak daytime)			
Quantization:	12 bits			
Spatial Resolution:	250 m (bands 1-2) (at nadir): 500 m (bands 3-7), 1000 m (bands 8-36)			
Design Life:	5 years			

Primary Use	Band	Bandwidth <sup>1</sup>	Spectral Radiance <sup>2</sup>	Required SNR <sup>3</sup>
Land/Cloud	1	620-670	21.8	128
Boundaries	2	841-876	24.7	201
Land/Cloud	3	459-479	35.3	243
Properties	4	545-565	29.0	228
	5	1230-1250	5.4	74
	6	1628-1652	7.3	275
	7	2105-2155	1.0	110
Ocean color/	8	405-420	44.9	880
Phytoplankton/	9	438-448	41.9	838
Biogeochemistry	10	483-493	32.1	802
	11	526-536	27.9	754
	12	546-556	21.0	750
	13	662-672	9.5	910
	14	673-683	8.7	1087
	15	743-753	10.2	586
	16	862-877	6.2	516
Atmospheric	17	890-920	10.0	167
Water Vapor	18	931-941	3.6	57
	19	915-965	15.0	250

Primary Use	Band	Bandwidth <sup>1</sup>	Spectral Radiance <sup>2</sup>	Required NE $\Delta$ T(K) <sup>4</sup>
Surface/Cloud	20	3.660-3.840	0.45	0.05
Temperature	21	3.929-3.989	2.38	2.00
	22	3.929-3.989	0.67	0.07
	23	4.020-4.080	0.79	0.07
Atmospheric	24	4.433-4.498	0.17	0.25
Temperature	25	4.482-4.549	0.59	0.25
Cirrus Clouds	26	1.360-1.390	6.00	150 <sup>3</sup>
Water Vapor	27	6.535-6.895	1.16	0.25
	28	7.175-7.475	2.18	0.25
	29	8.400-8.700	9.58	0.05
Ozone	30	9.580-9.880	3.69	0.25
Surface/Cloud	31	10.780-11.280	9.55	0.05
Temperature	32	11.770-12.270	8.94	0.05
Cloud Top	33	13.185-13.485	4.52	0.25
Altitude	34	13.485-13.785	3.76	0.25
	35	13.785-14.085	3.11	0.25
	36	14.085-14.385	2.08	0.35

<sup>1</sup>Bands 1 to 19, nm; Bands 20-36,  $\mu$ m  
<sup>2</sup>(W/m<sup>2</sup>- $\mu$ m-sr)  
<sup>3</sup>SNR=Signal-to-noise ratio  
<sup>4</sup>NE $\Delta$ T=Noise-equivalent temperature difference } Performance goal is 30%-40% better than required

The sensor on-orbit calibration coefficients and other calibration parameters are determined and updated from its on-board calibrators (OBCs) that include a solar diffuser (SD), a solar diffuser stability monitor (SDSM), a v-groove flat panel blackbody (BB), and a spectro-

radiometric calibration assembly (SRCA). Figure 1 shows the MODIS scan cavity and its on-board calibrators. The MODIS uses a two-sided paddle wheel scan mirror that rotates at 20.3 rpm or a scan period of 1.478s making alternate data collections with both mirror sides. Each scan the sensor views its on-board calibrators (SD, SRCA, BB, and space view (SV), and the Earth view (EV) sector sequentially. The solar diffuser stability monitor (SDSM) is used to monitor on-orbit degradation of the SD bi-directional reflectance factor (BRF)<sup>3-5</sup>.

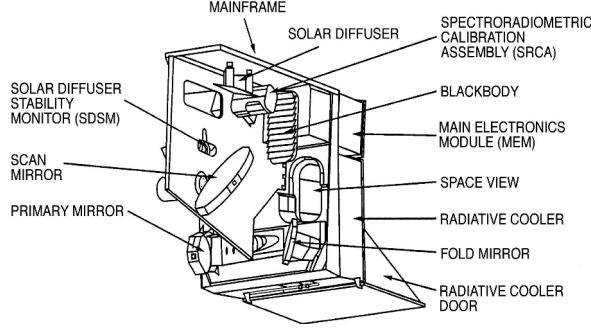


Figure 1 MODIS scan cavity and on-board calibrators

### RSB calibration using the SD and SDSM

For the reflective solar bands (RSB), the MODIS L1B primary data product is the top of the atmosphere (TOA) reflectance factor,  $\rho_{EV}\cos(\theta_{EV})$ . It is calculated by

$$\rho_{EV}\cos(\theta_{EV}) = m_1 \cdot dn_{EV}^* \cdot d_{ES\_EV}^2 \quad (1)$$

where  $\theta_{EV}$  is the Earth view (EV) pixel's solar zenith angle,  $m_1$  is the reflectance factor calibration coefficient determined from SD observations,  $d_{ES\_EV}$  is the EV pixel's Earth-Sun distance in AU, and  $dn_{EV}^*$  is the sensor's EV digital response corrected for instrument background, viewing angle, and temperature effects. Applying the same expression to the SD observations (replacing subscripts of EV with SD), the calibration equation is given by

$$\rho_{SD}\cos(\theta_{SD}) = m_1 \cdot dn_{SD}^* \cdot d_{ES\_SD}^2 \quad (2)$$

The SD BRF,  $\rho_{SD}$ , was characterized pre-launch. Its on-orbit time dependent degradation must be corrected. For a few RSB high gain bands (bands 8-16 for ocean color), a solar diffuser screen (SDS) is needed in order to attenuate the direct sunlight in the SD calibration. Thus the reflectance factor calibration coefficient,  $m_1$ , is determined by the following expression,

$$(\rho_{SD}\cos(\theta_{SD}) \cdot \Delta_{SD}) = m_1 \cdot (dn_{SD}^* / \Gamma_{SDS}) \cdot d_{ES\_SD}^2 \quad (3)$$

where  $\Delta_{SD}$  is the SD BRF degradation factor determined by the SDSM during each SD calibration and  $\Gamma_{SDS}$  is the SDS vignetting function (equal to 1 for bands that do not use the SDS). The SDSM tracks the SD degradation with alternate views of attenuated direct sunlight and diffuse solar reflection from the SD panel. Figure 2 is an example of normalized RSB response trending of  $m_1$  from over 4 years of Terra MODIS SD calibration data sets for bands 9 and 17 at wavelengths of 442nm and 904nm (all detectors, mirror side 1). The RSB calibration is band, detector, sub-sample, and mirror side dependent.

The RSB calibration coefficients, including RVS updates, are provided using time dependent look-up tables (LUTs) for the L1B code.

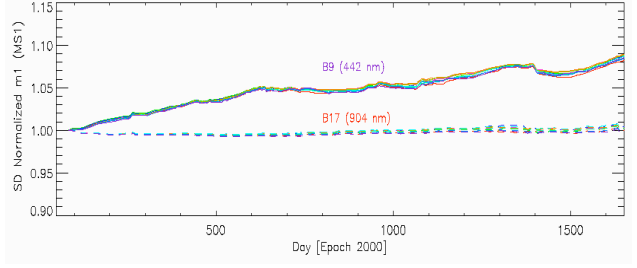


Figure 2 Terra MODIS bands 9 (442nm) and 17 (904nm) response trending of  $m_1$  (all detectors, mirror side 1)

### TEB calibration using the BB

For the thermal emissive bands (TEB), the MODIS L1B primary data product is the TOA radiance,  $L_{EV}$ . These bands are calibrated using a quadratic approach,

$$RVS_{EV} \cdot L_{EV} + (RVS_{SV} - RVS_{EV}) \cdot L_{SM}, \quad (4)$$

$$= a_0 + b_1 \cdot dn_{EV} + a_2 \cdot dn_{EV}^2$$

where  $dn_{EV}$  is the detector's EV digital response with instrument background (SV) subtracted, the offset and nonlinear coefficients  $a_0$  and  $a_2$  are updated from BB on-orbit warm-up and cool-down observations. The linear coefficient  $b_1$  is determined each scan from sensor's response to the BB. The second term on the left hand side (LHS) is the viewing angle (RVS) dependent scan mirror emission ( $L_{SM}$ ). When applying Eqn. 4 to the BB observations, an additional term,  $L_{CAV}$ , representing the scan cavity thermal emission reflected from the BB, must be included. Therefore the following equation is used to compute the linear coefficient  $b_1$  each scan,

$$RVS_{BB} \cdot \epsilon_{BB} \cdot L_{BB} + (RVS_{SV} - RVS_{BB}) \cdot L_{SM} +$$

$$RVS_{BB} \cdot (1 - \epsilon_{BB}) \cdot \epsilon_{CAV} \cdot L_{CAV} \quad (5)$$

$$= a_0 + b_1 \cdot dn_{BB} + a_2 \cdot dn_{BB}^2$$

The emissivities of the MODIS BB ( $\epsilon_{BB}$ ) and that of its scan cavity ( $\epsilon_{CAV}$ ) used in Eqn. 5 were determined from pre-launch calibration and characterization. Figure 3 shows the TEB calibration coefficient  $b_1$  determined on a scan-by-scan basis for Terra MODIS band 31 using an entire orbit of BB calibration data.

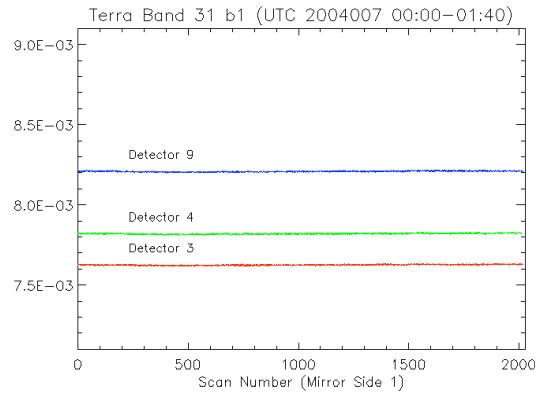


Figure 3 Terra MODIS band 31 (detectors 3, 4, and 9, mirror side 1) scan-by-scan response ( $b_1$ )

The corresponding long-term stability of Terra MODIS band 31 is shown in Figure 4 where each point is averaged over a 5 minute granule. The noticeable response changes in the long-term trending are either due to variations of the focal plane temperature or changes of the operational configuration (marked by the vertical lines). These changes do not impact MODIS TEB calibration since it is performed on a scan-by-scan basis.

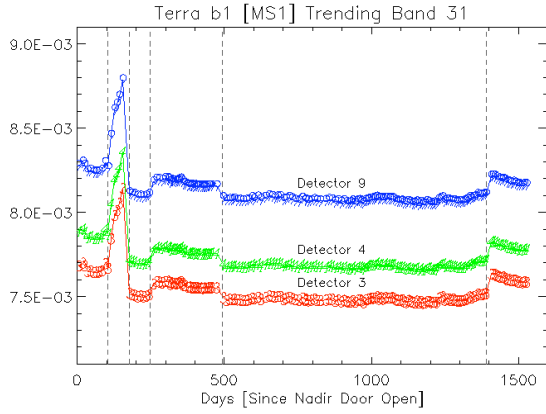


Figure 4 Terra MODIS band 31 (detectors 3, 4, and 9, mirror side 1) response ( $b_1$ ) trending

#### Spatial and spectral calibration using the SRCA

When the SRCA is used in its spatial mode, it consists of three components: (1) light sources, (2) an optical relay system, and (3) a collimator. Two reticles in the SRCA, one for along-scan and the other for along-track, are used for spatial characterization. Five phase-delays, that shift the detector's sampling start time, with an equivalent step size of 0.2km IFOV are applied in the spatial characterization to improve measurement precision. For a given band/detector, the centroid value of the response profile, i.e. the detector's position in the along-scan direction, is given by

$$\bar{x}(b, d) = \frac{\sum_{x=0}^{N_x} dn(b, d, x) \cdot x}{\sum_{x=0}^{N_x} dn(b, d, x)} \quad (6)$$

where  $dn(b, d, x)$  is the digital response for a given band, detector, and data sampling position, and  $N_x$  is the total number of data samples. The difference between the measurements of two detectors is their relative shift. The difference between two measurements at different time for a given detector is its position shift. The average value from all detectors in a band yields the band-to-band registration (BBR). For the along-track direction, the spatial characterization applies only on a band-by-band basis since the response profile is constructed from the responses of all detectors in a band.

In Spectral mode, the SRCA also consists of three components: (1) light sources, (2) a monochromator, and (3) a collimator. The monochromator becomes an optical

relay system (for spatial mode) by replacing its grating with a mirror. The SRCA spectral characterization is based on the grating equation which provides the relationship between the grating angle,  $\theta$ , and the wavelength,  $\lambda$ ,

$$\lambda = \frac{2A}{m} \cdot \sin(\theta + \theta_{off}) \cdot \cos \beta \quad (7)$$

where  $A$  and  $m$  are the grating spacing and diffraction order,  $\theta_{off}$  the grating offset angle, and  $\beta$  the half angle between incident and diffractive beams. The SRCA's spectral self-calibration (RSB only) is provided via a didymium filter with well-calibrated spectral peaks and a pair of silicon photo-diodes (SiPD): a calibration SiPD and a reference SiPD.

In addition to using its on-board calibrators, lunar observations (monthly) have also been used for the MODIS on-orbit calibration and characterization, especially for tracking RSB radiometric stability at different angles of incidence (AOI) to the scan mirror and studying the impact of detector crosstalk<sup>6</sup>.

With extensive on-orbit calibration and characterization efforts, both Terra and Aqua MODIS have been performing according to their specified design parameters (excluding a few minor problems identified pre-launch and on-orbit). The spectral performance of both sensors is satisfactory (less than 0.5nm center wavelength shift) and the spatial characterization is stable with no significant BBR change after launch. The sensors' radiometric calibration coefficients are regularly updated based on the calibration data sets from its on-board calibrators and lunar observations.

## References

- [1] Salomonson VV, Barnes WL, Xiong X, Kempler S, Masuoka E, (2002) An overview of the Earth Observing System MODIS instrument and associated data systems performance, *Proceedings of IGARSS*
- [2] Barnes WL, Pagano TS, Salomonson VV, (1998) Pre-launch characteristics of the Moderate Resolution Imaging Spectroradiometer (MODIS) on EOS AM-1, *IEEE Transactions on Geoscience and Remote Sensing*, 36, 1088-1100
- [3] Xiong X, Chiang K, Esposito J, Guenther B, Barnes WL, (2003) MODIS on-orbit calibration and characterization, *Metrologia*, 40, 89-92
- [4] Xiong X, Sun J, Esposito J, Guenther B, Barnes WL, (2002) MODIS reflective solar bands calibration algorithm and on-orbit performance, *Proceedings of SPIE*, 4891, 95-104
- [5] Xiong X, Chiang K, Guenther B, Barnes WL, (2002) MODIS thermal emissive bands calibration algorithm and on-orbit performance, *Proceedings of SPIE*, 4891, 392-401
- [6] Xiong X, Sun J, Chiang K, Xiong S, Barnes WL, (2002) MODIS on-orbit characterization using the Moon, *Proceedings of SPIE*, 4881, 299-307

## Calibration And Validation Of Satellite Sensors At Noaa/Nesdis/Ora: Summary Of Methods And Recent Results

J. G. Yoe, C. Cao, X. Wu, L. McMillin, S. I. Gutman, D. L. Birkenheuer, M.K. Rama Varma Raja, and J. Zhao

### ABSTRACT

The NESDIS Office of Research and Applications performs sensor calibration and data product validation (cal/val) for NOAA's polar and geosynchronous operational environmental satellites, as well as for a number of non-NOAA spacecraft and instruments. This paper summarizes the scope of these efforts, describes some of the unique methods developed and used by ORA and its partners, and presents and discusses selected recent results. Particular attention is paid to the Simultaneous Nadir Overpass (SNO) method for the on-orbit inter-calibration of like sensors on successive iterations of NOAA's Polar-orbiting Operational Environmental Satellites (POES). Developed to check the channel by channel performance of the High Resolution Infrared Sounder (HIRS) instruments on NOAA-17 and -18, the SNO method has now been applied to test the effectiveness of calibration corrections made to Advanced Very High Resolution Radiometer (AVHRR) observations and to Advanced Microwave Sounding Unit (AMSU) data. The use of a network of surface-based GPS receivers to determine atmospheric integrated precipitable water vapor (IPW) accurately and

precisely with 30-min temporal resolution now provides an effective and rapid means of validating satellite moisture retrievals. The method has been used successfully to validate observations from the Atmospheric Infrared Sounder (AIRS) and sounders on NOAA's Geosynchronous Operational Environmental Satellites (GOES). Although the method does not provide a vertical profile of moisture, it is shown to provide an effective scaling constraint for satellite and radiosonde intercomparisons.

### INTRODUCTION

The utility of the large and growing volume of satellite observations and derived data products for operational applications such as numerical weather prediction and climate research is dependent on the proper calibration of the instruments and validation of the products. NOAA is both operator of the POES and GOES systems and an end-user of satellite observations provided by a variety of operational and research spacecraft. It is not surprising therefore, that expertise in cal/val has been established at NOAA. These efforts are centered in NESDIS/ORA, however, many of them benefit from the cooperation with other NOAA Line Offices, NASA, other United States government agencies, universities, industry, and international partners.

*Corresponding Author: James G. Yoe  
5200 Auth Road, WWB Room 808, Camp  
Springs, MD, 20746, United States of  
America. [James.G.Yoe@noaa.gov](mailto:James.G.Yoe@noaa.gov)*

## OVERVIEW OF ACTIVITIES

ORA scientists have participated in pre-flight sensor calibration for GOES and POES imagers and sounders. These sensor characterizations permit optimal retrievals and direct data assimilation to be conducted. The extended lifetimes of operational and major research satellites require on-orbit sensor characterization periodically as well. Therefore ORA monitors the radiometric response of passive sensors on orbit, including the targeting of cold space, on-board sources, stable stars, and standard earth scenes for vicarious calibration.

ORA develops new products, refines retrieval algorithms, and guides the transition to operations for new and improved products. Data validation is an integral component of this process. For example, atmospheric motion vectors derived from consecutive scenes for the GOES or MODIS imagers are verified and quality-controlled via comparisons to radiosonde and wind profiler data and analyses. Ocean color data are validated using *in situ* sensors, as are sea surface temperature and surface wind products. The verification of new air quality products based on measurements of aerosol optical depths from GOES and MODIS relies on a variety of correlative data including *in situ* sensors, lidars, and sun photometers. SBUV ozone products are confirmed using Dobson station data. Typically ORA relies on its partners to provide the verification data for satellite measurements.

## SELECTED RECENT RESULTS

Examples of recent results that are expected to bear on future applications are presented in this section.

### a. Simultaneous Nadir Overpass (SNO)

The SNO method (Cao *et al*, 2004) significantly enhances capability to characterize POES sensors on-orbit when a pair of like instruments view the same nadir scene. Recently SNO has been used to reveal seasonal biases in the brightness temperatures of HIRS long-wave (stratosphere) channel on NOAA-15 and NOAA-16. This is illustrated by the blue (top) curve in Fig. 1. The bias is due to the interaction of seasonal temperature differences and the slight spectral response differences.

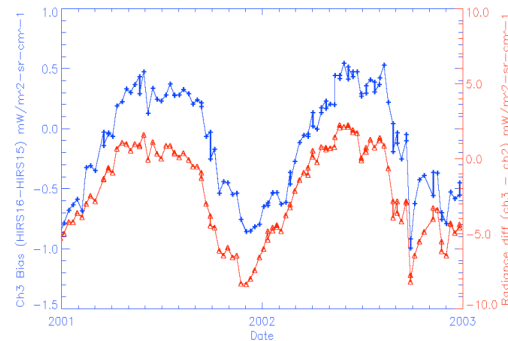


Fig. 1. Seasonal bias (blue, top) in HIRS channel 3 revealed using SNO data.

### b. GPS IPW verification for AIRS

With the NOAA Forecast Systems Laboratory, ORA scientists now use surface-based GPS sensors to validate AIRS moisture retrievals over the United States. The 30-min resolution of the GPS data enables significant data sets to be accumulated quickly, as illustrated by the monthly scatter plot in Fig. 2. There is very high correlation overall, but indications that the AIRS retrieval may be biased too dry in very moist and too moist in very dry cases, respectively. GPS IPW is being used as a constraint for validating AIRS vertical water vapor profiles (McMillin *et al*, 2005) and to

evaluate the GOES sounder moisture products at asynoptic times (Birkenheuer and Gutman 2005) also.

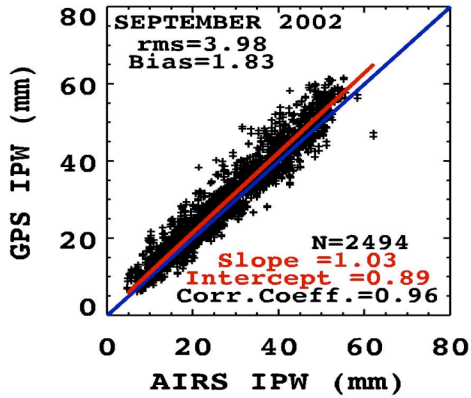


Fig. 2. Scatter plot of matched GPS and AIRS IPW data over the United States.

c. Multi-sensor NDVI validation

Normalized differential vegetation index (NDVI) are shown in Fig. 3 for a scene dominated by corn fields during the growing season. MODIS and AVHRR data give excellent agreement in this case. Reproducing a like result using different sensors is a key goal for a requirements-based observing system.

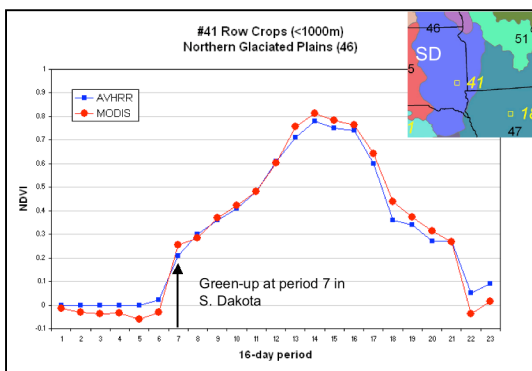


Fig. 3. NDVI estimates of a single scene from AVHRR (blue) and MODIS (red.)

However, doing so requires adequate instrument calibration. For example, the differences in AVHRR spectral response functions can result in very different

NDVI estimates for the same scene, as shown in Fig. 4.

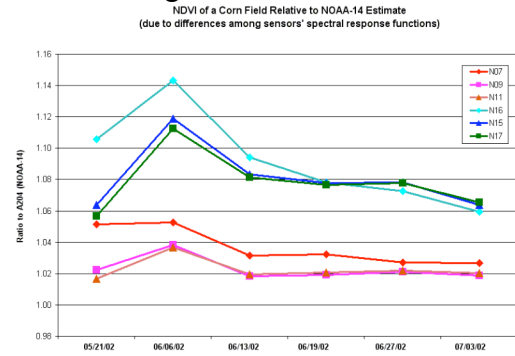


Fig. 4. Ratios of NDVI values from 6 AVHRR instruments relative to the corresponding NOAA-14 values.

SUMMARY

As the quantity of sensors and products grows, ORA refines and applies proven cal/val methods and develops new ones. These efforts depend on partners. Global monitoring over extended periods in the future is expected to require even more rigorous inter-calibration in the future.

REFERENCES

Birkenheuer, D.L., and S. I. Gutman, 2005: Comparison of the GOES moisture-derived product and GPS-IPW during IHOP. Submitted to *J. Atmos. Oceanic Tech.*

Cao, C., M. Weinreb, and H. Xu, 2004: Predicting SNO among polar-orbiting meteorological satellites for the intersatellite calibration of radiometers. *J. Atmos. Oceanic Tech.*, **21**, 537-542.

McMillin, L.M., J. Zhao., M.K. Rama Varma Raja, S.I. Gutman, and J.G. Yoe, 2005: Validation of AIRS moisture products using three-way intercomparisons with radiosondes and GPS sensors. Submitted to *J. Atmos. Oceanic Tech.*

## Abstract Sheet - Abstract number: 3

Author Name: Zibordi, Giuseppe  
Organisation: Joint Research Centre  
Country: ITALY  
Authors: Zibordi, Giuseppe, Joint Research Centre, ITALY (P)  
Melin, Frederic, JRC, ITALY  
Berthon, Jean-Francois, JRC, ITALY  
van der Linde, Dirk, JRC, ITALY  
Hooker, Stanford, NASA-GSFC, ITALY  
Holben, Brent, NASA-GSFC, ITALY  
Topic: 7 Post-launch sensors inter-comparison & calibrati

### **Inter-comparison of water leaving radiance data from operational ocean color sensors through in situ measurements**

The primary product of space sensors looking at the sea in the visible and near infrared is the water leaving radiance  $L_w$ . The accurate determination of remote sensing  $L_w$  values requires the absolute calibration of the space sensor and the removal of the atmospheric perturbing effects, i.e., the discrimination of  $L_w$  from the total radiance  $L$  measured by the spaceborne sensor viewing the sea through the atmosphere. The accuracy of the absolute calibration and the effectiveness of the atmospheric correction can be determined by comparing contemporaneous satellite derived and in situ  $L_w$  data or, alternatively, derived quantities like the normalized water-leaving radiance,  $L_{wn}$ , and remote sensing reflectance,  $R_{rs}$ . The in situ  $L_w$  values can be produced using above- or in-water optical measurement methods. An operational system for autonomous above-water radiance measurements, called the SeaWiFS Photometer Revision for Incident Surface Measurements (SeaPRISM), was deployed at the Acqua Alta Oceanographic Tower in the northern Adriatic Sea and used for the validation of remote sensing radiometric products in coastal waters. The SeaPRISM data were compared with simultaneous data collected from an independent in-water system for a wide variety of sun elevations along with different atmospheric, seawater, and sea state conditions. Comparisons were then made between normalized water-leaving radiances computed from SeaWiFS, MODIS and MERIS remote sensing data and SeaPRISM in situ measurements. The results suggest the feasibility of operational coastal networks of autonomous above-water radiometers deployed on fixed platforms (towers, lighthouses, navigation aids, etc.) to support ocean color validation activities.

# Using MERIS and MODIS for Land Cover Mapping in The Netherlands

**R. Zurita Milla, M.E. Schaepman and J.G.P.W. Clevers**

*Centre for Geo-Information, Wageningen University, P.O. Box 47, 6700 AA Wageningen, The Netherlands  
E-mail: Raul.zurita@wur.nl*

## **ABSTRACT**

The medium resolution sensors MERIS and MODIS are playing an important role in global and regional studies since they are fulfilling the information gap between the high and the low resolution sensors.

In this paper, we compare their performance for land cover mapping over The Netherlands. The use of spectral unmixing techniques will be evaluated as well because due to the fragmentation of most of the landscapes at the spatial resolution of these sensors the recorded images mainly contain heterogeneous pixels. Two study cases were tested by unmixing and classifying a MERIS full resolution and a MODIS image (both recorded in mid July 2003). The first one consisted in bringing the MODIS 250 and 500 meter bands to the spatial resolution of MERIS full resolution (300m) and then performing an unmixing of the 6 main land cover classes of The Netherlands. Subsequently, a second comparison was done by doing the classification only with the most similar bands shared by these sensors (3 main land cover classes).

In addition, this paper presents an endmember selection procedure based on existing fine resolution land cover maps. In our case, the LGN, which is the Dutch land cover map, was aggregated from 25m to 300m. At the same time, a standard purity index (SPI) was calculated for each aggregated pixel in order to identify the most homogeneous pixels at the medium resolution scale.

Results showed that the radiometric and geometric properties of these 2 sensors are quite good and that the classification accuracies were very similar (and promising). Following our results we finally recommend a combined use of MERIS and MODIS for land cover classification at a medium resolution scale.

## **1. INTRODUCTION**

Due to the growing recognition of the importance of land use and land cover mapping for agricultural and environmental applications an important number of initiatives and projects are taking place to provide this information to end users and if possible at different spatial scales [1]. In this respect, medium resolution sensors might be able to provide a great monitoring tool as they can distinguish different land cover types over large areas and they have a high temporal resolution (global coverage in 1-3 days). The aim of this paper is to compare the performance of the two current medium resolution sensors, namely MERIS and MODIS, for land cover mapping.

Because of the fragmentation of most of the landscapes at the spatial resolution of these 2 sensors the recorded images mainly contain heterogeneous pixels or mixels. Thus, this paper will focus on the use of spectral unmixing techniques for classifying and intercomparing MERIS and MODIS images.

## **2. MATERIALS AND METHODS**

Since MERIS and MODIS have a number of different features, two study cases were designed to study and compare their performance. The first study case consisted in bringing the 2 MODIS 250m bands and the 5 bands at 500m to the spatial resolution of MERIS full resolution (300m) and then performing a spectral unmixing of the main 6 classes that cover The Netherlands.

After this, a second comparison was done by limiting the number of bands to the most similar ones between MERIS and MODIS. This resulted in working with only 4 bands and, therefore, in mapping the 3 main classes (the dimensionality of the problem is the restrictive factor for selecting the number of classes that can be identified). The next 2 subsections describe with further detail these study cases as well as the remotely-sensed and the validation datasets used in this study.

### **2.1. Remotely-sensed data**

A MERIS full resolution and a MODIS/Terra level 1b image (radiance Top of Atmosphere) were selected for the 14th of July 2003. First the images were georeferenced to the RD Dutch coordinate system using the tie-points provided with the images. Then, both images were corrected: the MERIS image from the SMILE [2] effect and the MODIS image for the bow-tie deformation [3]. Next, the 2 MODIS bands at 250m and the 5 bands at 500m were resampled to 300m using the nearest neighbor method. At the same time, the MERIS bands 1, 2, 11 and 15 were excluded from the analysis since they are severely affected by the

atmosphere (scattering and absorption) [4]. The software packages BEAM (Basic ENVISAT Toolbox for (A)ATSR and MERIS) and MRT-Swath (MODIS Reprojection Tool) were used to carry out these pre-processing steps.

In order to minimise the possible errors due to georeferencing inaccuracies, an image to image co-registration with the aggregated Dutch land use map (LGN) was done with ENVI. 30 ground control points were selected throughout The Netherlands to have a good coverage. After that, both images were warped using all the points and a third degree polynomial equation so that the LGN was matched as close as possible. The image warping yielded a RMSE of 0.4347 and of 0.4406 for the MERIS and MODIS images, respectively.

For the second study case, the most similar bands of both sensors (i.e. bands having more or less the same spectral coverage) were selected. Accordingly, the first 4 MODIS bands and the MERIS bands 3, 5, 6, 7 and 13 were chosen. As MODIS band 1 lies in between of MERIS bands 6 and 7, the average of these two bands was taken to resemble the MODIS band as much as possible.

## 2.2. Land use database

The Dutch land use database (LGN) was used as reference [5]. The database uses a grid structure with a cell size of 25 meters. The nomenclature of the LGN4 database contains 39 classes covering urban areas, water, forest, various agricultural crops and ecological classes. The LGN was created for an important part based on satellite imagery, but ancillary datasets were also integrated into it. Currently four versions exist, spanning a time period between 1986 and 2000. In this study, only the LGN4, which is based on satellite data of 1999 and 2000, was used. The overall classification accuracy of this dataset is about 90 %.

The initial LGN4 legend was aggregated into the main 6 and 3 land cover classes so that it could be used as a validation dataset for the first and the second study cases, respectively. The selected 6 main classes were: grassland, arable land, deciduous forest, coniferous forest, water and built-up areas, whereas the 3 classes map contained: low vegetation, forest and built-up areas. Note that despite the importance of the class water for The Netherlands it was left out of the analysis because a low spectral confusion was expected for this class and because we were working with 4-band images (which implies that only 3 endmembers could be defined).

After this thematic aggregation, a spatial aggregation took place to resample the original pixel size of 25m to the one of MERIS full resolution (300m). The aggregation method consisted in using a majority filter with a kernel size of 12 pixels (25m \* 12 = 300m). The land use with the highest abundance in this kernel was used to label the aggregated map. The proportion of every class within this kernel was also recorded during the spatial aggregation process, so that a so-called standard purity index (SPI) could be calculated from each window, as noted in equation 1:

$$SPI = \sqrt{\frac{\sum_{i=1}^{i=n} (f_i - f_{\max class})^2}{n - 1}} \quad (1)$$

Where:  $f$  represents the fraction of each land use in the kernel,  $f_{\max class}$  is the maximum fraction (the class driving the labeling process), and  $n$  is the number of classes. Consequently  $SPI = 1$ , when only one class is present in the kernel window and  $SPI=0$  when all the classes are present in the same proportion. A threshold of  $SPI = 0.95$  was used to mask the most homogeneous areas. After this, a moving window filter of 3 by 3 pixels was applied in order to minimise possible adjacency effects. Thus, only 'pure' pixels surrounded by the same land use class were finally selected [6].

## 2.3. Spectral unmixing

After having identified the most homogenous areas in The Netherlands for each one of the 6 (or 3, for the second test case) classes, the spectral signatures of the pure land use types, or endmembers, were derived and the angle among the different spectra was compute to assess eventual confusion among classes [7].

Subsequently, two unmixing methods were applied to evaluate the classification accuracy: unconstrained linear spectral unmixing [8] and matched filtering [9]. The latter approach turned out to be very useful, since it maximizes the response of a known endmember and suppresses the response of the composite unknown background, thus matching the known signature. On the other hand, the linear spectral unmixing method offers the possibility of getting the root mean square error (RMSE) per pixel

### 3. RESULTS

After computing the angle for all the possible pairs of endmembers we assigned to these combinations the name of the sensor having the highest value (better separability). At the end, we observed that the number of pairs per sensor was quite similar both for 6 and 3 classes. Nevertheless, MERIS was performing slightly better: especially for all the pairs involving either the class water or the class built-up.

Table 1 illustrates the classification results for both study cases. Notice that the first classification accuracies refer to the 6 classes 300m pixel size case and that the last 2 columns correspond to the second study case where only similar spectral bands were selected.

Table 1. Classification results for 6 and 3 classes.

Sensor	# of bands	Method	Class. Accuracy (%)	# of bands	Class. Accuracy (%)
MERIS	11 <sup>a</sup>	LSU	57.087 [RMSE: 0.157]	4 <sup>z</sup>	82.542 [RMSE: 0.387]
MERIS	11 <sup>a</sup>	MF	60.256	4 <sup>z</sup>	76.617
MODIS	7 <sup>b</sup>	LSU	40.579 [RMSE: 0.128]	4 <sup>δ</sup>	82.350 [RMSE: 0.864]
MODIS	7 <sup>b</sup>	MF	61.292	4 <sup>δ</sup>	78.469

<sup>a</sup> Excluding MERIS bands 1, 2, 11 and 15; <sup>b</sup> MODIS bands 1 & 2 aggregated from 250 m to 300 and MODIS bands 3-7 resampled from 500 m to 300; <sup>z</sup> MERIS bands 3, 5, average of 6&7 and 13; <sup>δ</sup> MODIS bands 1 & 2 aggregated from 250 m to 300 and MODIS bands 3 & 4 resampled from 500 m to 300.

The classification results are very similar and consistent with the previous studies [4]. In general, we can say that MERIS was performing somewhat better when using linear spectral unmixing (LSU) because its classification accuracies were slightly higher and the root mean square error (RMSE) was lower. On the other hand, the differences are not significant and MODIS was performing a bit better when doing a matched filtering classification (MF).

### 4. CONCLUSIONS, RECOMMENDATIONS AND OUTLOOK

The geometric and radiometric properties of MERIS and MODIS seem to be fine for land cover mapping at a medium resolution scale. Both instruments showed an equal and good performance for classifying land use in The Netherlands. Following our findings regarding the angle among spectra we recommend to investigate the possibilities of combining MERIS and MODIS in a hierarchical scheme in order to improve the classification accuracy. Further research will consist in exploring the influence of the radiometric (in)accuracies on the final land use product.

### REFERENCES

1. Rogan, J. and D.M. Chen, *Remote sensing technology for mapping and monitoring land-cover and land-use change*. Progress in Planning, 2004. **61**: p. 301-325.
2. *BEAM 3.0*. 2004, Brockmann Consult. <http://scipc3.scicon.gkss.de/services/beam2/software/>.
3. Gomez-Landesa, E., A. Rango, and M. Bleiweiss, *An algorithm to address the MODIS bowtie effect*. Canadian Journal of Remote Sensing, 2004. **30**(4): p. 644-650.
4. Clevers, J.G.P.W., et al. *Using MERIS on ENVISAT for land cover mapping*. In *ENVISAT Symposium*. 2004. Salzburg (Austria).
5. De Wit, A.J.W. and J.G.P.W. Clevers, *Efficiency and accuracy of per-field classification for operational crop mapping*. International Journal of Remote Sensing, 2004. **25**(20): p. 4091-4112.
6. Zurita Milla, R., et al. *Long-term MERIS land product accuracy assessment based on vicarious calibration and regional validation*. In *ENVISAT Symposium*. 2004. Salzburg (Austria).
7. Price, J.C., *How unique are spectral signatures?* Remote Sensing of Environment, 1994. **49**(3): p. 181-186.
8. Hu, Y.H., H.B. Lee, and F.L. Scarpace, *Optimal linear spectral unmixing*. IEEE Transactions on Geoscience and Remote Sensing, 1999. **37**(1): p. 639-644.
9. Harsanyi, J.C. and C.I. Chang, *Hyperspectral Image Classification and Dimensionality Reduction - an Orthogonal Subspace Projection Approach*. IEEE Transactions on Geoscience and Remote Sensing, 1994. **32**(4): p. 779-785.